UNIVERSITY OF KWAZULU-NATAL

A STUDY OF FIRE-INDUCED AIR-GAP VOLTAGE BREAKDOWN CHARACTERISTICS UNDER HVDC CONDITIONS

MARCH 2012

ZOLA NTSHANGASE

A STUDY OF FIRE-INDUCED AIR-GAP VOLTAGE BREAKDOWN CHARACTERISTICS UNDER HVDC CONDITIONS

By

Zola Ntshangase, B.Sc. (Eng.)(Elec.)

A dissertation submitted in partial fulfilment (50%) of the requirements for the degree of

Master of Science in Electrical Engineering

(Power & Energy Studies)

In the Faculty of Engineering

University of KwaZulu-Natal

Supervisor: Professor N.M. Ijumba

Co-Supervisor: Professor A.C. Britten

Durban, South Africa

07 March 2012

I dedicate all this work to my late mother,

Ziningi Regina Dlamini

and my late father,

Zwelihle Royal Ntshangase

May your souls rest in peace and I know that each day you always look down on us and offer us protection.

Declaration

As the candidate's supervisor, I have/have not approved this dissertation for submission.

Signed:.....

Name: ..... **Date**: .....

I, **Zola Ntshangase,** the undersigned, hereby declare that:

(i) The research reported in this dissertation, except where otherwise indicated, is my original work.

(ii) This dissertation has not been submitted for any degree or examination at any other university.

(iii) This dissertation does not contain other persons' data, pictures, graphs or other information, unless specifically acknowledged as being sourced from other persons.

(iv) This dissertation does not contain other persons' writing, unless specifically acknowledged as being sourced from other researchers. Where other written sources have been quoted, then:

a) their words have been re-written but the general information attributed to them has been referenced;

b) where their exact words have been used, their writing has been placed inside quotation marks, and referenced.

(v) Where I have reproduced a publication of which I am an author, co-author or editor, I have indicated in detail which part of the publication was actually written by myself alone and have fully referenced such publications.

(vi) This dissertation/thesis does not contain text, graphics or tables copied and pasted from the Internet, unless specifically acknowledged, and the source being detailed in the dissertation/thesis and in the References sections.

.....

Z. Ntshangase

206521431

Date: .....

Acknowledgements

The author would like to thank the Lord Almighty for giving him the strength and the will to go on even in the midst of uncertainties and doubts. He has guided me through and with his love and grace; He has delivered me to this point.

My utmost thanks go to my supervisor, Professor N.M. Ijumba for his extensive guidance and dedication throughout my research work. His love for his work has given me renewed strength and zeal about the career path that I have chosen. I have certainly grown under his supervision and I hope that we will still work closely together in the near future.

My loving soon-to-be wife Nozipho Mqadi for her unwavering support, she is one in a million and I am blessed to have her in my life.

My sons, Mbhele, Lizwelihle and Buhlebonke, I trust that my efforts in ensuring that you have a decent education and up-bringing will inspire you to do far greater things in your lifetimes then I ever will during mine!

Additionally the author would like to thank the following people:

- Professor A.C. Britten (Co-supervisor and Eskom Corporate Consultant - HV)
- Leena Rajpal (Business manager – HVDC Centre)
- Neetu Rama (Former Postgraduate Administrator – HVDC Centre)
- Anand Naidoo (Former Laboratory Technician – HVDC Centre)
- Aaron Mutombo (Laboratory Technician – HVDC Centre)
- HVDC Centre MSc students (Ojo and Cedrick)
- The Ntshangase families in Port Shepstone, Bulwer & Pietermaritzburg

Abstract

This dissertation investigates the role that is played by high temperatures of air gaps on the breakdown voltage levels under DC positive and negative polarity applied voltages. Due to past experience of AC transmission lines tripping as a result of sugar-cane fires that occur under these lines during cultivation seasons, this study was initiated to investigate this effect under DC applied voltages.

Results were obtained from laboratory work conducted and these were closely analysed to understand the behaviour of air gaps under these conditions. A 17mm^2 square-cut brass rod-rod electrode configuration was used to carry out these tests at the various air gap temperatures. These were induced by a gas burner for both the positive and negative polarities at 20^{0}C – 300^{0}C for the 10 mm – 150 mm air gap range and 20^{0}C – 150^{0}C for the 200 mm – 500 mm air gap range. Later particles were introduced into the air gap to determine the subsequent behaviour. These were introduced vertically from the top into an air gap via a vibrating micro sieve mechanism to regulate the consistency of the introduction of these particles in the air gap.

A reduction of 55% and 50% was observed on the breakdown voltage under positive and negative polarity applied voltages respectively from ambient conditions to 300^{0}C. Additionally the breakdown behaviour of both negative and positive DC was found to be linear which is similar to the AC case. However, air gaps subjected to positive DC applied voltages were found to portray an inferior dielectric strength as opposed to the equivalent negative DC polarity.

The study found that the effect of particles in the air gap is practically negligible and that for practical purposes, only the temperature effect plays a role due to the reduced air density at high temperatures.

Empirical models for both the positive and negative DC polarities have been proposed by the study that incorporate the effect of the temperature in the air gap to enable the determination or prediction of the breakdown voltage level at various temperatures. These models may be utilised for DC transmission line design for servitudes in areas that are known to be prone to fires.

List of Abbreviations

AC (ac)	-	Alternating current
DC (dc)	-	Direct current
EPRI	-	Electric Power Research Institute (USA)
HV	-	High voltage
HVDC	-	High voltage direct current
IEC	-	International Electrotechnical Commission
IEEE	-	Institute of Electrical & Electronic Engineers
kV	-	Kilovolt
LI	-	Lightning impulse
RMS (r.m.s.)	-	Root mean square
SI	-	Switching Impulse
STP	-	Standard Temperature & Pressure
UK	-	United Kingdom
UKZN	-	University of KwaZulu- Natal
USA	-	United States of America

List of Symbols

I_0	-	Initial photocurrent from the cathode
δ	-	Cathode separation
α	-	Primary ionization coefficient
γ	-	Secondary ionization coefficient
E	-	Electric field
p	-	Gas pressure
n_0	-	Initial number of electrons emitted by the cathode
n_a	-	Number of electrons that reach the anode
η	-	Attachment coefficient
E_0	-	Original electric field
x_c	-	Critical avalanche length
E_r	-	Radially directed space charge field strength
x	-	Avalanche progression distance
N_{cr}	-	Critical electron concentration in an avalanche
V_s (U_s)	-	Breakdown voltage under STP Conditions
V_t (U_t)	-	Breakdown voltage at actual temperature conditions

D (δ)	-	Relative air density
T	-	Actual temperature
p_0	-	101.3kPA
T_0	-	20^0C

List of Illustrations

List of Tables

Table of Contents

CHAPTER 1

INTRODUCTION

1.1. Background

It is well known that the presence of fire under transmission lines reduces the dielectric strength of the air in the vicinity of the conductors [1]. This leads to breakdown occurring at a value lower than it normally would under standard temperature conditions [2]. Over the years Eskom has experienced flashover problems caused by bush and sugar cane fires under 275 and 400 kV transmission lines [3]. In the northern coastal region of KwaZulu-Natal where sugar cane farming is a major agricultural activity, farmers burn the sugar cane crops as a harvesting aid thus causing line outages [4]. Similar problems have also been reported in other countries such as Brazil, Canada and Mexico, where agricultural fires were resulting in transmission line outages [5]. As a result various authors such as Cowan *et al.* [6], Sadurski and Reynders [3], Sukhnandan and Hoch [7] in South Africa, Lanoie and Mercure [8] in Canada, Fonseca, *et al*. [5] in Brazil and Robledo-Martinez *et al.* in Mexico [9] have carried out studies to understand the effect of fire on the reduction of the insulation strength of air thus its effect on the line performance. However, these have been conducted under AC applied voltages, except in the case of [8] where studies were also conducted on a ±450 kV experimental bipolar dc line.

1.1.1. Sugar cane fire study

Cowan [6] in 1991 collaborated a research study with Eskom (South African power utility) to establish the mechanism of insulation breakdown, the fault impedance and the extent of electromagnetic induced noise prior to flashover. The study had emanated from problems experienced on high voltage lines in the coastal region of KwaZulu-Natal during sugar cane harvesting in which sugar cane is burnt as a means of aiding in harvesting. Flashovers that would occur on these lines could potentially damage transmission line hardware and as a result of large fault currents, severe voltage depressions would occur [6].

Figure 1.1 A typical sugar cane flame completely engulfing conductors of an Eskom transmission line [10]

A typical sugar cane fire burning under a transmission line is illustrated in Figure 1.1 [10], and it can be observed that the intensity and height of the fire flames can be such that they completely engulf the three phases of an AC transmission line. This would inadvertently lead to a severe deterioration in the dielectric strength of the air between the adjacent phases.

In investigating the mechanism of insulation breakdown, the authors of [6] documented empirical observations which showed that the following factors influenced the probability of flashovers (for an AC line):

1) the voltage gradient (i.e. transmission line phase spacing),
2) fire intensity and duration (i.e. temperature) and
3) ash particles and smoke density.

Cowen *et al.* [6] further noted that ambient temperature, humidity and other environmental conditions had little apparent influence.

Additional data from three previous years (1988 – 1990) was presented and it indicated the following significant findings:

- 400 kV lines (47 kV/m) experienced 1.5 flashovers/100km/annum while
- 132 kV lines (21 kV/m) only experienced 0.3 flashovers/100km/annum

- 400kV lines with 44 kV/m phase-to-phase and 47kV/m phase-to-earth wire voltage gradient generally flash phase-to-earth while
- 275 kV lines with 37 kV/m and 33 kV/m voltage gradients respectively flash mainly phase-to-phase.

Laboratory studies conducted by Cowan [6] showed that temperatures of 1100 ^{0}C reduced the dielectric strength of air from 2120 kV/m to 110 kV/m. These results are only valid for small and uniform air gaps and field observations indicated that the fire had to be intense and sustained for flashover to occur. For large and non-uniform gaps experienced in practice, the insulation breakdown was found to take place according to the streamer mechanism, rather than the classical Townsend mechanism, thereby reducing the dielectric strength from the 110 kV/m stated above. Ash particles and smoke were observed to be assisting in the streamer breakdown, thus reducing air dielectric strength even further. The Townsend and Streamer mechanism of breakdown is discussed further in *Section 2.1.1.1.* and *2.1.1.2.* respectively.

The study drew a conclusion that the phase-to-phase and phase-to-earth wire voltage gradient statistically predict where the flashover will occur. Thus to ensure less severe voltage depressions, the phase-to-earthwire voltage gradient must be greater than the phase-to-phase voltage gradient (i.e. forcing phase-to-earth faults).

There currently exists no documented (or none could be located) full scale literature on a field study conducted on the effects of fire on the dielectric air gap breakdown characteristics of HVDC lines. Such a study would have been of great value to this research as it could have been comparatively analysed with outcomes obtained by Cowan *et al.* [6]. However, available literature on the subject under AC and DC is discussed further in later chapters of this study.

1.2. Motivation

With limited studies on the topic carried out under DC applied voltages, as part of a strategic partnership this study was initiated jointly by Eskom, the South African utility company and the HVDC Centre of the University of KwaZulu-Natal. For a combination of technical and economical reasons, long-distance transmission using HVDC systems has over the past two decades become a viable alternative to HVAC for various utilities across the world. Thus as

such, knowledge on the various technical aspects of HVDC transmission is sought; more especially in the African context, the effects of fires on the air dielectric degradation.

The behaviour of air as a dielectric was studied under DC applied voltages in the presence of fire, with special reference to its voltage breakdown characteristics. The ultimate objectives of the study were thus to investigate the following critical aspects of the voltage breakdown characteristics of air gaps:

1) the DC voltage breakdown mechanism compared with the AC breakdown mechanism;
2) the effect of increased temperatures in the air gap;
3) the comparative effect of the voltage polarity (negative or positive) and
4) the effect of the presence of particles at high temperatures in the air gap.

In addition, the outcomes of the investigations into these aspects were comparatively studied with the same phenomena as observed from literature on the subject under AC voltages. A rod-rod gap configuration was used to conduct the air gap voltage breakdown tests. All experiments were conducted in the HVDC laboratory, which is part of the HVDC Centre at UKZN in Durban.

Ultimately, this study sought to investigate whether air as a dielectric under AC voltage stresses and subjected to elevated temperatures would portray similar behaviour under DC voltage stresses. Further practical field aspects such as the nature of the DC polarity voltage and the advent presence of particles in the vicinity of the air gap are qualified on the basis of their influence on the breakdown voltage characteristics.

1.3. Research methodology

This study was conducted as follows:

- A literature survey of available data under AC and DC (both polarities).
- A comparative analysis of the literature.
- Experimental results that were obtained were presented citing information as discussed and presented in the literature survey.
- A model was proposed based on the experimental results and various conclusions and recommendation were presented.

1.4. Study outcomes

Ultimately the empirical and theoretical findings of this study may be used in the design of insulation systems for HVDC lines, more especially where the line is to pass through an area that is known to be prone to fires. Furthermore with the recent increase in HVDC transmission systems, it further enforces the need for an in-depth understanding of air gap voltage breakdown characteristics under DC conditions [2]. Presently the Apollo HVDC scheme between South Africa and Mozambique is the only HVDC scheme that is in operation in South Africa, however with the Westcor HVDC project still under consideration, findings from this study will certainly be of particular interest and application.

1.5. Dissertation outline

With the background of this study having been elaborated on in this chapter; in *Chapter 2* a literature review of the topic is presented with reference to both AC and DC voltages with an objective of introducing the basis for experiments conducted in this study and the data presented in subsequent chapters. Experimental procedures used and the layout of the experiments conducted are discussed in *Chapter 3*. In *Chapter 4*, findings of the study are presented and a thorough and an in-depth interpretation and analysis of the results obtained is conducted. The ultimate conclusions drawn on the study are discussed in *Chapter 5*.

CHAPTER 2

LITERATURE REVIEW

Insulation systems in high voltage transmission lines are designed for a certain level of electric field strength, taking into account critical intensity levels before onset corona activity occurs. Since air is used as the main insulation in high voltage transmission [11], a safe operating distance between adjacent conductors must exist. This minimises the possibility of interruptions due to insulation failures on that particular power transmission system. Discussions to follow in this section will exclude insulation breakdown conditions such as those observed due to either lightning or switching impulses. Only insulation breakdown that occurs as a result of continuous electric field stresses emanating from applied voltages will be discussed.

2.1. Basic gaseous insulation breakdown

Insulation is effective up to the breakdown threshold [12] and the manner in which breakdown occurs is a progressive process from partial to complete breakdown [13]. It is thus imperative that phenomena leading to complete breakdown of gaseous mediums be empathised for various insulation systems under various conditions.

2.1.1 Ionization processes in a gas

2.1.1.1 Townsend mechanism

The Townsend theory has often been used by researchers to explain gaseous dielectric breakdown. However, this theory is limited in that it only holds for uniform fields under quasi-static conditions and needs to be complemented by the Streamer criterion in order to be of effective use and importance in engineering [14]. It assumes that during the avalanche process, the applied voltage remains constant, however in practice breakdown is accompanied by a collapse of voltage [15]. Nevertheless, it forms a fundamental basis for an understanding of breakdown processes that occur in air, thus forming a foundation for breakdown of solid, liquid and glass dielectrics.

This theory of electrical breakdown in gases is well documented [16] – [25] and as such will not be explicitly reviewed as part of this Chapter. However, throughout the report various citations relating to this fundamental principle will be made.

2.1.1.2. Streamer mechanism

At higher pressures, larger electrode gap spacing and higher potential gradients the formation of a discharge will deviate from that as explained by the Townsend mechanism and follow the *Streamer ('Kanal')* mechanism of voltage breakdown. For a better understanding of this theory it will have to be elaborated on first under uniform electric field conditions and then further extending its applicability to non-uniform electric fields.

(i) Plane uniform gap

The theory assumes that the breakdown process starts off by a single electron avalanche which then becomes unstable creating fast moving streamers directed towards the anode and cathode from its head [15]. A process known as photo-ionisation is pivotal in the conversion of these electron avalanches into streamers. *Raether* [25] in his studies of the effect of space charge of an avalanche on its growth observed that when the charge concentration was higher than 10^6, but lower than 10^8, the growth of an avalanche was weakened. He further illustrated that when the ion concentration exceeded 10^8, the avalanche current was followed by a steep rise in current and breakdown of the gap followed thereafter.

(ii) Non-uniform gap

In non-uniform fields, e.g. in point-plane, point-point, sphere-plane gaps or coaxial cylinders, the field strength and hence the effective ionisation coefficient α vary across the gap [22]. For a streamer to be initiated at the high-voltage electrode and for it to bridge the gap two conditions have to be satisfied; one for the streamer inception and the other for the streamer propagation.

The streamer mechanism is also a widely documented principle with various authors [15], [22], [25] – [35] having elaborated on the fundamentals of streamer formation and space charge influence in both uniform and non-uniform gaps.

2.1.1.3. The Streamer mechanism applied to high temperatures

The limitations of the Townsend theory to uniform fields have been alluded to in *Section 2.1.1.1* and the need to rely on the Streamer mechanism of breakdown to better explain the air breakdown mechanism has also been discussed in *Section 2.1.1.2*. Prevailing climatic parameters influence the electrical discharges in air, resulting in a dependence of the

breakdown voltage on these parameters. Discussions in this particular section will however, only seek to elaborate on the influence of temperature on the Streamer breakdown in air, pressure and humidity will not be considered due to their practical insignificance. Thermal ionization has been excluded from discussions as it is attained when a gas is heated to temperatures of the order of 10,000*K* [36], [37] which is outside of the application for purposes of this study. To incorporate the influence of temperature on the breakdown mechanism, it is more convenient to introduce the 'relative gas density', δ (D) – a dimensionless quantity. This quantity takes care of the effect of temperature on the mean free path of electrons in the gas at constant pressure [37] and is defined as:

$$\delta = \frac{\rho}{760}\frac{293}{273+t} = 0.386\frac{\rho}{273+t} \quad ...(2.1)$$

Where,

p = the gas pressure in Torr and

t = Temperature in ^{0}C

The temperature influences the electrical discharges in air via the motion of the particles [38]. As the temperature in the air gap is increased, the mean free path of the particles also increases linearly with the corresponding increase in temperature. The electron and ion concentrations in the air gap rise with the result that the distortion of the electric field by the field of the space charge of positive ions increases [37].

McDaniel [39] in his book defines the "mean free path" as the distance that a molecule travels between successive collisions. He further explains that each collision marks an end of two free paths (one for each of the two collision partners), and the total number of free paths executed per cm^3/sec is $\sqrt{2}\pi N^2 D^2 v'$.

Where,

N = gas number density (molecules/cm^3)

D = molecular diameter (assuming that molecules are elastic spheres)

v' = mean velocity of molecule

The total length of all these free paths is Nv' and the average length of a free path is given by the expression [39]:

$$\lambda = \frac{1}{\sqrt{2}\pi N D^2} \quad ...(2.2)$$

which is designated as *Maxwell's mean free path*. He [39] defines the average collision frequency for a single molecule of a gas with a Maxwellian distribution (Figure 2.8) as:

$$\nu = \sqrt{2}\pi N D^2 v' \qquad ...(2.3)$$

Thus according to the elastic sphere model, the collision frequency varies directly with the density of the gas (Equation 2.1) and the square root of the absolute temperature, variation with temperature arising from the proportionality of *v* to *v'*. The mean free path on the other hand, varies only with the density and is inversely proportional to it.

The Maxwell's distribution function of Figure 2.1 is expressed in the form [39]:

$$f(v)dv = N_t \left(\frac{2}{\pi}\right)^{1/2} \left(\frac{m}{kT}\right)^{3/2} v^2 e^{\left[-mv^2/2kT\right]} dv \qquad ...(2.4)$$

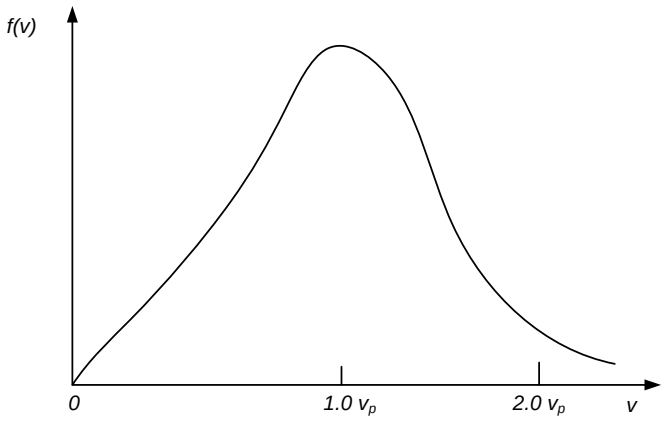

Figure 2.1. Maxwell distribution function for the speeds of molecules of a gas in thermodynamic equilibrium [39]

Where,

f(v)dv = the number of molecules with speeds between *v* and (*v* + *dv*) cm/sec,

m = the mass of one of the molecules in grams,

T = the absolute temperature in ^{0}K, and

k = 1.3806 x 10^{-16} erg/^{0}K (Boltzmann's constant)

v_p = the most probable velocity of the distribution

N_t = the total number of molecules in the gas, defined by the following equation

$$\int_0^\infty f(v)\, dv = N_t \qquad ...(2.5)$$

Elaborating further, it further follows that Equation 2.6 [22], [35] defines N_{cr}, the critical electron concentration in an avalanche that gives rise to the initiation of a streamer.

$$exp\left\{\int_0^{x_c \leq \delta} \alpha dx\right\} = N_{cr} \quad \ldots(2.6)$$

Where,

N_{cr} = the critical electron concentration in an avalanche giving rise to initiation of a streamer

This is directly proportional to α, the Townsend coefficient of ionization by electrons corresponding to an applied field *E*. In a non-uniform electric field distribution in the air gap, α is stated as not being a constant [25], [34], but rather as a function of the parameter *x* as defined in Equation 2.7 [34].

$$E_r = 5.3 \times 10^{-7} \frac{\alpha e^{\alpha x}}{\left(\frac{x}{\rho}\right)^{1/2}} volts/cm \quad \ldots(2.7)$$

Where,

x = the distance (in cm) which the avalanche has progressed

p = the gas pressure in torr and

α = Townsend coefficient of ionization by electrons corresponding to the applied field *E*

At the first instance the formation of charge carriers from neutral gas molecules is as a result of the impact or collision of particles amongst each other, accelerated under the electric field. The introduction of elevated temperatures promotes more frequent collisions, thus subsequently more electrons and positive ions are formed. In Figure 2.2 the effect of an increased temperature in the air gap is schematically illustrated. The values that have been used in this figure are only illustrative and are not to be taken as measured values.

Assuming that charge carriers were already present before applying the electric field, at *STP* conditions, an electron avalanche travels a distance x_1 and as a result creates nx_1 number of new electrons and ny_1 number of positive ions after a time t_1 in traverse. During the same time, at an elevated temperature (e.g. 50^0C) the same electron avalanche would have travelled a distance x_2, where $x_2 > x_1$ in which during its traverse it would have collided with more neutral atoms to release more electrons, positive ions and vibrational (excited) molecules.

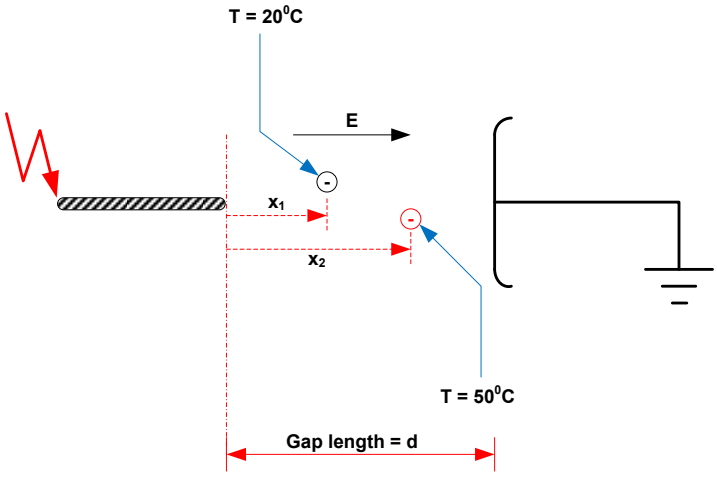

Figure 2.2 Illustration of temperature effect on air gap breakdown voltage

This will then lead to a canal/ streamer formation sooner than it would have under STP and leading to a premature breakdown of the air gap.

This effect can further be explained with reference to energy. The total energy of an electron while still attached to the molecule can be divided into two types of energies [37]: First the kinetic energy W_{KE}, which depends upon its mass and velocity, and second the potential energy W_{pot}, depending upon its charge in the Coulomb field of the nucleus of a molecule. These energies are given as,

$$W_{KE} = \frac{1}{2} m_e v_e^2 = \frac{1}{8\pi\varepsilon} \frac{e^2 z}{r_e} \quad \text{...(2.8)}$$

and

$$W_{pot} = -\frac{1}{4\pi\varepsilon} \frac{e^2 z}{r_e} = -2W_{KE} \quad \text{...(2.9)}$$

Where,

m_e = the electron mass

v_e = electron velocity

ε = the permittivity of the dielectric (air) and

z = the atomic number representing z electrons with negative elementary charge e = -1.6 x 10^{-19}, as lying in the discrete circular orbits r_e of the atom.

Once the electron attains enough energy to be ejected from the atom shell, the potential energy of the electron tends to be zero. Then the only energy it has is the kinetic energy

acquired externally (high temperature). Elevated gas temperatures results in many of the gas atoms or molecules acquiring high velocities, thus the ionisation by electron impact (α-process) and ionisation by positive ion impact ($\beta -$ process) as illustrated in Figure 2.3 and 2.4 [37] is more frequent leading to a rapid formation of streamers and subsequently the complete breakdown of the air gap. From Equation 2.2 – 2.5, the significance of the velocity v_e and v_m (to a limted extent) can be witnessed.

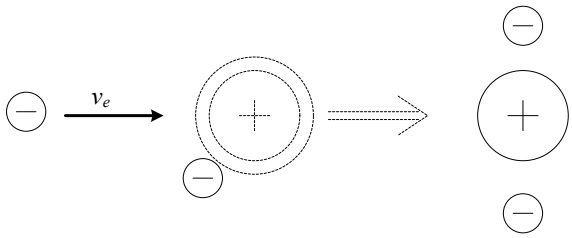

Figure 2.3 Ionization by electron impact [37]

Corresponding equation: $$\frac{1}{2}m_e v_e^2 \geq e.U_I \quad ...(2.10)$$

Where, U_I = Ionisation potential

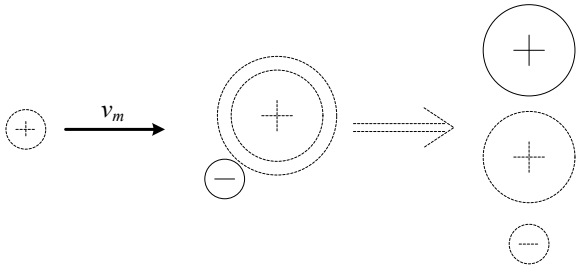

Figure 2.4 Ionization by positive ion impact [37]

Corresponding equation: $$\frac{1}{2}m_m v_m^2 \geq 2e.U_I \quad ...(2.11)$$

In 1993, *Allen et al*. [40] investigated the temperature and density effects on streamer propagation in air over the temperature range $-14^0\text{C} < \text{T} < 148^0\text{C}$ using direct voltages up to 125 kV. Experiments were conducted using a plane parallel electrode system, enclosed in an oven permitting a maximum electrode separation of 20 cm under a uniform field. The oven was thermally insulated and designed for a maximum temperature of 200^0C (573 K), while ambient atmospheric pressure and humidity were maintained.

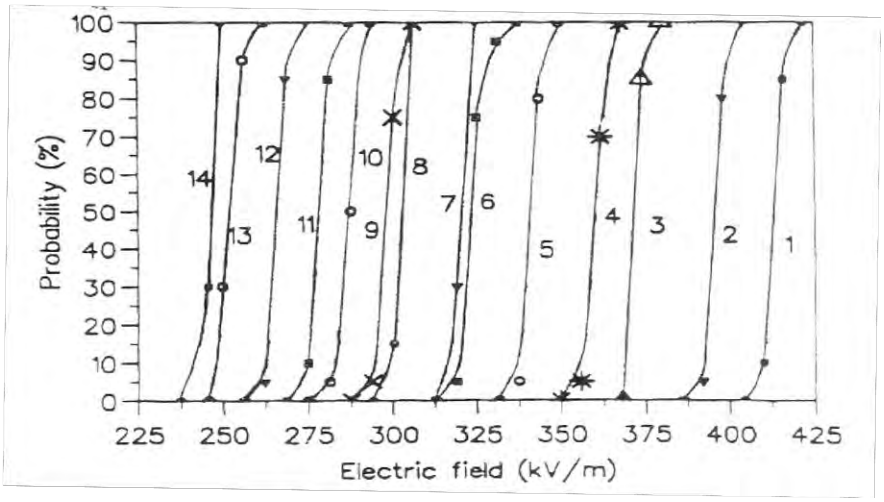

Figure 2.5 Probability of streamer propagation
as a function of electric field [40, pp. 6]

Figure 2.5 [40] illustrates the probability curve of streamer propagation as a function of the electric field intensity. From this it is apparent that streamer propagation commences at a lower field intensity at higher temperatures than it is required for lower air gap temperatures.

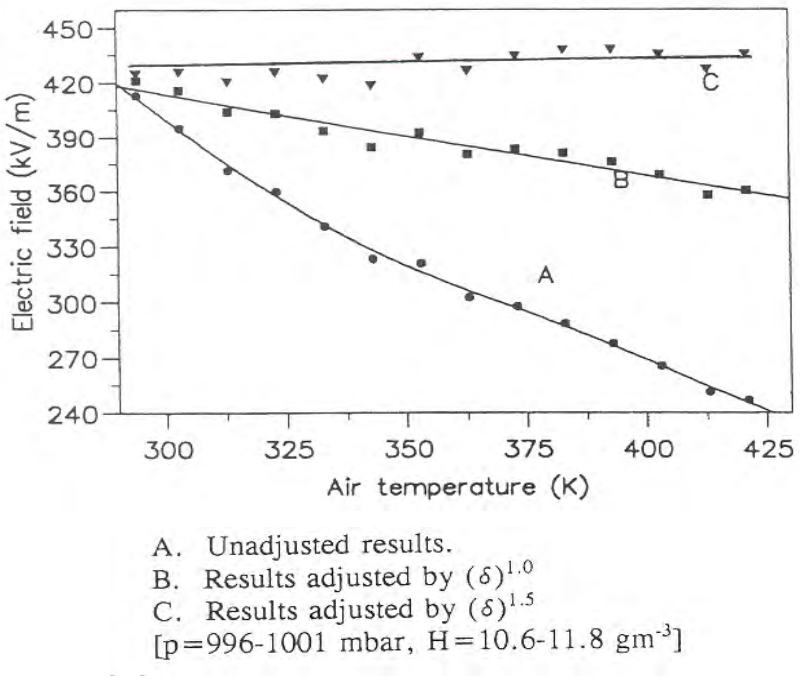

Figure 2.6 Streamer propagation field (50%)
as a function of air temperature [40, pp. 8]

The authors reported that at standard atmospheric conditions, the minimum electric field required for propagation of a streamer is 422 kV/m. This was reported to be reduced by the increase of temperature; however this was attributed to the resulting reduction in density rather than to the specific temperature effects on ionic and neutral species. Additionally, the density dependence (scaled as relative air density to the power 1.5) was found to be constant over the temperature range $-14^0C < T < 148^0C$. This is illustrated in Figure 2.6 [40].

2.2. Voltage breakdown characteristics of air gaps

In the overall problem of total insulation requirements, the factor of adequate clearance between the energized components of a DC transmission line and ground is of major importance [41]. Furthermore, as air is used as the main insulation between these energized components, its dielectric properties need to be well understood as well and all the parameters that the properties are dependent on. Of these, external influencing parameters play a pivotal role in defining the dielectric properties of air gaps [2]. External influencing parameters can be grouped into three categories: the geometrical, the electrical and the climatic parameters [42]. However, in this section, in line with the study the literature that will be reviewed shall be limited to external influencing parameters (temperature and density, excluding humidity) for various electrode gap configurations. Further, the effect of the applied voltage polarity and floating particles in the air gap will also be discussed.

2.2.1. Breakdown at room temperature

Various studies around the world have been conducted with the main aim of understanding the voltage breakdown characteristics of air gaps under various voltage applications, i.e. continuous AC and DC voltages, switching impulses (SI), and lightning impulses (LI). These have been conducted using various gap configurations, e.g. rod-rod (point-point), rod-plane (point-plane) etc., electrode shapes (i.e. cylindrical flat cut, hemispherically ended etc.) and gap sizes.

2.2.1.1 AC breakdown characteristics

EPRI [43] in 1998 published a report on the spark over performance and gap factors for gaps below 1m. In this publication, results observed both under AC (Appendix C) and DC (Positive polarity - Appendix A & Negative Polarity – Appendix B) were reported on. In [43]; for ease of reference and comparison of experimental results obtained in this study and the published literature, the spark over performance of the horizontal rod-rod electrode gap

configuration under both alternating and direct current applied voltages are of particular interest.

In Figure 2.7, AC voltage breakdown characteristics (r.m.s.) of a horizontal rod-rod air gap configuration are illustrated for the 0.02 m – 1.6 m range as observed by different authors. The rods that were used in all instances were flat cut squares with a varying edge width of between 12.5 mm and 25 mm and were made of brass. Results obtained by Fonseca *et al.* [5] and Robledo-Martinez *et al.* [9] were extrapolated for larger air gaps as these were obtained only for the 0 – 200mm air gap range. In the overall range it is evident that a linear behaviour exists (or can be estimated) between the breakdown voltage and the air gap length. Such an observation is imperative to note as scrutiny of obtained experimental results is still to be discussed in later chapters. It is of interest to note that results obtained by Razevig [23] and those obtained by EPRI [43] are in direct agreement with each other.

The observed mean withstand voltage gradient from both these authors is approximately 3.5 kV/cm which also represents the median.

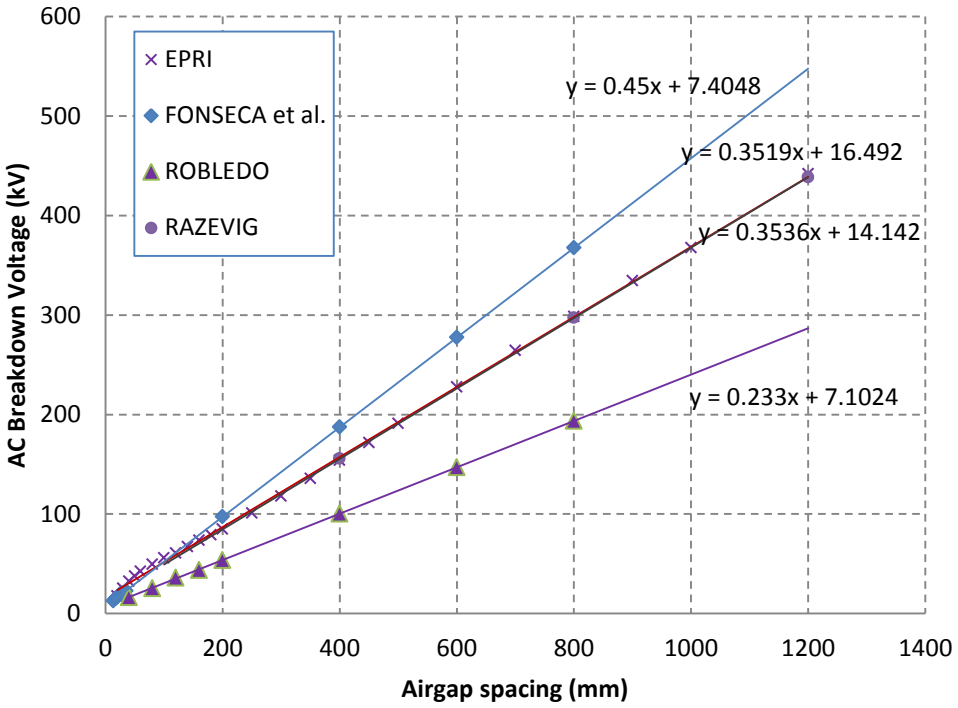

Figure 2.7 AC breakdown characteristics of rod-rod air gaps
{Based on [5], [9], [24] and [43]}

Fonseca *et al.* [5] obtained a higher gradient than [23] and [43] with an observed mean withstand voltage gradient of 4.5 kV/cm. Further Robledo-Martinez *et al.* [9] obtained a

mean withstand voltage gradient of 2.3 kV/cm, the least of the authors that have been discussed in this section.

2.2.1.2 DC breakdown characteristics

Figures 2.8 and 2.9 illustrate work on breakdown characteristics of rod-rod air gaps up to 2m under positive and negative DC applied voltages respectively. The median of the mean withstand voltage breakdown gradients observed under positive DC applied voltage can be approximated at 4.3 kV/cm, which is 23% higher than the 3.5 kV/cm observed under AC applied voltage discussed in *Section 2.2.1.1* above. This ultimately indicates that given an air gap of a specific length, it will portray inferior dielectric strength properties under an AC applied voltage as opposed to a DC applied voltage.

In Figure 2.8, air gap voltage breakdown characteristics under positive DC voltages as reported by EPRI [43], Abraham *et al.* [44] and Gobbo *et al.* [45] obtained in the smaller 0 – 500 mm air gap range had to be extrapolated to allow for a comparative analysis of the literature from different authors. Similar to results observed under AC applied voltage, a linear relationship exists between the breakdown voltage and air gap length for positive DC applied voltage. Allen *et al.* [46] reported that this linearity resulted from the fact that breakdown is determined by the movement of positive streamers initiating from the anode and approaching the negative electrode. Thus as a result, negative streamers which are determined to be shorter are formed.

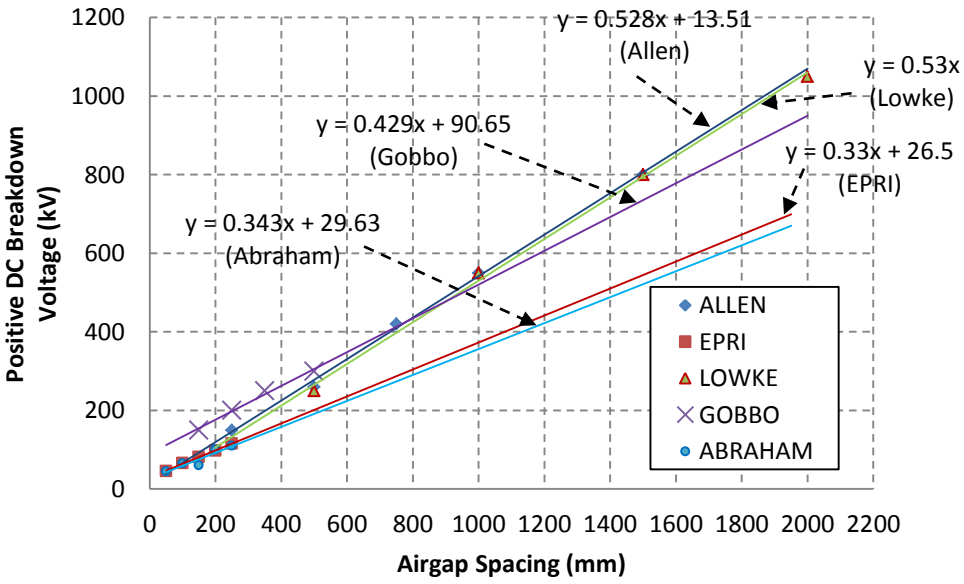

Figure 2.8 Positive DC breakdown characteristics of rod-rod air gaps
{Based on [43], [44]-[47]}

The authors of [46] in this study conducted a review of the breakdown characteristics of rod-plane and rod-rod air gaps stressed under direct current voltages, ultimately to determine the range of DC voltage measurements for which these may be applicable.

Figure 2.9 illustrates air gap voltage breakdown characteristics under negative DC voltages investigated by different authors. The linear relationship between the breakdown voltage and the air gap length is also clearly observed under negative DC voltages, as was observed under AC and positive DC voltage applications. The maximum mean withstand voltage gradient, 5.7 kV/cm was obtained by Lowke [47] and Gobbo *et al.* [45]. In this study the authors were investigating the validity of the data provided by the IEC [48] standard and sensitivity to the shape of electrode termination for rod-rod gap configurations. The least mean withstand voltage gradient as illustrated in Figure 2.16 is 3.4 kV/cm obtained by Abraham *et al.* [44] in which flashover characteristics of several type gaps including the rod-rod gap were investigated. The rods used in this study were 12.5 mm x 12.5 mm square cut brass rods.

The median of the mean withstand voltage gradients observed in Figure 2.9 is approximated at 4.7 kV/cm. This is approximately 10% and 34% higher than the mean gradient observed under positive DC and AC voltages respectively. Further, this indicates that the performance of air as a dielectric (under ambient temperature conditions) is superior when subjected to negative DC voltages than AC and positive DC voltages.

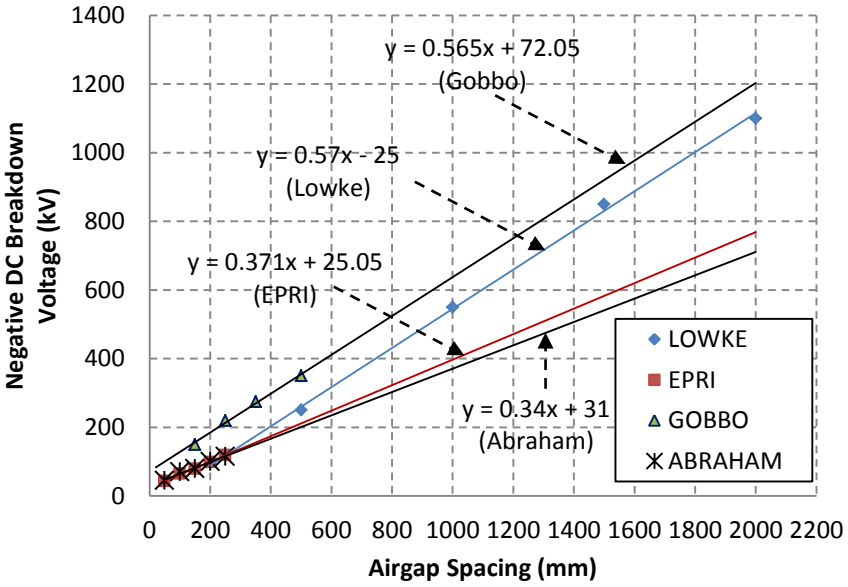

Figure 2.9 Negative DC breakdown characteristics of rod-rod air gaps
{Based on [43], [45]-[47]}

This observation is very important as it will be used as the basis for a comparative analysis of experimental data to be discussed in later chapters. Results obtained by the various authors whose literature was discussed in this section on air gap voltage breakdown characteristics under DC applied voltages may be attributed to the various corona modes that an air gap undergoes before complete breakdown.

2.2.2. Effect of increased temperatures and solid particles

The insulation strength of air is decreased by the reduction in air density due to the temperature increase caused by the fire [4]. The breakdown of air depends on temperature and humidity, however in the presence of fire the humidity correction factor, *H* is minimal, and hence it is ignored resulting in the reduced Equation 2.12 from Equation 2.11 [40]:

$$U_s = U_t \frac{H}{D} \quad ...(2.11)$$

$$U_t = U_s \frac{2.892\rho}{T} \quad ...(2.12)$$

Where, U_s = Breakdown voltage under STP conditions,

V_t = Breakdown voltage at actual temperature conditions,

p = the barometric pressure and (kPa)

T = is the actual temperature in Kelvin (K)

D = the relative air density (usually denoted δ) defined by the equation:

$$\delta = \frac{\rho}{\rho_0} \frac{273+T_0}{273+T} \quad ...(2.13)$$

Where, T = is the actual temperature in ^{0}C, assuming that

p_0 = 101.3kPa and

T_0 = 20 ^{0}C under STP conditions.

If p is expressed in *mmHg* in Equation 2.11, this results in the following equation:

$$U_t = U_s \frac{0.392P}{273+T} \quad ...(2.14)$$

The authors in [5] also cited that the reduction of the dielectric strength of an insulator due to increased temperature can be approximately determined by the following equation:

$$U_t = U_s \frac{0.386p}{273+T} \quad \ldots(2.15)$$

Where,

U_t = Flashover/breakdown voltage at actual temperature conditions,

U_s = Flashover/breakdown voltage in STP conditions,

p = the barometric pressure (*mmHg*) and

T = Actual temperature (^{0}C)

Thus taking a temperature of 120^{0}C and applying it in Equation 2.15, neglecting the pressure reduction, yields $U_t = 0.76\ U_s$. Equation 2.14 and 2.15 are very close to each other and can be approximated to yield equal results.

2.2.2.1 Millimetric experimental tests

For characteristics of discharges in high temperature air, Alston [49] conducted measurements of the breakdown voltage under uniform electric field air gaps. He confirmed in high temperature air up to 1200^{0}C, the validity of Paschen's Law for millimetric air gaps.

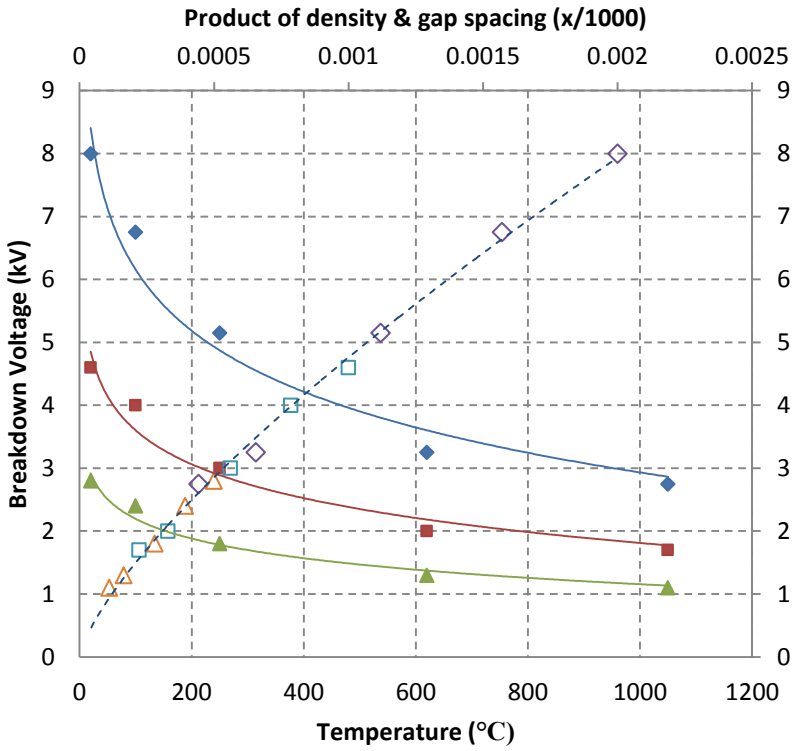

Figure 2.10 Breakdown characteristics for 0.5 mm –2.0 mm gaps at temperatures up to 1100^{0}C and atmospheric pressure
{Based on [49]}

Symbol (T, V)	Symbol (x, V)	Gap, mm
◆ 2mm	◇ 2mm	2
■ 1mm	□ 1mm	1
▲ 0.5mm	△ 0.5mm	0.5

In Figure 2.10 [49], Alston first plotted the breakdown voltage to a base temperature, *T* (full curves), and then re-plotted it (dotted curve) as a function of a parameter *x*, which is proportional to the product of gas density and gap spacing (mm) and was defined by the equation:

$$x = \delta d \qquad ...(2.16)$$

This significant reduction in breakdown voltage with an increase in temperature as observed in Figure 2.10 [49] is in agreement with other literature [3]-[5], [6], [9], [42], [50]-[51]. It can be observed that the three voltage/temperature curves resulted in only one *V/x* curve which articulates that the breakdown voltage is a function of the parameter *x* alone.

2.2.2.2 Field experimental tests under AC voltages

In 1991, Robledo-Martinez *et al.* [9] sought to illustrate the practical significance of high temperatures and investigated the dielectric properties using a model transmission line which was subjected to fire conditions. He performed his experiments on a 70 kV AC model transmission line as illustrated in Figure 2.11 [9].

Robledo-Martinez *et al.* [9] cited several factors that could be attributed to the reduction in breakdown levels of air gaps in the presence of fire:

1) Ionization produced by the flame
2) solids carried by the convection currents associated with combustion,
3) the reduction in air density resulting from high temperatures and
4) a combination of these factors.

Results that were obtained from burning various fuels portrayed a significant reduction in breakdown levels in comparison with the experiments that were conducted in the absence of fire with a fixed height of 1.15 m and a conductor spacing of 12 cm. The reduction levels were found to be 49% for gas, 37% for sugarcane leaves, 29% for sugarcane bagasse and 27% for wood. As the withstand voltage gradient with no fire was recorded to be approximately 4.5 kV/cm, it thus means that the mean withstand voltage gradients were reduced to 2.3 kV/cm for gas, 2.8 kV/cm for sugarcane leaves, 3.2 kV/cm for sugarcane bagasse and 3.3 kV/cm for wood.

The study concluded that the most dangerous air insulation degradation factors were temperature and/or ionization.

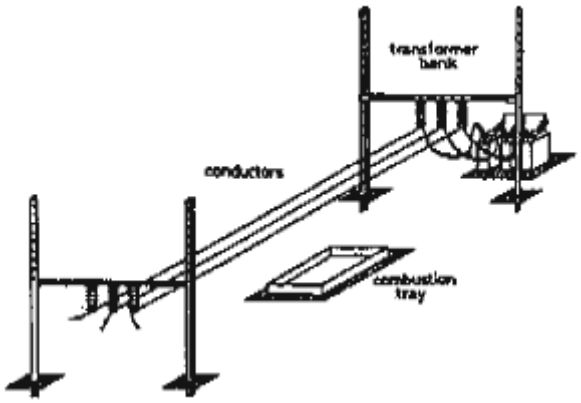

Figure 2.11 Experimental setup of a 70 kV AC model transmission line [9, pp. 2].

It was further indicated that during the combustion process, as a result of the solid particles that are released, these would play a significant role only with shorter spans between conductors. Additionally, this significance is also subject to physical properties such as the concentration and the size.

The 49% reduction in the breakdown level reported in [9] is in good agreement with [3] where a 50% reduction in breakdown voltage was observed for a gap spanned by the flame for the 15 mm – 30 mm air gap size. However, for larger air gaps (200 mm – 1000 mm) the reduction in breakdown voltage was of the order of 75%. The shape of the electrode was found to have played no role. The presence of floating particles in the air gap resulted in the reduction of breakdown voltage by between 20 – 30%, but the mechanism to breakdown remained the same (linear).

In [3] it was shown that the air density effect (reduction of) played a more prominent and significant role than the degree of ionization. Further, if a gap is completely engulfed in flames, due to the introduction of micrometric particles this would act to significantly reduce the level at which the air gap will breakdown. Such an observation is in agreement with the factors that were cited in [9] attributed to the reduction in voltage breakdown levels.

Sadurski *et al.* in [3] further made reference to important field observations that were made by Moreno [53] through experience in 1985. These observations were:

1) Maximum temperature in the flame: 800^0C – 900^0C,
2) temperature of the conductor: 60^0C – 80^0C and

3) temperature of the air near the conductor: 110^0C – 120^0C.

Fonseca *et al.* [5] in 1990 published a paper of tests under fire from sugar cane leaves performed in Brazil, in a 1m conductor-to-conductor and conductor-to-plane configurations with AC voltage stresses. The reported withstand voltage gradients were 2.5 kV/cm for an air gap at ambient temperature conditions (T_0 was taken to be 15^0C), 1.9 kV/cm & 1.7 kV/cm for an air gap temperature (air gap not spanned by flames) of 100^0C and 120^0C respectively. For a fire of sugar cane leaves, the withstand voltage gradient was reported to be 0.5 kV/cm. Air gap temperatures of 100^0C and 120^0C represent an equivalent 31% and 32% reduction in voltage breakdown levels respectively in comparison with breakdown at 15^0C. Further, spanning the air gap with fire made from sugar cane leaves represented an 80% reduction in breakdown levels. The voltage breakdown levels obtained by spanning the air gap with fire were observed to be significantly lower than when the fire did not span the air gap length.

The 80% obtained for an air gap spanned by a fire from sugar cane leaves is in close agreement with the 75% reduction reported in [3]. It is noted that the breakdown voltage is minimum when the gap is bridged by flames of sugar cane leaves. The significant presence of floating particles reaching the air gap resulted in the observation of the highest reduction [5] in voltage breakdown levels. This articulates findings reported in [3] and [9]. Fonseca *et al.* also recorded a temperature of 120^0C close to the flames which is similar to observations made in [3].

Table 2.1 The effect of floating particles on flashovers for various voltage level lines [55].

Nature of the Flame	Portion of Gap bridged	Line Voltage kV								
		400	275	220	132	88	66	44	32	22
Clean	100%	Y	N	N	N					
With Floating Particles	100%	Y	Y	Y	Y	Y	Y	Y	N	N
	80%	Y	Y	Y	Y	Y	N	N	N	N
	70%	Y	Y	Y	Y	N	N	N	N	N
	60%	Y	Y	N	N	N	N	N	N	N
	50%	N	N							

Sarduski [54] in 1977 conducted experiments with air gaps between live and earthed components and with flames spanning part and the total distance of the gaps. His experiment showed that with as little as 60% of the gap between the ground and the conductor of 400 kV

and 275 kV lines bridged by flames with particles, was sufficient for the line to experience a flashover [55]. These results are shown in Table 2.1. [55].

In Table 2.1 the areas indicated in red (Y areas) are those that resulted in a flashover. It is of interest to note that only a 400kV line with a clean flame experienced a flashover when the entire air gap was bridged by a flame.

2.2.2.3 Field experimental tests under DC voltages

Lanoie *et al.* [56] in Canada in 1987 conducted a study to investigate the characteristics of a bipolar ±450 kV DC model line exposed to burning trees and vegetation. This model line had a 13.7 m clearance at mid-span, a phase-to-phase (pole-to-pole) distance of 11.75 m and a 70m span length. Each pole consisted of a hollow aluminium tube, 4.4cm in diameter. The test line configuration is illustrated in Figure 2.12 [56]. This study represents the most practical experimental test setup done for a DC line.

Temperatures of the flame reached 1000^0C, which is equivalent to a relative air density of approximately 0.2. According to IEEE standards one would expect a 50% reduction in the efficiency of air insulation based on temperature effects alone but the test results obtained by Lanoie *et al.* yielded a figure of approximately 90%. Such a major reduction in voltage breakdown levels is in huge contrast to the literature that has been discussed in this particular section. This reduction in this study was to a certain extent attributed to the chemical characteristics of the flame, in addition to their thermal properties [56].

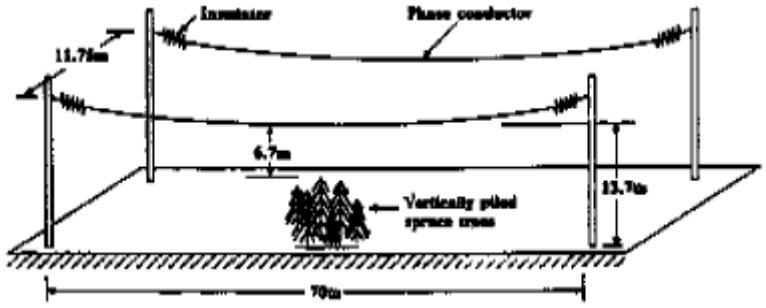

Figure 2.12 Experimental setup of a ±450 kV DC model transmission line [56].

2.2.3. Space charge influence and polarity effect

The space charge influence introduced in *Section 2.1.1.2(i)* plays a major role on the breakdown characteristics of air gaps, especially those that are characterized by a non-uniform electric field distribution, e.g. point-plane, point-point etc. This influence further portrays a dependency on the polarity of the applied voltage, and as such this section seeks to elaborate on this inter-dependency. Fundamentals of the space charge influence are first discussed in detail with reference to the influence on both the positive and negative polarity. To conclude the discussion, literature by a number of authors on the polarity effect is presented on prior experimental work and subsequent outcomes.

2.2.3.1 Fundamentals of the space charge influence

Using the point-plane electrode configuration illustrated in Figure 2.13(a) [21], [37] as a reference, the space charge influence on the breakdown voltage of an air gap with a positive polarity point is explained as follows [25], [37], [57]:

1. Electrons because of their higher mobility are readily drawn into the anode, leaving the positive space charge behind.
2. The space charge will cause a reduction in the field strength close to the anode and at the same time will increase the field further away from it.
3. The field distortion caused by the positive space charge is illustrated in Figure 2.13(b).
4. The high field region is in time moving further into the air gap, thus increasing or extending the region for ionization.
5. A cathode directed streamer will be initiated due to the high electric field strength which is on the tip of the space charge. This will ultimately lead to breakdown.

With reference to the negative point-plane electrode configuration illustrated in Figure 2.14(a); the space charge influence for this configuration is explained as follows [25], [37]:

1. Simplified, the space charge will build up on the negative point-plane gap and cause distortion of the electric field Fig. 2.14(b).
2. Various ionization stages will occur, resulting in the formation of ion clouds and ultimately the weakening of the field.
3. On the termination of the ionization processes, it may then become possible to start the formation of new avalanches.

4. Due to the doubling effect of the ion clouds, it is necessary to apply higher voltages to the air gap in order to achieve complete breakdown. This forms the basis for the explanation of why under negative DC voltages, higher voltage breakdown levels may be expected in comparison with positive DC voltages in highly inhomogeneous fields.

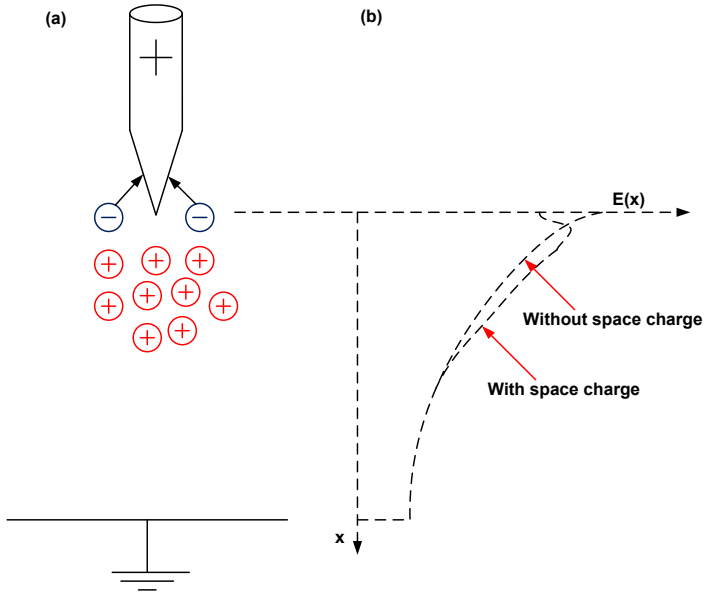

Figure 2.13 (a) Space charge build-up in positive point-plane gap.
(b) Field distortion by space charge [21], [37]

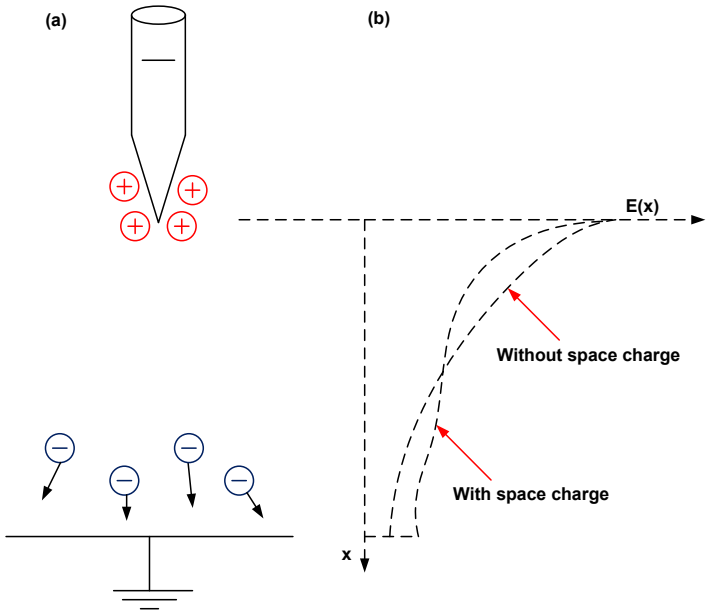

Figure 2.14 (a) Space charge build-up in negative point-plane gap.
(b) Field distortion by space charge [21], [37]

2.2.3.2 The polarity effect reviewed

Alston [49] in his 1958 paper observed that hot spots result in a very considerable lowering of flashover voltage in nearly uniform fields. He showed that breakdown values were higher on negative than on positive polarity for a 0.5 cm gap, confirming discussions in *Section 2.2.3.1*. Furthermore he conducted a test run with a 20 cm sphere and a 1000°C hot spot in the plate. He found that the polarity effect was reversed at a gap spacing of approximately 2.0 cm, positive breakdown values were higher at bigger gap spacings. This finding was in agreement with findings of *Broadbent et al.* [58] in which positive breakdown voltage values were higher than negative values, by an amount which varied with the gap spacing. Further, *Sletten et al.* [59] also recorded the same polarity effect for Trigatron gaps in which this was observed at an air gap spacing of 1.8 cm. However, *Alston et al.* further concluded that a hot spot can lower the breakdown voltage to a value approaching, but not smaller than that obtained by heating the whole gap. This effect decreases as the field departs from uniformity [49].

Tests conducted by *Hernandez-Avilla et al.* [60] in which DC breakdown in an air gap bridged by a flame was investigated, yielded opposite results to those obtained in [49]. It was observed that the electrode polarity influences the current levels of the discharge, this being the higher for positive voltages [60]. The theory of higher breakdown voltages for negative polarity was maintained. Furthermore, it was observed that the effective ionization follows the same overall behavior but the positive coefficients have higher values than the corresponding negative ones. The mean withstand voltage gradient recorded in this study under fire conditions was 2.5 kV/cm which is in agreement with [9] where a mean withstand voltage gradient of 2.3 kV/cm was observed.

CHAPTER 3

EXPERIMENTAL LAYOUT & PROCEDURES

All experimental work was conducted in the HVDC Centre laboratory in the Westville campus at the University of KwaZulu-Natal. Experimental results obtained in the laboratory were pivotal in the conduction of an in-depth comparative analysis of the phenomena governing breakdown of air gaps under both AC and DC applied voltages. This chapter presents a description of the experimental layout and procedures that were followed in obtaining the results discussed herein this report.

3.1. Laboratory facilities

The HVDC laboratory at UKZN has a two-stage Walton-Cockcroft HVDC generator with a maximum output voltage of +500 kV and –540 kV and a continuous output current of 7.5 mA. However, this generator set can only go up to ±300 kV due to height restrictions in the laboratory. The ripple factor at maximum load is less than 3% [61]. Figure 3.1 [61] illustrates the schematic of the generator.

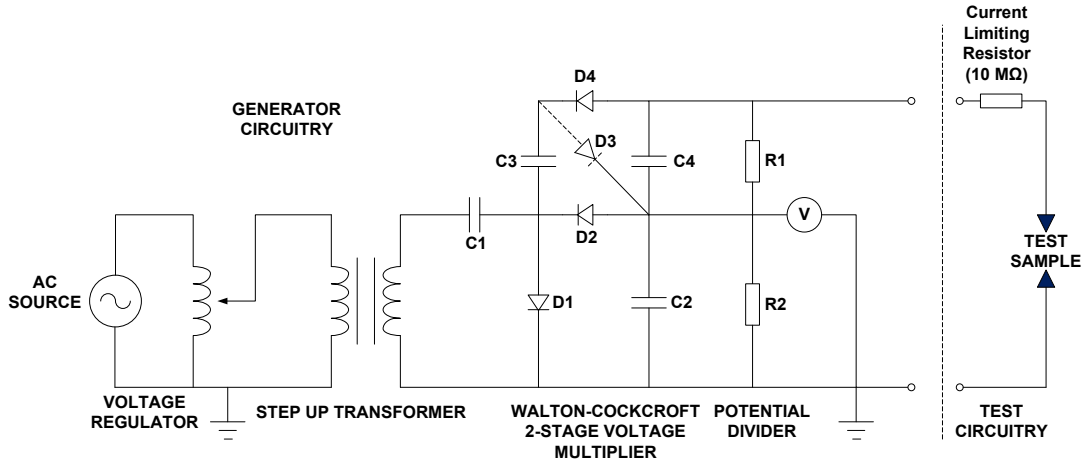

Figure 3.1 HVDC Centre Walton-Cockcroft ±533 kV DC generator
{Based on [61]}

Tests to investigate the effect of floating particles on the air gap breakdown level were conducted in a wooden shed as the soot could not be allowed to be dispersed throughout the HV laboratory. Thus a *Glassman HV* rack mount and fully enclosed 4 kW, ±125 kV DC generator set with a continuous current output of 30 mA was used to conduct the experiments. This generator has a ripple factor of 0.1% RMS of rated voltage at full load up to 125 kV and a -20^0C to $+50^0$C ambient temperature operating range. Figure 3.2 below illustrates the schematic of the front panel of this DC generator set.

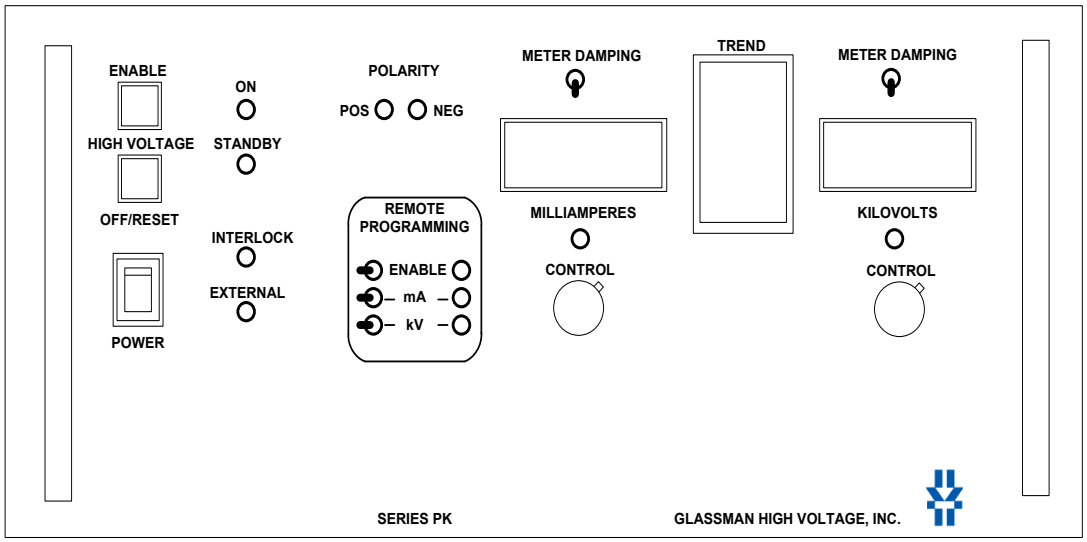

Figure 3.2 Glassman HV front panel of rack-mount ±125 kV, 4 kW DC generator power supply {Based on [62]}

3.2. Test setup and design

The tests were conducted with a rod-rod air gap configuration with one electrode energized to either positive or negative DC voltage and the other earthed. The experimental setup is illustrated in Figure 3.3.

3.2.1 High air gap temperature tests

For smaller air gaps (10 mm – 150 mm) the gas burner used was of the annular type, however this became inadequate for larger air gaps, hence for gaps in the 200 mm – 500 mm range, an 800 mm long, longitudinal gas burner was used to adequately induce the required heat levels along the entire length of the air gap.

This was setup in the laboratory so as to create a controlled environment as opposed to outdoors where conditions vary daily thus making it difficult to obtain consistent or near-consistent results. Furthermore, it would have been extremely difficult to induce the required temperatures in the air gap as the wind speeds vary throughout the day.

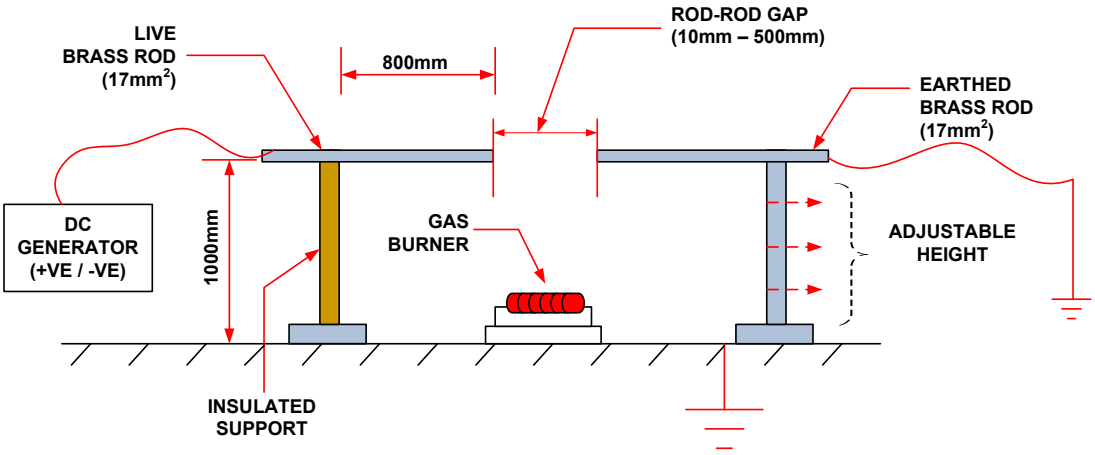

Figure 3.3 Experimental setup of the air gap configuration

3.2.2 Particle tests

To introduce particles into the air gap, a mesh wire rack had to be made and this is illustrated in Figure 3.4. This was made of a steel top basin, 100 cm (L) x 20 cm (H) in size. The bottom of the rack was made of a 30 cm width micro-mesh wire sieve so that it could be able to carry the ash particles of the saw dust. These would then be carried up into the air gap by the natural upward direction of the heat convection from the gas burner. However, the experimental results obtained from this experimental setup were found to be highly inconsistent and thus ultimately inconclusive. This setup had the following shortfalls:

1. The particles carried by the upward convection of the fire stream were inadequate to effect any significant introduction of particles in the air gap. This at times resulted in sample readings that were evidently only due to the effect of only the increased temperature in the air gap and not the combined effect of particles as well.
2. The amount of particles introduced in the air gap would vary greatly and thus affect the breakdown voltages obtained.

This resulted in this particular experimental setup to be abandoned and a more effective manner of introducing particles in the air gap had to be sought. This culminated in the design

of the experimental setup illustrated in Figure 3.5. Critical aspects of the experimental setup that could not be achieved previously with the setup shown in Figure 3.4 were corrected in the latter experimental setup.

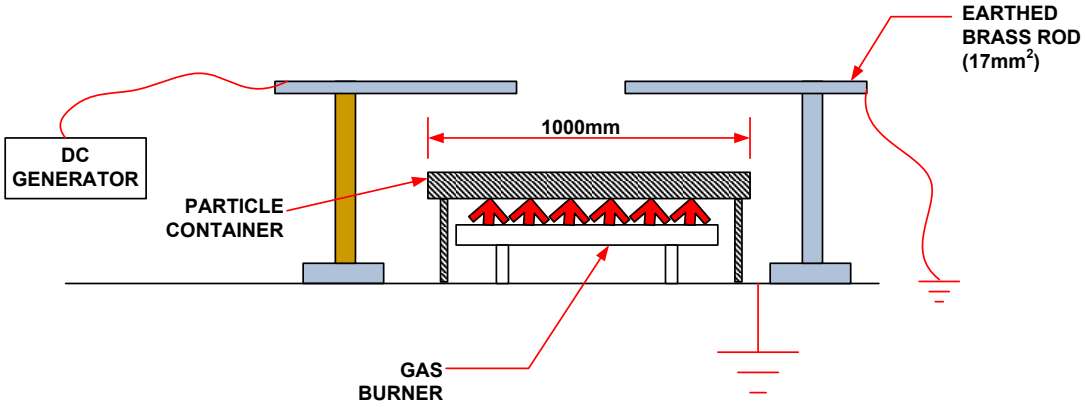

Figure 3.4 Initial particle tests setup

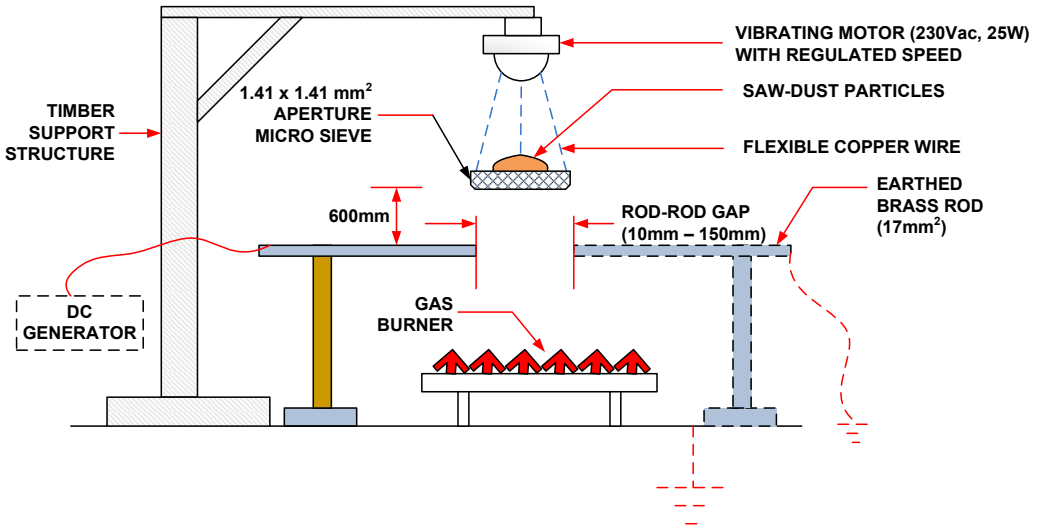

Figure 3.5 Experimental setup used for particle tests

In this experimental setup, a speed regulated vibrating motor was used to generate vibrations on a micro sieve comprising of apertures with an area of *1.41* x *1.41mm*^{2} that carried saw-dust particles. A combination of this vibrating mechanism and the upward convection of the fire stream enabled a constant introduction of particles in the air gap. The motor generated a rotating motion parallel to the ground which stirred the particles in the sieve and they would be lifted off the surface on an upward direction and then come back down vertically on gravitational force into the air gap. Further particles would land on the gas burner, and get burnt before moving up into the air gap as ash as a result of the upward convection of the fire

stream. The exact rate of the supply (m^3/s) of the particles into the air gap was not quantified as this would have involved a series of mathematical models to incorporate the various experimental influences on the final number of particles that make it to the air gap and their relative speed and direction.

As the speed of the vibrating motor could be regulated, the amount of particles introduced in the air gap could therefore be controlled as well. This eliminated possible errors as contemplated in the former experimental setup as discussed earlier in this section.

3.3. Experimental procedures

Rods that were used were made of steel and of 17 mm^2 square-cut size. These were erected and supported as per Figure 3.3. Only the gap size was varied for the tests, the distance from the flame base to the air gap was fixed at 60.5 cm for reasons elaborated on further on in this paragraph. The target temperature range was 100^0C – 150^0C to obtain results that were closely aligned with practical findings reported on in [3] and [5].

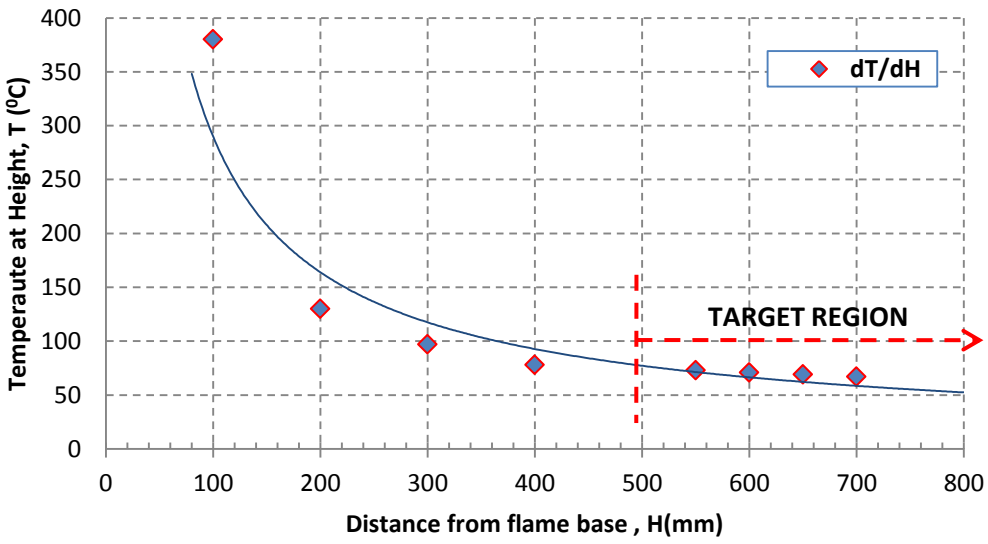

Figure 3.6 Gas burner temperature profile indicating temperature measurement target region

A thermocouple temperature probe (Type K) was used to measure the temperature in the air gap. It was, however, imperative to ensure that temperature measurements were taken in the region where the rate of change of the temperature (T) with the height (h) from the base of the gas burner (dT/dh) was reasonably low, i.e. ≈ constant. A number of these readings were taken and Figure 3.6 illustrates a typical temperature profile plot clearly indicating the region in which it was observed reasonable to obtain temperature readings. Thus the fore-mentioned

height was selected bearing in mind the latter statement. Additionally, careful consideration had to be taken so that the air gap was placed at an optimum height that will enable the induction of the required temperature levels in the air gap.

For each of the temperatures, prior to the application of the voltage; the air gap temperature would be measured, and once again after the measurement to ascertain that there had been no significant variation in the temperature in the air gap. The maximum allowable temperature variation between the two temperature readings was $\pm 5^0$C, if this limit was breached the measurement would be discarded.

With the air gap fixed, the voltage would be raised until breakdown occurred. This would be repeated 5 times to obtain an average breakdown voltage for that specific temperature in the air gap. A flame was introduced into the air gap (but not bridging the air gap) to vary the temperature. As a precaution to ensure that the generator set operating conditions were being maintained, ambient temperature readings were also always noted before, during and after the tests.

In addition to the procedures discussed above, there were further steps that were incorporated when tests with particles were conducted. These include:

1. The cleaning of the brass electrodes between each successive sample reading. This was done so as to ensure that the soot particles that settle on the rods did not influence the breakdown behavior of the air gap due to the possible introduction of a number of particles which may distort the field between the brass electrodes. Furthermore, such an effect would have been more significant at smaller air gaps as the accumulation of these particles could possibly have acted as an “extension” of the rod thus advertently reducing the air gap length which would reduce the breakdown voltage. This effect may however had been regarded as negligible in the greater scheme of the experimental results. Nonetheless, as far as it was reasonably practicable; necessary precautions needed to be taken to preserve the consistency and integrity of the results obtained.
2. Prior to varying the gap length, the amount of particles (mass) in the sieve would be measured using a marked beaker to ensure that the amount of particles introduced in the air gap did not vary. Depending on the weight carried by the sieve, the resulting vibrations would vary accordingly, i.e. for a smaller weight, there are greater vibrations, and thus more particles are stirred and carried into the air gap even when the speed of the motor remains constant.

Figure 3.7 Gas mask used for particle tests [63]

Furthermore, due to the associated health risk of dust and millimetric particles being continuously present in the room, it was essential that the tests were conducted while a gas mask was worn to minimize the risk of harmful exposure such as inhalation and the ingress of foreign particles into the eyes. The mask that was used for this purpose is shown in Figure 3.7 [63].

CHAPTER 4

EXPERIMENTAL RESULTS AND DISCUSSION

In this chapter all work carried out on the breakdown characteristics of a rod-rod air gap configuration under DC applied voltage will be presented for both the negative and positive polarities. Experimental results obtained will be comparatively analyzed with previous work which has been discussed in earlier chapters.

4.1. Breakdown at high temperatures

4.1.1. Small air gaps [10 mm – 150 mm]

4.1.1.1. Positive polarity

Presented in Figure 4.1 are breakdown voltage results as a function of the air gap size (10 mm – 150 mm) for temperatures up to 300°C for the positive polarity. It is shown that breakdown characteristics illustrate a linear relationship with the air gap spacing. This relationship is observed over the entire temperature range. It must however be noted that even with an increase in the air gap temperature, this linear dependence is preserved, but at higher temperatures air gaps breakdown at lower voltages than they normally would in ambient temperature conditions. This is in agreement with observations discussed in *Section 2.2* under both the positive and negative DC and AC applied voltages.

The maximum withstand voltage gradient as illustrated in Figure 4.2 is 4.5 kV/cm obtained at 32^0C (ambient temperature conditions without fire). This value is in direct agreement with the value of 4.5 kV/cm value obtained by *Fonseca et. al*.[5] as discussed in *Section 2.2.1.1* obtained under an AC applied voltage. The median of the mean withstand voltage gradient as discussed in *Section 2.2.1.1* under AC was reported as 3.5 kV/cm, this is 22% lower than the value of 4.5 kV/cm reported on in this section. The experimental results obtained under positive DC applied voltages at room temperature represent an approximate increase of a quarter $(1/4)$ in the withstand voltage gradient when compared with that discussed in literature presented in earlier sections.

In *Section 2.2.1.2,* the median of mean withstand voltage gradients observed under positive and negative DC applied voltages (for various authors at room temperature) was reported as

4.3 kV/cm and 4.7 kV/cm respectively. This further indicates an agreement with experimental results obtained herein and this represents a 4% increment and a 4% decrement deviation from the positive and negative DC breakdown voltages respectively as discussed in the literature surveyed.

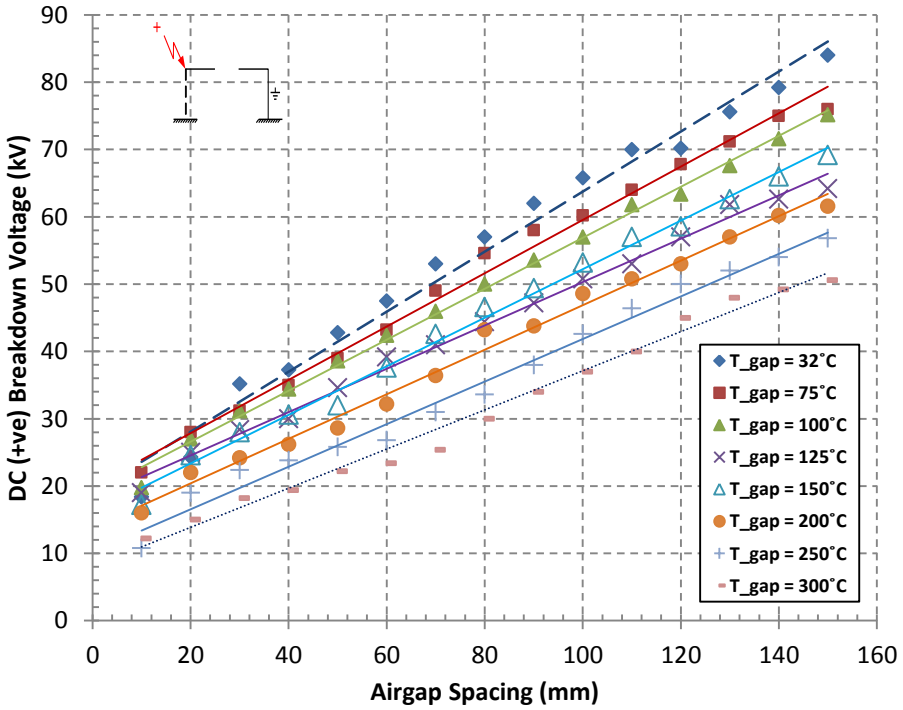

Figure 4.1 Positive DC voltage breakdown characteristics at high temperatures for small air gaps

This reaffirms what was discussed in *Section 2.2.1.2*, that air gaps at ambient temperature conditions under negative DC applied voltages have a higher dielectric strength when compared with an equivalent air gap size subjected to positive DC voltage stresses.

The minimum withstand voltage gradient observed in Figure 4.2 is 2.9 kV/cm at an air gap temperature of 300^0C. This means that the equivalent reduction in the withstand voltage gradient is approximately 55% from ambient temperature conditions to 300^0C. This advertently means that the dielectric strength of an air gap at 300^0C is reduced to a value just below half of what it would have been at STP conditions which is quite significant. This is in good agreement with results obtained by *Robledo-Martinez et al* [9] as discussed in *Section 2.2.2.2* where a reduction of 49% (withstand gradient of 2.3 kV/cm) was observed in the breakdown voltage using gas as a fuel to generate fire under an AC applied voltage.

Figure 4.3 illustrates the reduction in breakdown voltage as a function of air gap temperature for specific air gap lengths. The breakdown voltage from ambient temperature conditions to

300°C is reduced by a maximum of 51%; this is observed on the 60 mm and 80 mm air gaps. This reduction is in agreement with that observed in [3] and [9] discussed in *Section 2.2.2*. At an air gap spacing of 120 mm, the least reduction in breakdown levels was observed, this was found to be approximately 32%. Over the entire 10 mm – 150 mm air gap range, the average reduction in the breakdown voltage was observed to be 46%, which is considerably high. A further observation is the pronounced linear behavior of the reduction in breakdown voltage with an increase in temperature over this air gap range

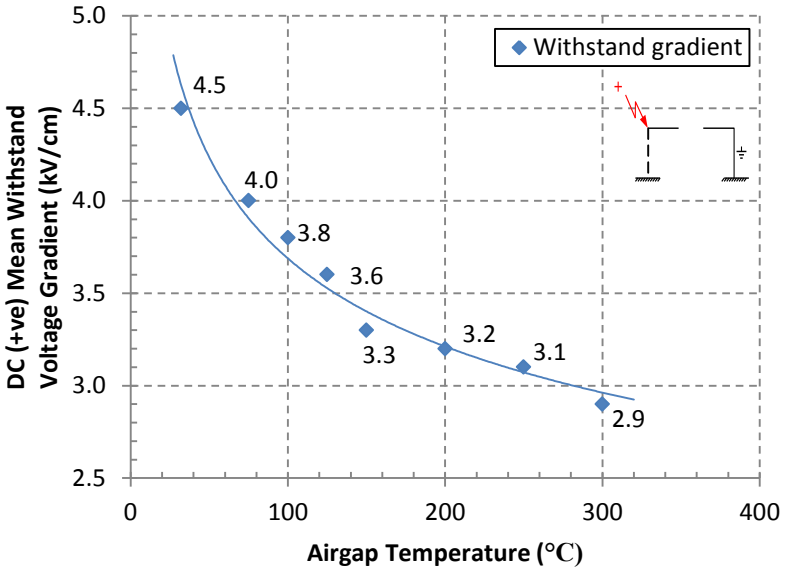

Figure 4.2. Positive DC mean withstand voltage gradient as a function of air gap temperature for small air gaps.

In Figure 4.4 a *V/x* (*x* as defined in *Equation 2.16*) plot is illustrated of the experimental results as discussed above. It is observed from Figure 4.4 that the *V/x* curve takes the form of a logistic curve of the form:

$$f(x) = \frac{c}{1+a.e^{-bx}} \qquad ...(4.1.)$$

Where,

a, b and *c* are constants derived from the data.

It further follows that experimental results illustrated in Figure 4.4 are in agreement with Alston's [49] observation that the breakdown voltage is a function of the parameter *x* alone. However, the validity of the latter statement is assumed to be limited only to the experimental work done as part of this study.

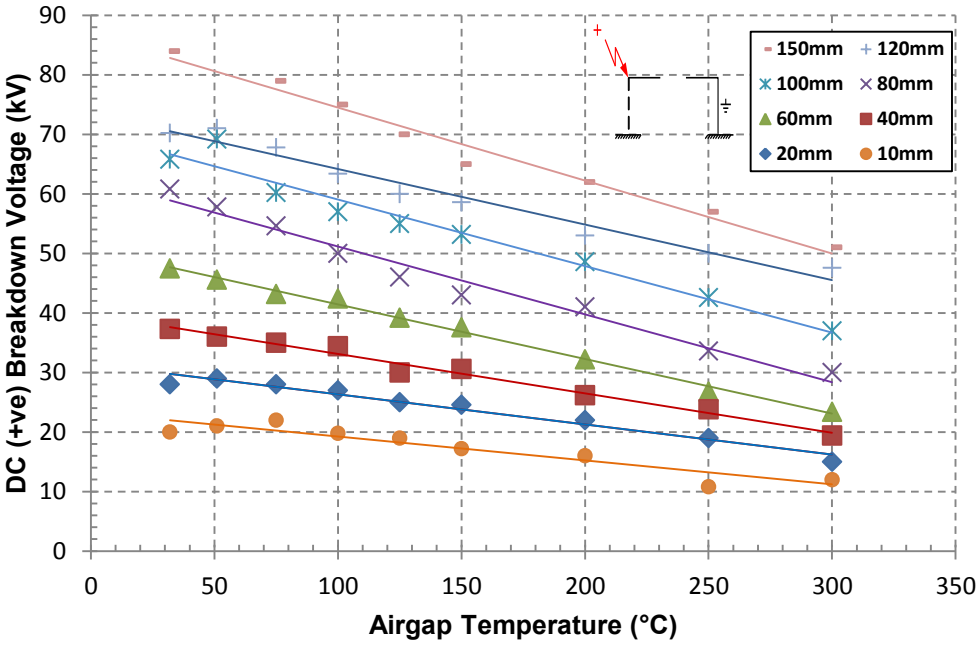

Figure 4.3 Temperature effect on positive DC breakdown voltage characteristics for small air gaps.

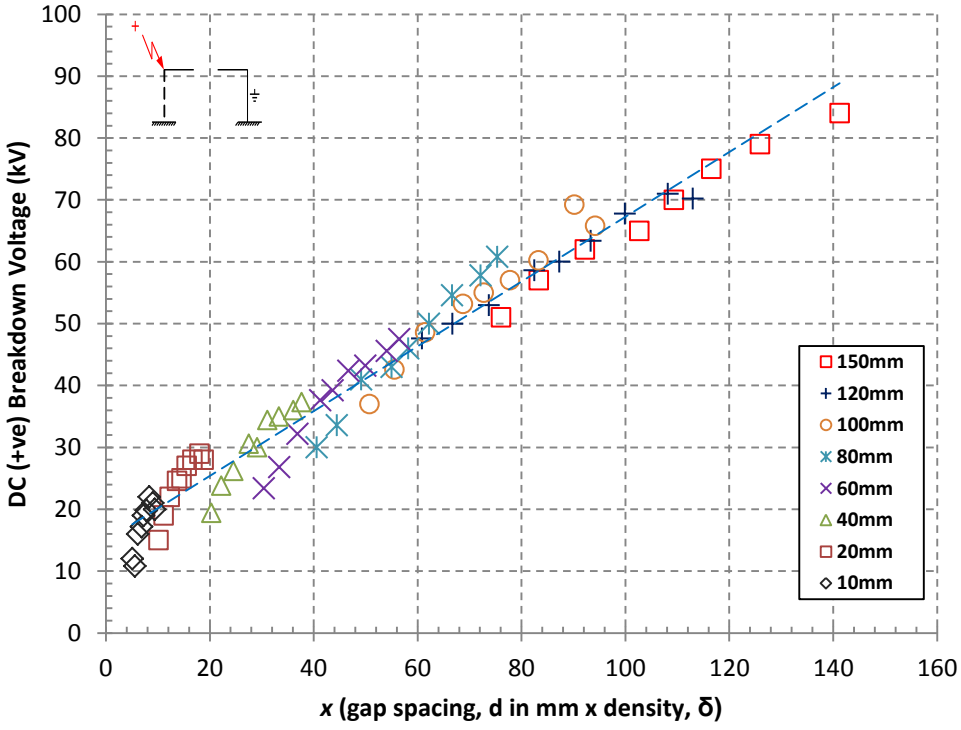

Figure 4.4 *V/x* curve illustrating the temperature effect on positive DC breakdown voltage characteristics for small air gaps.

4.1.1.2. Negative polarity

Observations from Figure 4.5. illustrate that a linear relationship exists between the breakdown voltage and the air gap spacing, a similar observation was made under positive DC applied voltages discussed in *Section 4.1.1.1* above. This relationship is also observed over the entire temperature range. Similarly, at higher temperatures air gaps breakdown at lower voltages than they normally would in ambient temperature conditions. This is in agreement with observations discussed in *Section 2.2.2* under both positive and negative DC and AC applied voltages.

The maximum withstand voltage gradient illustrated in Figure 4.6 is 5.1 kV/cm obtained at 25^0C (ambient temperature conditions without fire) and it is in close agreement with [47] and [45] discussed in *Section 2.2.1.2* in which a value of 5.7 kV/cm was obtained. Further in *Section 2.2.1.2,* the median of mean withstand voltage gradients observed under negative DC applied voltages (for various authors) was reported as 4.7 kV/cm; this represents an ≈ 20% variation between the withstand voltage gradients. The result obtained herein is ≈ 13% higher than that observed under positive DC applied voltages which is presented in *Section 4.1.1.1*. A higher dielectric strength under negative DC applied voltages is further confirmed at ambient temperature conditions. This can be explained by the space charge effect which becomes notable in air gaps with trenchantly asymmetrical electric fields as discussed in *Section 2.2.3.1*.Similar observations were also presented in *Section 2.2.1.2*.

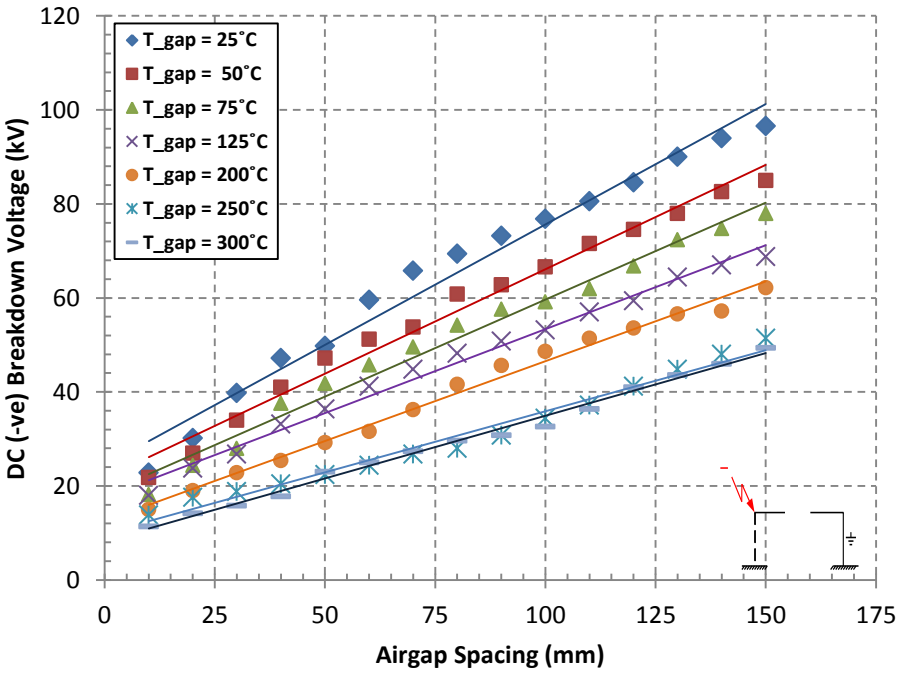

Figure 4.5 Negative DC voltage breakdown characteristics

at high temperatures for small air gaps

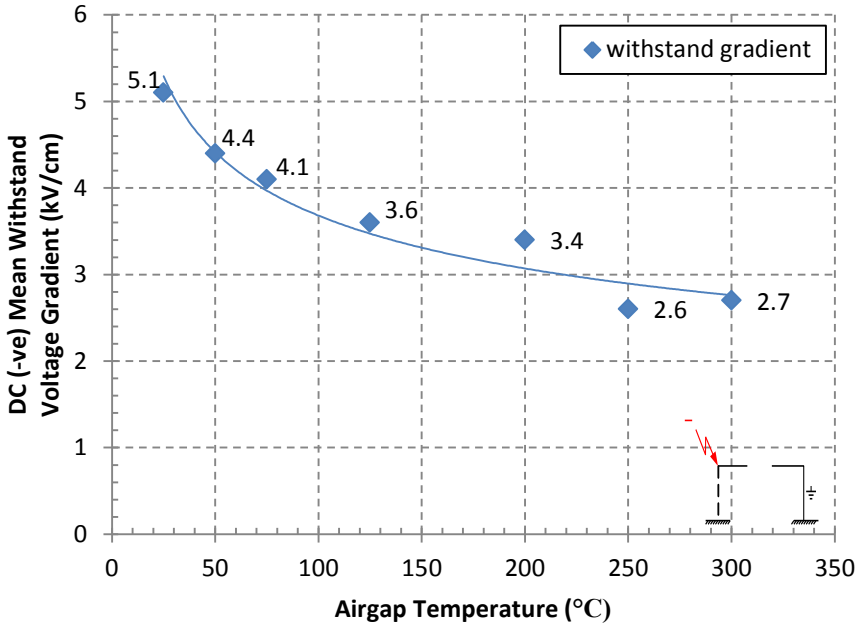

Figure 4.6 Negative DC mean withstand voltage gradient as a function of air gap temperature for small air gaps

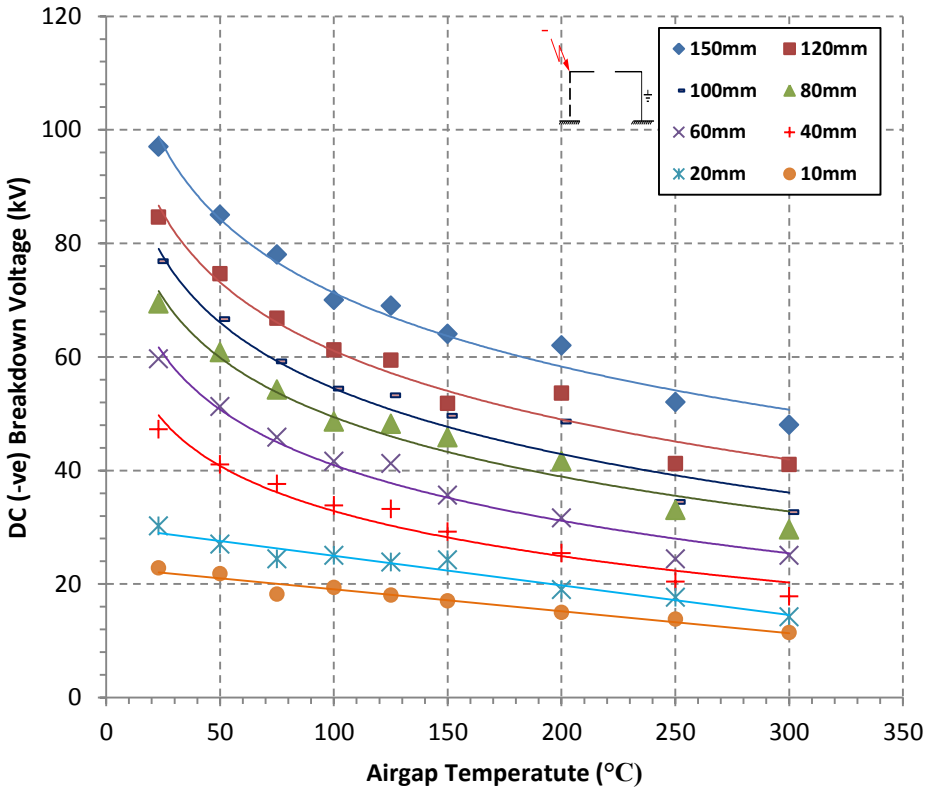

Figure 4.7 Temperature effect on negative DC breakdown characteristics for small air gaps

The minimum withstand voltage gradient observed in Figure 4.6 is 2.6 kV/cm. This is an equivalent 51% reduction in the withstand voltage gradient from the 5.1 kV/cm discussed above. It further follows that as also observed under positive DC polarities (*Section 4.1.1.1);* the dielectric strength of an air gap at 300^0C is reduced to a value just below half of what it would have been at STP conditions. Over the 20 – 300^0C temperature range, the negative polarity portrays a lesser degree of dielectric deterioration by 7% as compared to the equivalent positive polarity. The space charge effect may still be assumed to play a role in the level of breakdown voltage observed under both the positive and negative DC applied voltages.

Figure 4.7 illustrates the reduction in breakdown voltage as a function of air gap temperature for specific air gap lengths under negative DC applied voltages. The breakdown voltage from ambient temperature conditions to 300°C is reduced by a maximum of 50%; this is observed in the 10 mm air gap. This reduction is in agreement with that observed in [3] and [9] discussed in *Section 2.2.2.2*. An average of 47% reduction in breakdown levels is observed, the least value obtained was 42%.

The behaviour between the air gap temperatures and the breakdown voltage observed for the negative polarity is logarithmic as opposed to being linear which was observed in under positive polarity. The negative breakdown voltage plots deviate from this linearity for air gaps greater than 20 mm.

It can further be noted that for the air gap range of 40 mm – 150 mm, a significant reduction in the breakdown voltage is observed for temperatures up to 100°C. This logarithmic behavior of the breakdown voltage as observed in Figure 4.7 for the negative polarity suggests a vulnerability of negatively charged poles under increased temperature conditions up to 100^0C. This behavior is in agreement with results obtained by Alston [49] and discussed in *Section 2.2.3.2*.

Figure 4.8 further illustrates a *V/x* (dotted curve) curve of the experimental results as discussed in *Section 2.2.2.1.* Experimental results illustrated are in agreement with Alston's [49] observation that the breakdown voltage may be assumed to be a function of the parameter *x* alone. Nevertheless it is interesting to note that the scatter the of data shown in Figure 4.8 of the *V/x* curve portrays a greater deviation when compared to the scatter observed under the positive polarity. However, beyond this observation it is further noted that this scatter is more pronounced at air gaps below 100 mm for both the negative and

positive DC polarities. This can be attributed to the logarithmic behaviour of negative breakdown voltage with an increase in temperature as discussed in this section.

This behaviour suggests that with an increase in temperature and air gap spacing, values obtained from the *V/x* curve for the negative polarity would remain higher than the equivalent positive polarity values. This translates to a higher dielectric strength under negative polarity than the equivalent positive polarity.

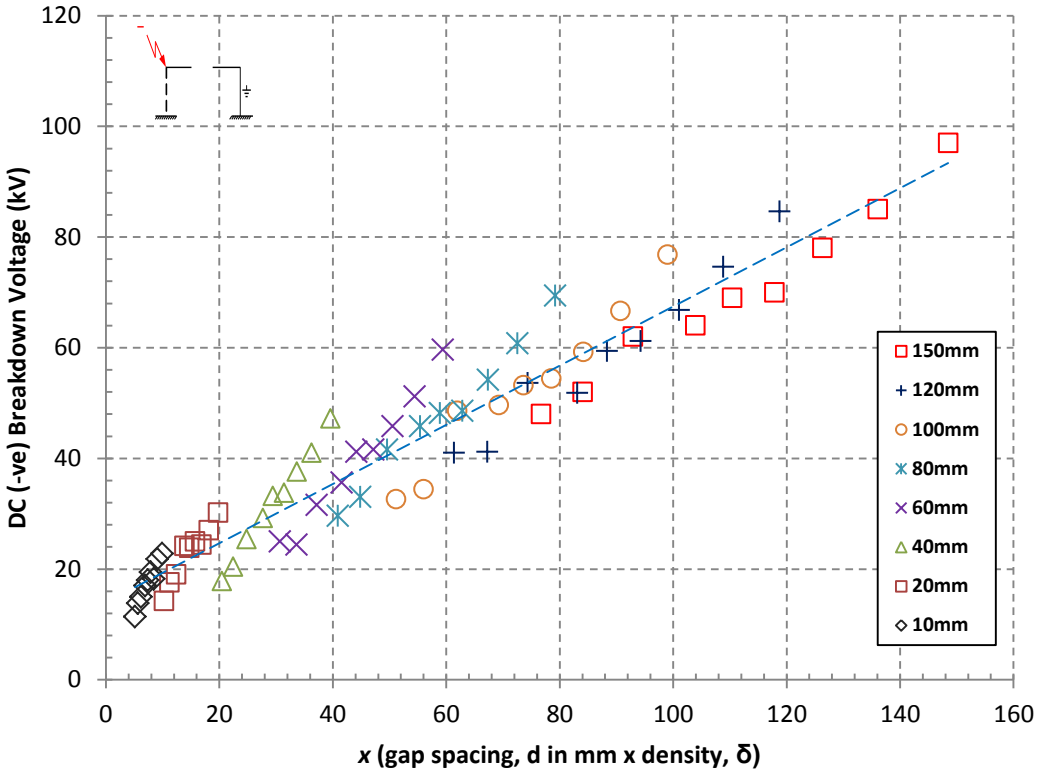

Figure 4.8. *V/x* curve illustrating temperature effect on negative DC breakdown characteristics for small air gaps

4.1.2. Large air gaps [200 mm – 500 mm]

4.1.2.1. Positive polarity

Figure 4.9. illustrates that a linear relationship exists between the breakdown voltage and the air gap spacing for large air gaps, a similar observation was made under both the positive and negative DC applied voltages discussed in *Section 4.1.1.1* and further in *Section 4.1.1.2* above. As already discussed, at higher temperatures air gaps breakdown at lower voltages than they normally would under ambient temperature conditions as elaborated on in *Section*

2.2.2. This is in agreement with observations discussed in *Section 4.1.1* and *4.1.2* under both the positive and negative DC and AC applied voltages.

The maximum withstand voltage gradient illustrated in Figure 4.10. is 5.7 kV/cm obtained at 24^0C (ambient temperature conditions without fire) and this is in direct agreement with [47] and [45] discussed in *Section 2.2.1.2* under negative polarity, in which a value of 5.7 kV/cm was also obtained. However, a value of 5.3 kV/cm is reported by Allen *et al.* [46] and Lowke [47] under the positive polarity, this is a variation of approximately 7.5% which is not that significant. The result obtained herein is ≈ 26% higher than that observed under the positive DC applied voltages for small air gaps, which is presented in *Section 4.1.1.1*.

The minimum withstand voltage gradient observed in Figure 4.10 is 5.1 kV/cm. This is an equivalent 12% reduction in the withstand voltage from ambient temperature conditions to 150^0C.

From Figure 4.11 it is observed that the relationship between the breakdown voltage and the air gap temperature initially portrays a higher voltage gradient in the 25^0C – 50^0C temperature range. This suggests a high dielectric strength loss of the air gap in this range. However, in the 50^0C – 150^0C range a more gradual, linear reduction in the breakdown voltage with an increase in temperature is evident.

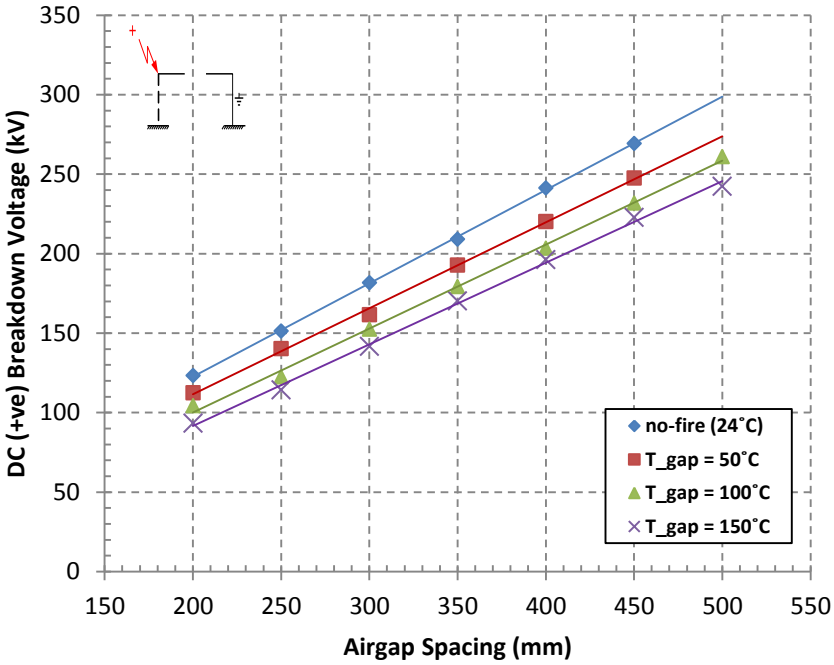

Figure 4.9 Positive DC voltage breakdown characteristics at high temperatures for large air gaps.

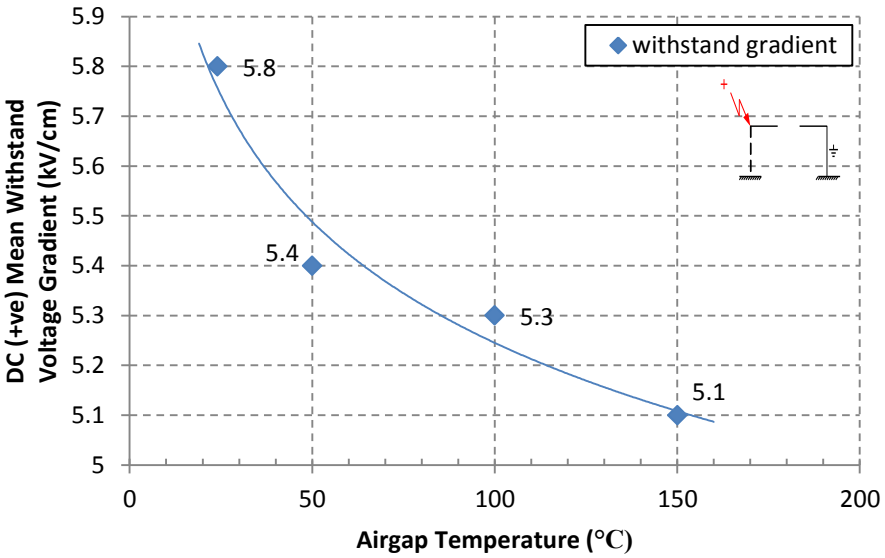

Figure 4.10 Positive DC mean withstand voltage gradient as a function of air gap temperature for large air gaps.

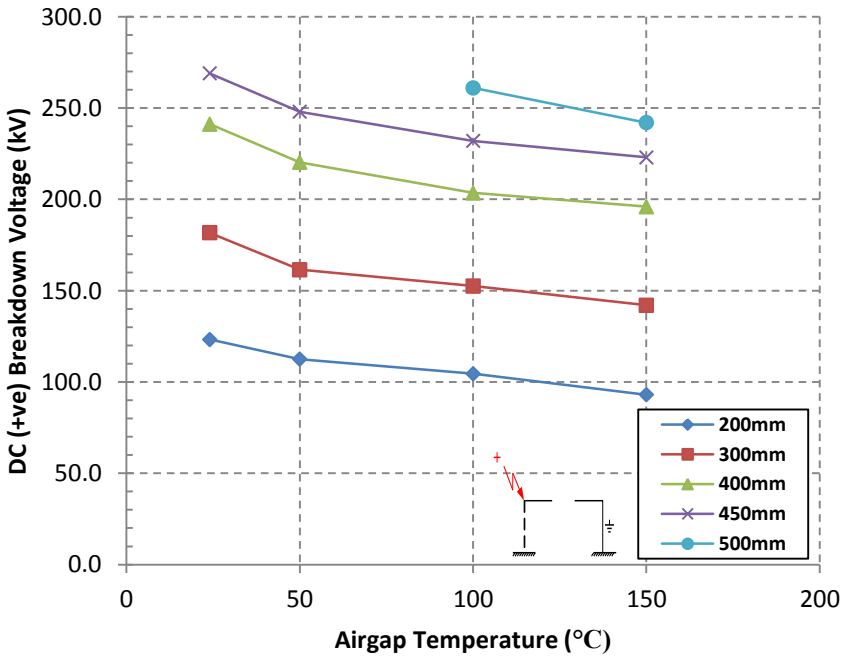

Figure 4.11 Temperature effect on positive DC breakdown characteristics for large air gaps

4.1.2.2. Negative polarity

Observations from Figure 4.12 also illustrate that a linear relationship exists between the breakdown voltage and the air gap spacing, an observation that has been made for both positive and negative DC applied voltages for small air gaps and also for large air gaps discussed in *Section 4.1.2.1* above. This relationship is also observed over the entire temperature range. Higher temperatures for air gaps also result in lower breakdown voltage levels than those observed under normal ambient temperature conditions. This is in agreement with observations discussed in *Section 2.2* under both the positive and negative DC and AC applied voltages.

The maximum observed withstand voltage gradient illustrated in Figure 4.13 is 6.0 kV/cm obtained at 24^0C (ambient temperature conditions without fire). This is in close agreement with [47] and [45] discussed in *Section 2.2.1.2* in which a value of 5.7 kV/cm was obtained. In *Section 4.1.2.1* a value of 5.7 kV was reported under no fire conditions under the positive polarity, which is ≈ 5% lower than the value obtained herein. A higher dielectric strength under negative DC applied voltages is further confirmed at ambient temperature conditions.

The minimum withstand voltage gradient observed in Figure 4.13 is 5.1 kV/cm. This is an equivalent 15% reduction in the withstand voltage gradient. A similar observation under positive DC polarity (*Section 4.1.1.1)* was witnessed.

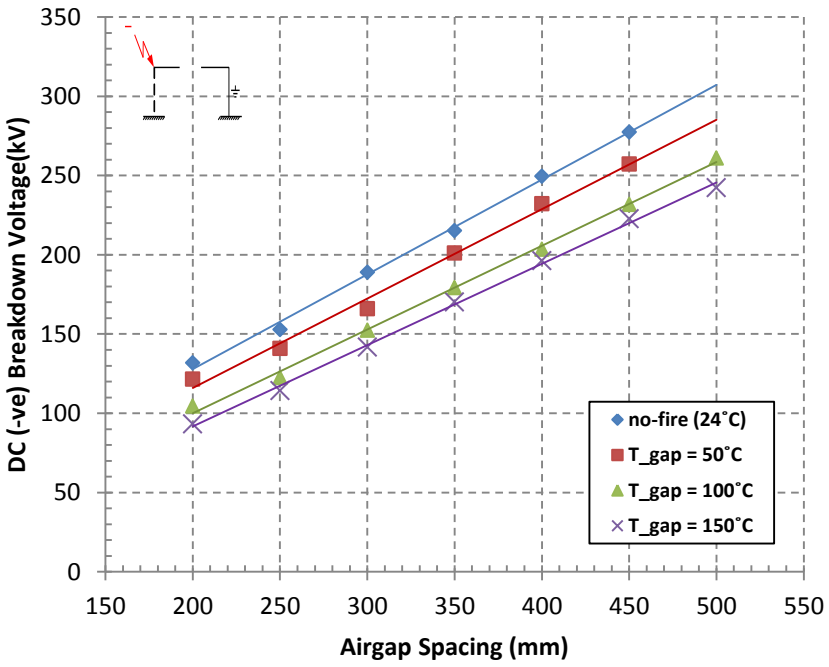

Figure 4.12 Negative DC voltage breakdown characteristics at high temperatures for large air gaps

However for large air gaps the reduction in breakdown voltage is 25% higher under the negative polarity when compared to the equivalent positive polarity. Throughout the experimental results discussed in earlier sections, there had not been such an observation.

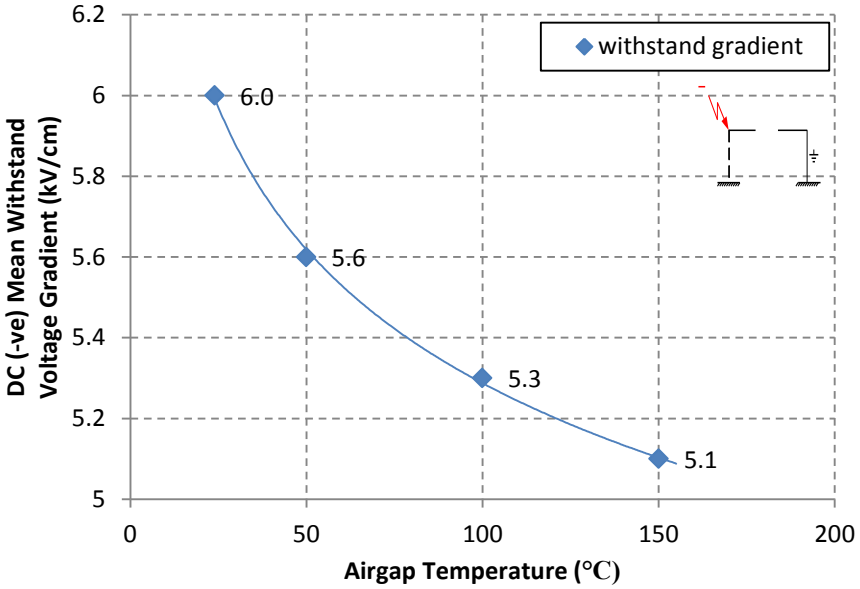

Figure 4.13 Negative DC mean withstand voltage gradient as a function of air gap temperature for large air gaps

As shown in Figure 4.14, it is evident that an almost similar behavioural pattern under negative DC applied voltages was observed as witnessed under the positive polarity.

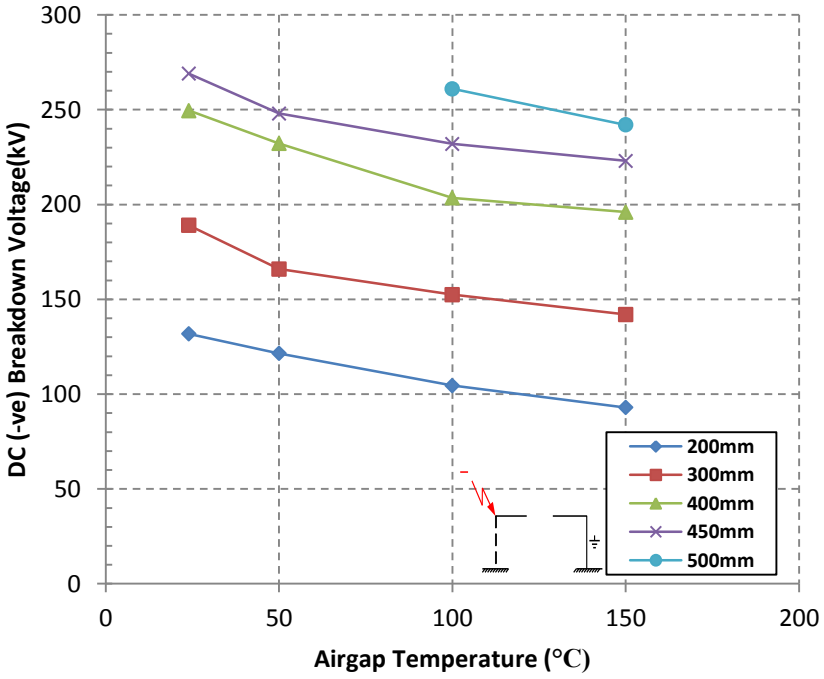

Figure 4.14 Temperature effect on negative DC breakdown characteristics for large air gaps

It is further confirmed that higher air gap temperatures result in lower breakdown voltage levels. However it is noted that for large air gaps, the reduction in air gap breakdown voltage observed was found to be higher in the negative polarity than in the positive polarity.

4.2. Effect of particles at high temperatures

The effect of particles was investigated for small air gaps up to a temperature of 200^0C and the results obtained are presented herein. The experimental setup for the introduction of particles into the air gap is discussed in detail in *Section 3.2.2*.

4.2.1. Positive Polarity

Figure 4.15 illustrates breakdown voltage results as a function of the air gap size (10mm-150mm) for temperatures up to 200°C for the positive polarity subjected to particles introduced into the air gap. It is shown that breakdown characteristics illustrate a linear relationship with the air gap spacing. This relationship is observed over the entire temperature range and the linear dependence is preserved. As already observed, at higher temperatures air gaps breakdown at lower voltages then they normally would in ambient temperature conditions. This is in agreement with observations discussed in *Section 2.2* and *4.1* under both the positive and negative DC and AC applied voltages.

The minimum withstand voltage gradient observed in Figure 4.17. is 3.1 kV/cm at an air gap temperature of 200^0C. This means that the equivalent reduction in the withstand voltage gradient is approximately 31% from ambient temperature conditions to 200^0C. While the withstand voltage gradient at the same temperature without particles was reported to be 3.2 kV/cm in *Section 4.1.1.1*, which is 4% higher than the latter value. This means that the dielectric strength of an air gap at high temperatures is further deteriorated by the presence of particles in the air gap. Although not quantified, *Robledo-Martinez et al.*[9] as discussed in *Section 2.2.2.2* acknowledged the role of solid particles on the breakdown voltage depending on their size and concentration.

4.2.2. Negative Polarity

Figure 4.18 illustrates breakdown voltage results as a function of the air gap size (10 mm – 150 mm) for temperatures up to 200°C for the negative polarity subjected to particles

introduced into the air gap. It is shown that breakdown characteristics illustrate a linear relationship with the air gap spacing. This relationship is observed over the entire temperature range and the linear dependence is preserved. As already observed, at higher temperatures air gaps breakdown at lower voltages as they normally would under ambient temperature conditions. This is in agreement with observations discussed in *Section 2.2* and *4.1* under both the positive and negative DC and AC applied voltages.

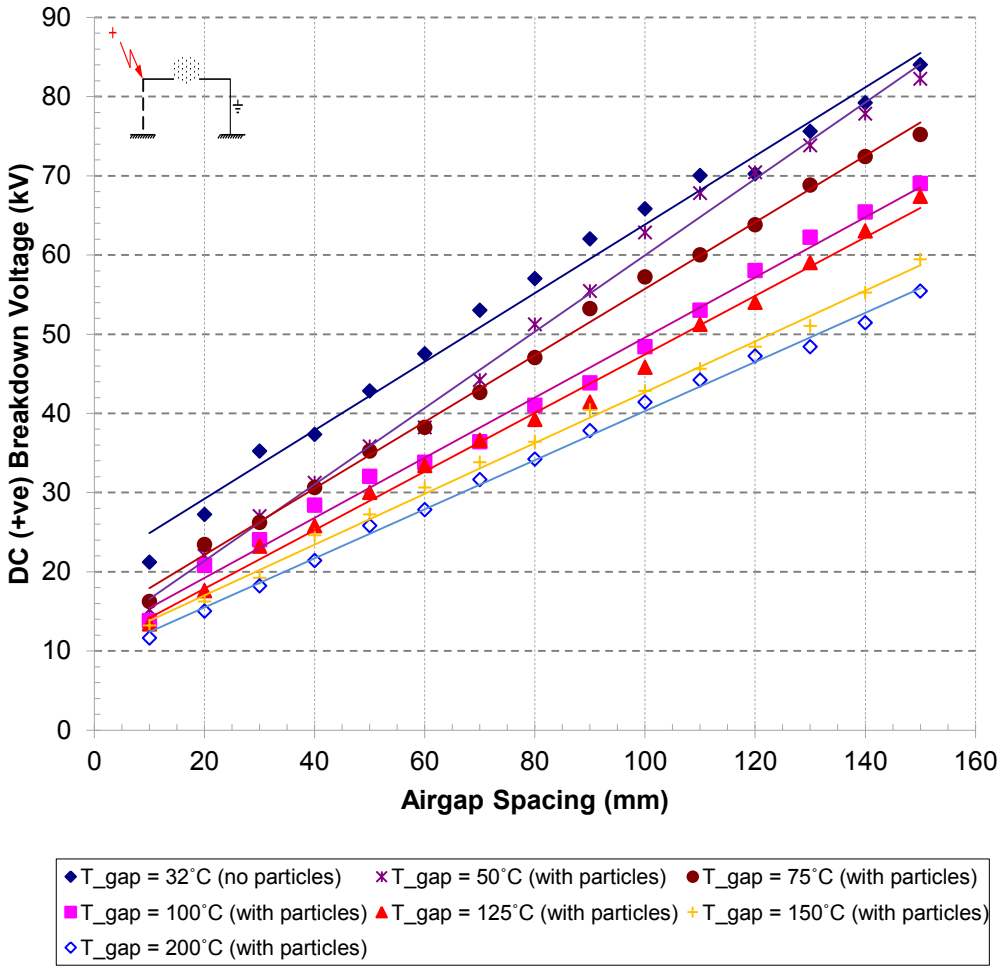

Figure 4.15 Positive DC voltage breakdown characteristics at high temperatures for small air gaps with particles

The minimum withstand voltage gradient observed in Figure 4.20 is 3.4 kV/cm at an air gap temperature of 200^0C. This means that the equivalent reduction in the withstand voltage gradient is approximately 33% from ambient temperature conditions to 200^0C. While the withstand voltage gradient at the same temperature without particles was also reported to be 3.4 kV/cm in *Section 4.1.1.1*. This means that the dielectric strength of such an air gap at high temperatures was not affected by the presence of particles in the air gap. This observation seem to re-iterate the finding of *Robledo-Martinez et al.*[9] as discussed in

Section 2.2.2.2 in which the role of solid particles on the breakdown voltage is dependent on their size and concentration.

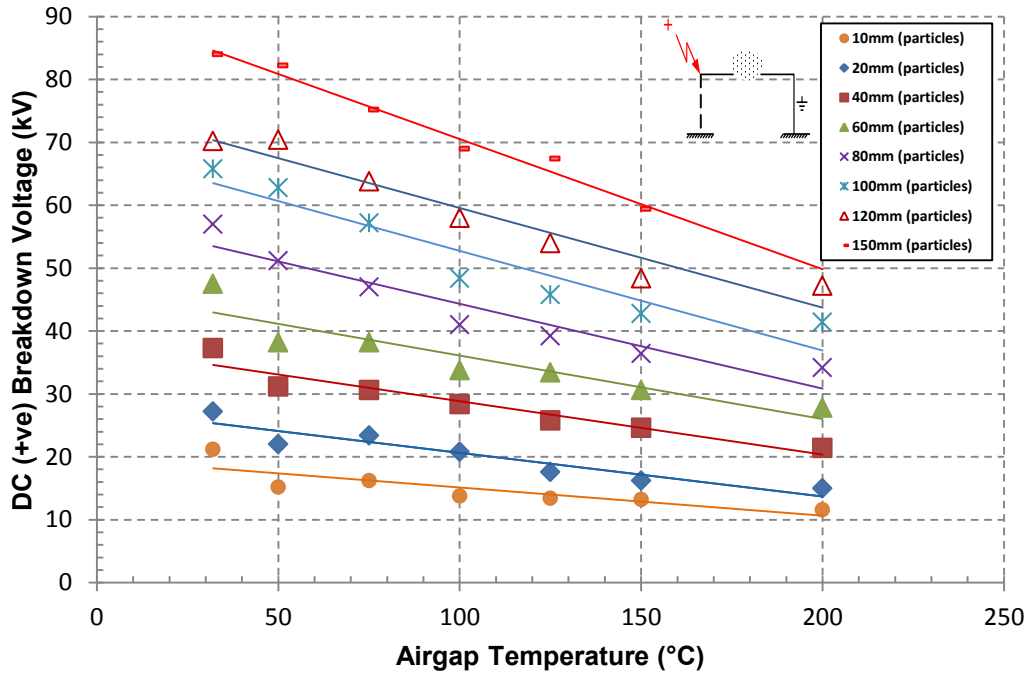

Figure 4.16 Positive DC voltage breakdown characteristics as a function of air gap temperature for small air gaps with particles

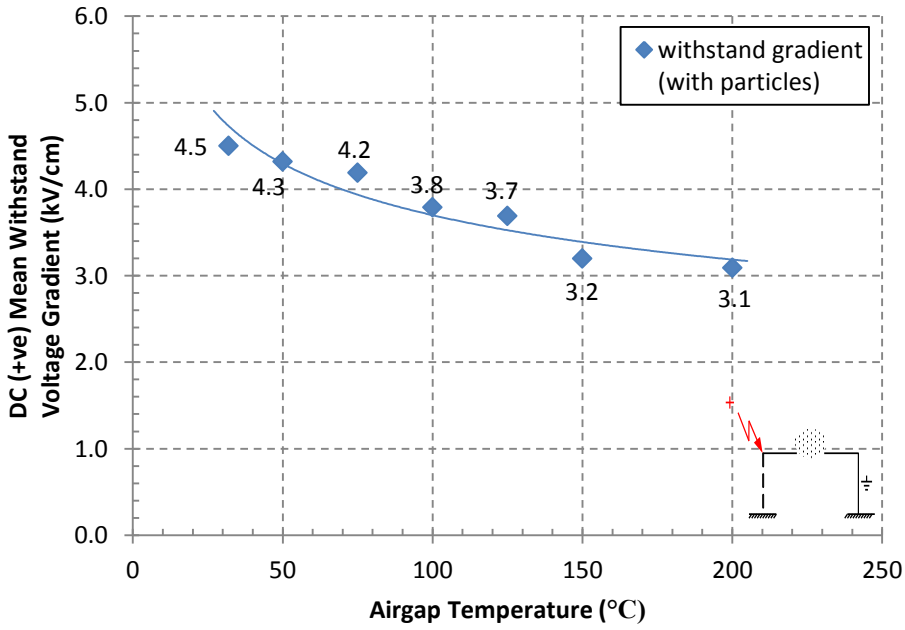

Figure 4.17 Positive DC mean withstand voltage gradient as a function of air gap temperature for small air gaps with particles

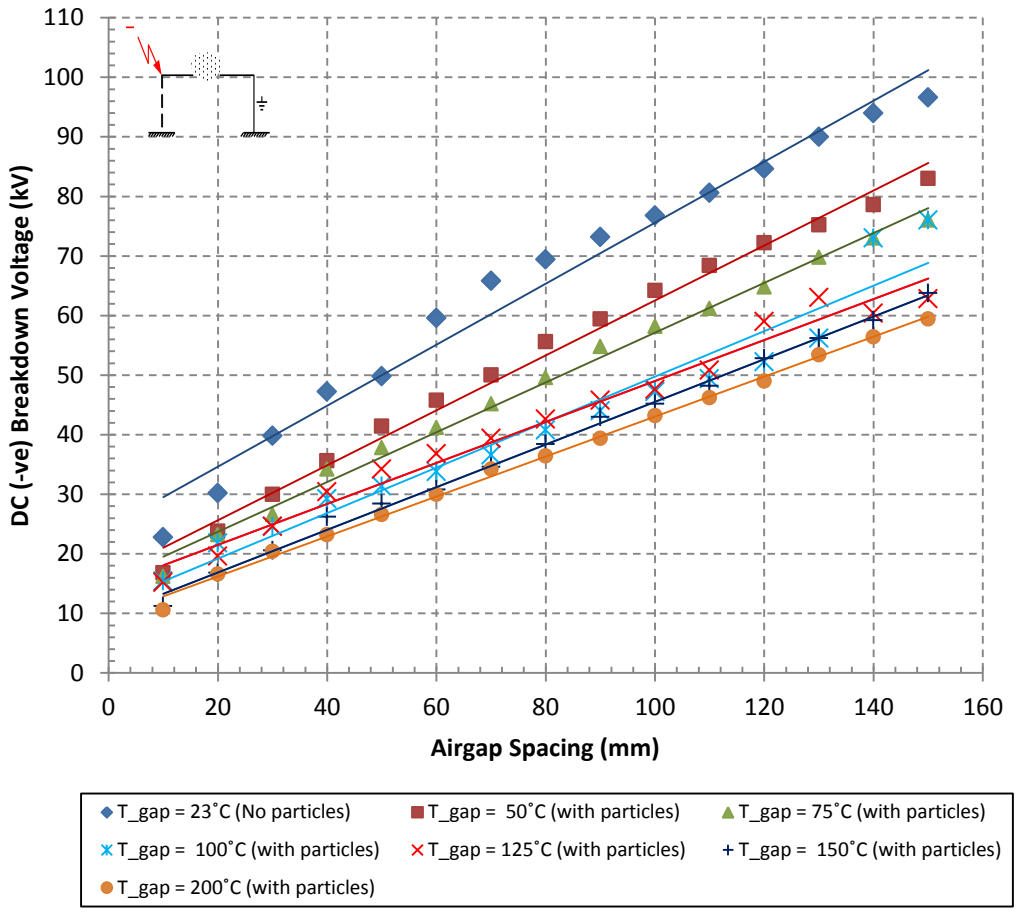

Figure 4.18 Negative DC voltage breakdown characteristics at high temperatures for small air gaps with particles

The behavior between the air gap temperatures and breakdown voltage observed for the negative polarity is logarithmic as opposed to linear which was observed in positive polarity. The negative breakdown voltage plots deviate from this linearity for air gaps greater than 20 mm.

It can further be noted that for the air gap range of 40 mm – 150 mm, the significant reduction in breakdown voltage as observed for temperatures up to 100°C under the negative polarity without particles in the air gap is not as clearly defined.

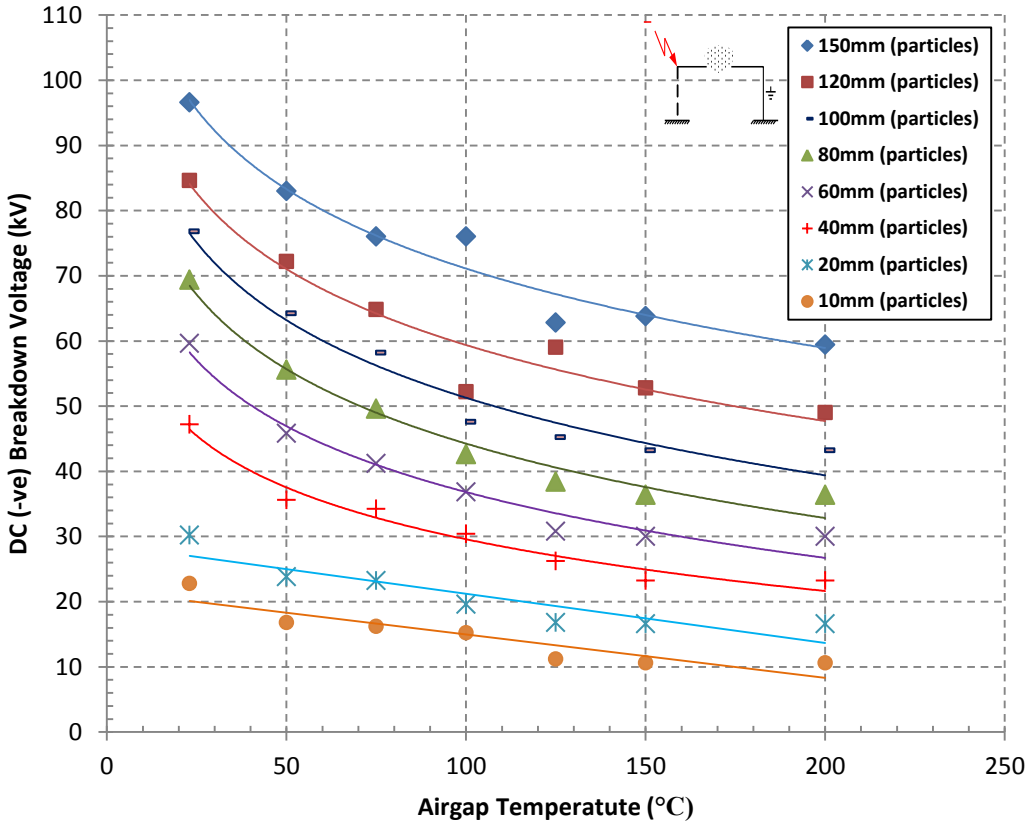

Figure 4.19 Negative DC voltage breakdown characteristics as a function of air gap temperature for small air gaps with particles

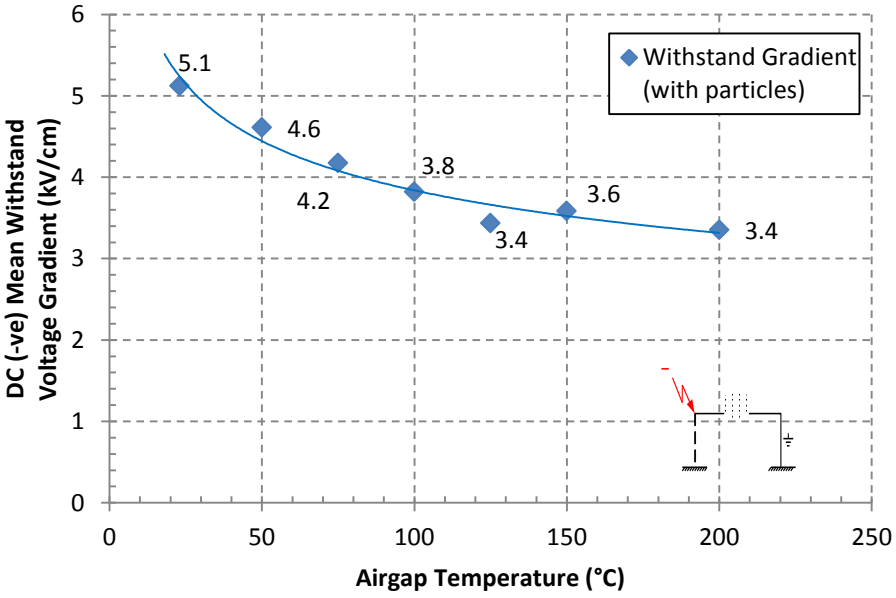

Figure 4.20 Negative DC mean withstand voltage gradient as a function of air gap temperature for small air gaps with particles

4.3. Empirical model for practical applications

In *Section 4.1* it was shown that the breakdown voltage can be approximated to be dependent on a parameter *x* (product of air density and the air gap spacing), which was defined in Equation 2.16 Figure 4.21 illustrates a proposed approximation of the breakdown voltage as a function of the product of the air density function and the air gap spacing under positive DC polarity. The density function is used to calculate the equivalent reduction as a result of an increase in temperature.

The resultant equation is:

$$V_{t\_positive} = 6.09x + 10.07 \quad \text{...(4.2)}$$

Where,

$V_{t\_positive}$ = The breakdown voltage at a temperature T (^{0}C), and air gap spacing d [cm].

Using Equation 4.2, a *1m* air gap at an air gap temperature of 100^0C (δ = 0.786) would breakdown at $V_{t_positive} \approx 488$kV.

Also illustrated in Figure 4.22 is an equivalent proposed model for the negative polarity. This results in the following model:

$$V_{t\_negative} = 6.1x + 13.36 \quad \text{...(4.3)}$$

Where,

$V_{t\_negative}$ = The breakdown voltage at a temperature T (^{0}C), and air gap spacing d [cm]. Given the same *1m* air gap at 100^0C, it would breakdown at $V_{t_negative} \approx 492$kV which is expectedly higher than its equivalent positive polarity.

These models have a single variable *x* which is influenced by both the temperature in the air gap and the actual air gap length. Previous models (AC and DC) that have been developed have attempted to define the breakdown voltage as a somewhat linear function of the air gap length at ambient temperature conditions. Where temperature effects have been incorporated, the breakdown voltage at ambient temperature conditions for a specific air gap has often been multiplied by a constant factor corresponding to the equivalent reduction in the air density at a specific temperature above ambient.

Table 4.1 and Table 4.2 illustrate the positive and negative DC experimental results respectively of breakdown voltages with their equivalent corrected values. These values were corrected using the density function defined in Equation 2.13.

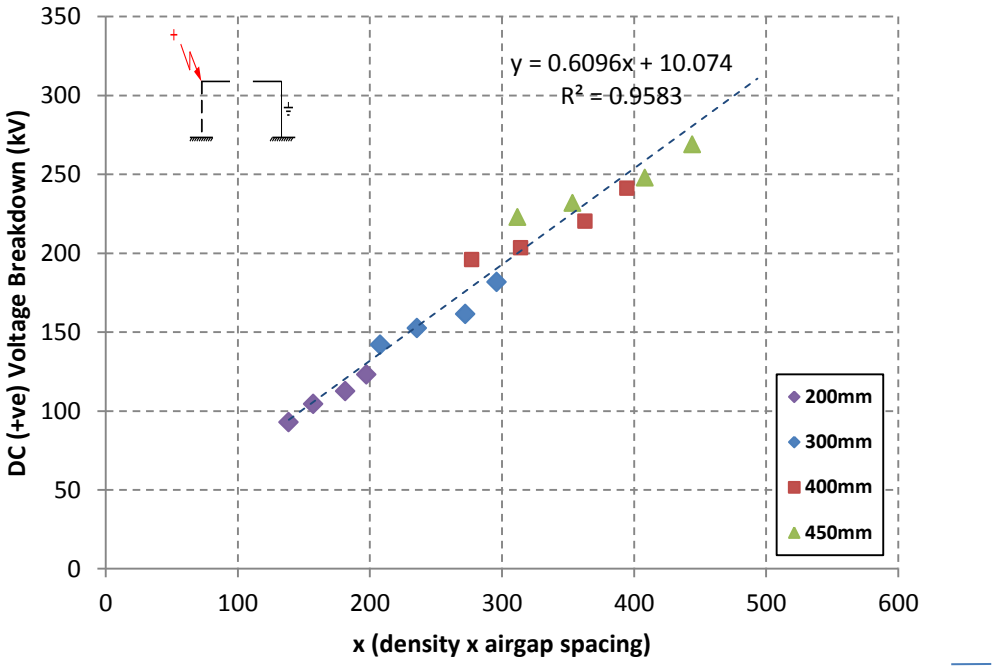

Figure 4.21 Positive DC breakdown as a function of *x* (product of density & air gap spacing)

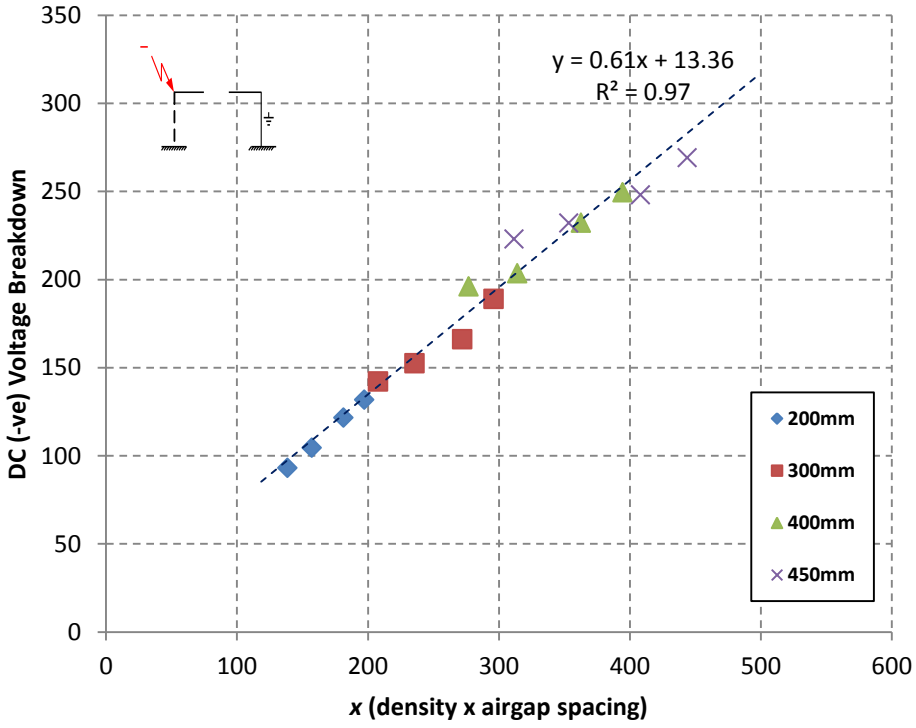

Figure 4.22 Negative DC breakdown as a function of *x* (product of density & air gap spacing)

These were corrected to STP conditions corresponding to the temperature, T_0 = 20^0C and pressure, p_0 = *1013mb* (*101.3kPa*) to illustrate the correlation between the proposed empirical formulae based on the experimental results and the calculated voltage breakdown values incorporating the reduction in density as presented in Equation 2.12, 2.14 and 2.15. Experimental results as obtained by EPRI [43] were also included in the comparison.

Figure 4.23 illustrates the results obtained from using the empirically derived model of Equation 4.2 to plot values of the positive DC breakdown voltage for a 200 mm air gap in the 20^0C – 300^0C range. These are plotted with the corrected experimental and EPRI results (presented in Table 4.1) applied to the reduced air density prediction model of Equations 2.14 and 2.15 neglecting the pressure reduction. These results are presented in Appendix J. It is to be noted that the derived empirical models for practical applications as presented in Equations 4.1 and 4.2 are purely from experimental results and no safety factor has been applied to these.

Table 4.1 Corrected experimental positive DC breakdown voltage characteristics at room temperature for large air gaps

Air gap Length d (mm)	Experimental Breakdown Voltage ▲ (kV)	Corrected Breakdown Voltage (kV)	EPRI Breakdown Voltage ■ (kV)
200	123.30	119.51	130
250	151.30	146.65	160
300	181.80	176.22	185
350	209.00	202.58	220
400	241.30	233.89	260
450	269.30	261.03	280

Note: ▲ Temperature: 24^0C; Pressure: 995.3*mb*

Note: ■ EPRI [43]

Table 4.2 Corrected experimental negative DC breakdown voltage characteristics at room temperature for large air gaps

Air gap Length d (mm)	Experimental Breakdown Voltage ▲ (kV)	Corrected Breakdown Voltage (kV)	EPRI Breakdown Voltage ■ (kV)
200	131.80	127.75	120
250	152.80	148.11	160
300	189.00	183.20	180
350	215.30	208.69	200
400	249.50	241.84	240
450	277.50	268.98	270

Note: ▲ Temperature: 24^0C; Pressure: 995.3*mb*

Note: ■ EPRI [43]

It can be observed that the percentage error as illustrated in Figure 4.23 gradually increases with the corresponding increase in temperature.

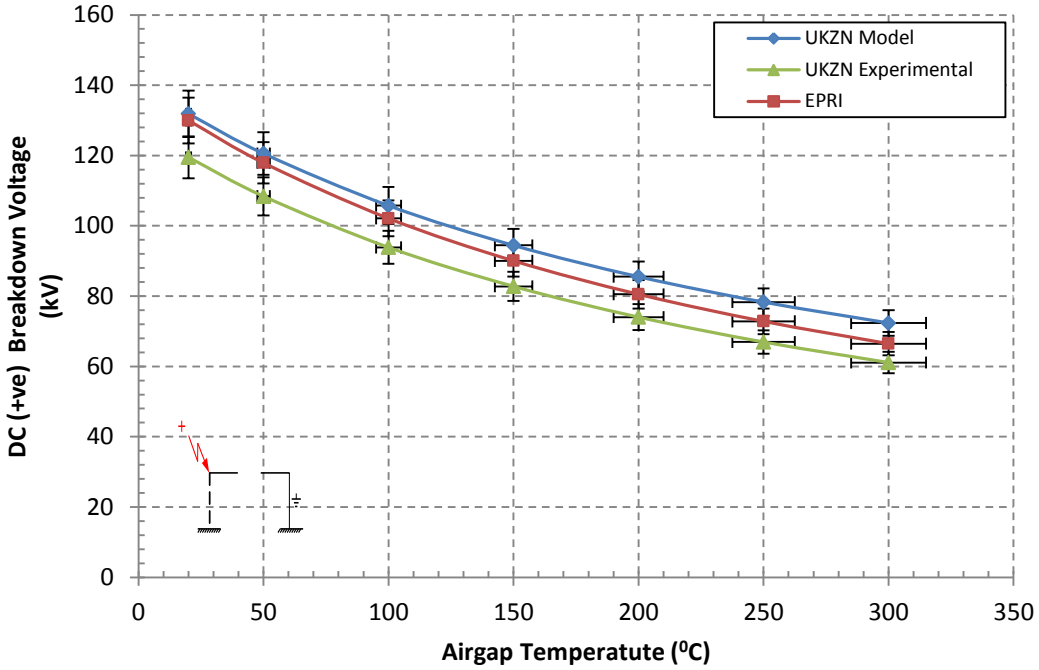

Figure 4.23 Plot of the positive DC breakdown voltage of a 200 mm air gap as a function of temperature using the derived model

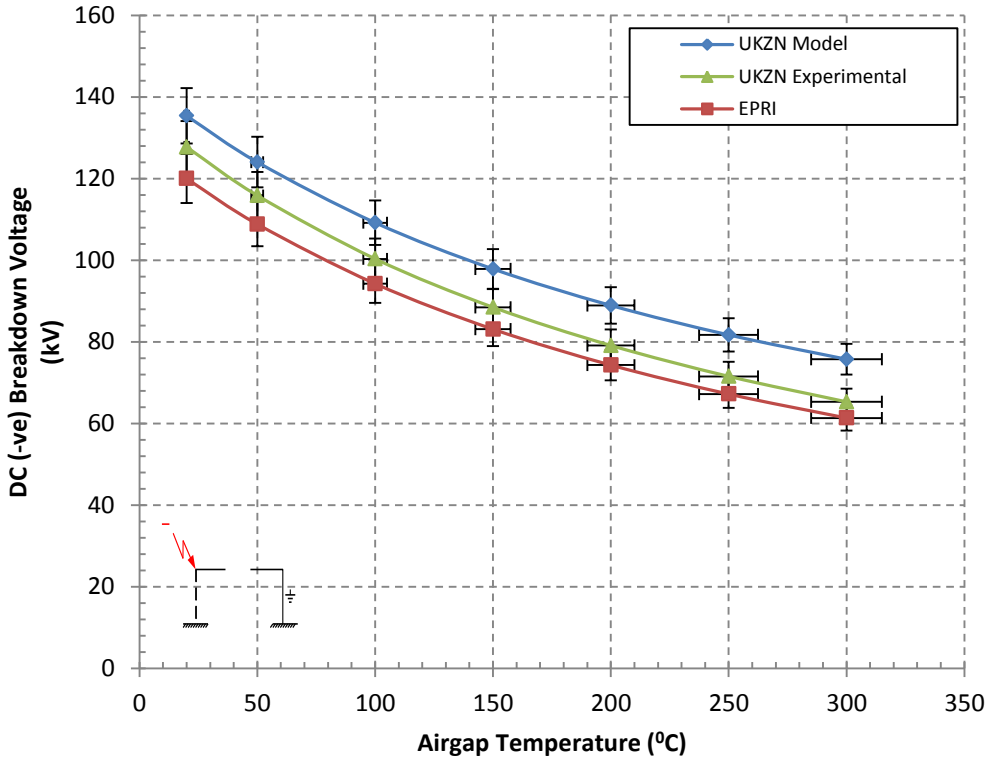

Figure 4.24 Plot of the negative DC breakdown voltage of a 200 mm air gap as a function of temperature using the derived model

This behaviour may be attributed to the dynamic behaviour of air at these elevated temperatures. Given the experimental setup this may have resulted from the difficulty to completely control the temperature in the air gap. However, the model illustrates a good correlation with the predicted values and this is a good indication of its validity for the simulation of Line-To-Tower minimum air gap clearances under dry conditions of positive polarity DC towers.

Figure 4.24 illustrates the results obtained from using the empirically derived model of Equation 4.2 to plot values of the negative DC breakdown voltage of a 200 mm air gap in the 20^0C – 300^0C range. These are plotted as per the DC positive polarity plots as discussed in this section. These results are also presented in Appendix J.

As observed in the positive polarity, the percentage error as illustrated in Figure 4.24 also seems to gradually increase with the corresponding increase in temperature. This behaviour has been attributed to reasons discussed above in this section. This model also illustrates a good correlation with the predicted values; however it is observed that a greater percentage error deviation is observed under the negative polarity when compared with the corresponding positive polarity. As it has been mentioned the empirical formulae presented in this chapter have not been applied with any safety factor and are purely experimental. However, if a safety of factor of 0.8 – 0.9 were applied; these empirical equations would yield results much closer to the predicated results presented in both Figure 4.23 and 4.24. Similar plots may be generated by varying the air gap length to extract voltage breakdown characteristics of varying lengths of Line-To-Tower clearances.

4.4. Conclusion

In *Section 4.1* and *4.2* experimental results of the voltage breakdown characteristics for small and large air gaps under both positive and negative DC applied voltages were presented and discussed. A thorough analysis and discussion was presented of the behavior of air gaps subjected to high temperatures up to 300^0C. Both the negative and positive DC cases were examined with reference to each other and with reference to the AC case. Further, results obtained from introducing particles in the smaller air gaps were also discussed. Lastly empirical models for practical applications for both polarities were proposed. These models enable the calculation of the breakdown voltage given the Line-To-Tower clearance and most importantly incorporating ambient air temperature around the vicinity of the conductor and the tower.

CHAPTER 5

CONCLUSIONS AND RECOMMENDATIONS

Based on the experimental work conducted as part of this study, the following conclusions are made:

1. The mechanism to breakdown for both the positive and negative DC applied voltage was found to be linear. A similar result had been obtained by various authors under AC applied voltages presented in the literature review.
2. Although at high temperatures breakdown occurs at a value lower than it normally would under ambient temperature conditions, the mechanism leading to breakdown remained linear. This was observed under both positive and negative polarities.
3. An approximately 55% and 50% reduction in breakdown voltage can be expected to be observed from ambient temperature breakdown levels to a temperature of 300^0C in the positive and negative polarities respectively.
4. For smaller air gaps, the dielectric withstand gradient observed under negative DC applied voltages at ambient temperature conditions was 5.1 kV/cm which is approximately 13% higher than that observed under positive polarity which was reported as 4.5 kV/cm. This confirmed a higher negative polarity dielectric strength compared to the positive polarity.
5. For larger air gaps it was further observed that air gaps have a higher dielectric strength under the negative polarity.
6. The dependence of the breakdown voltage of an air gap at high temperatures can be approximated by a model based on the dependence of the breakdown voltage to a parameter x (product of the relative air density at the temperature and the air gap spacing), for both the positive and negative polarity.
7. The models proposed can be used to approximate the breakdown voltage of a Line-To-Tower clearance at a given temperature.
8. The models developed may be further utilized for DC transmission line design for servitudes in areas known to be prone to fires.

9. The existence of particles in the air gap at high temperatures only influences the breakdown voltage levels to a very limited extent and thus depending on the size of the particles introduced and their orientation within the air gap their effect can be assumed to be close to negligible for practical purposes. Hence only the effect of high temperatures within the air gap can practically be assumed to influence the voltage breakdown levels.

It suggested that future work be commissioned to further investigate the following aspects of the study which were not conclusively exhausted:

1. The effect of the size of the particles on the breakdown voltage levels.
2. The effect of the various types of fuels.
3. The effect of a flame bridging the air gap on the breakdown characteristics for both the positive and negative polarities under DC voltages. This would provide insight into the role of high temperature plasmas on the voltage breakdown of bridged air gaps.

APPENDIX A*:

Positive DC sparkover data for horizontal Rod-to-Rod Air gap

Table A1

D (m)	U_{sp} (kV)	T/F	Gap Factor	Comments
0.05	+44	F	0.88	Temperature = 32°C, humidity = 12.5g/m^3
0.05	+46	F	0.92	Temperature = 32°C, humidity = 16g/m^3
0.05	+47	F	0.94	Temperature = 32°C, humidity = 17.5g/m^3
0.05	+48	F	0.96	Temperature = 32°C, humidity = 19.5g/m^3
0.05	+49	F	0.98	Temperature = 32°C, humidity = 21g/m^3
0.05	+44	F	0.88	Temperature = 35°C, humidity = 14g/m^3
0.05	+45	F	0.90	Temperature = 35°C, humidity = 15.5g/m^3
0.05	+46	F	0.92	Temperature = 35°C, humidity = 17.5g/m^3
0.05	+47	F	0.94	Temperature = 35°C, humidity = 19.5g/m^3
0.05	+49	F	0.98	Temperature = 35°C, humidity = 24g/m^3
0.05	+42	F	0.84	Temperature = 37°C, humidity = 14.5g/m^3
0.05	+43	F	0.86	Temperature = 37°C, humidity = 16.5g/m^3
0.05	+44	F	0.88	Temperature = 37°C, humidity = 18.5g/m^3
0.05	+45	F	0.90	Temperature = 37°C, humidity = 20.5g/m^3
0.05	+47	F	0.94	Temperature = 37°C, humidity = 24.5g/m^3
0.10	+63	F	0.84	Temperature = 32°C, humidity = 12.5g/m^3
0.10	+64	F	0.85	Temperature = 32°C, humidity = 16g/m^3
0.10	+65	F	0.87	Temperature = 32°C, humidity = 17.5g/m^3
0.10	+66	F	0.87	Temperature = 32°C, humidity = 19.5g/m^3
0.10	+68	F	0.91	Temperature = 32°C, humidity = 21.5g/m^3
0.10	+62	F	0.83	Temperature = 35°C, humidity = 14g/m^3
0.10	+64	F	0.85	Temperature = 35°C, humidity = 15.5g/m^3
0.10	+66	F	0.88	Temperature = 35°C, humidity = 17.5g/m^3
0.10	+68	F	0.91	Temperature = 35°C, humidity = 19.5g/m^3
0.10	+70	F	0.93	Temperature = 35°C, humidity = 24g/m^3;;

**Extracted from [43], however the original source is [44].*

Table A1 cont…

D (m)	U_{sp} (kV)	T/F	Gap Factor	Comments
0.10	+62	F	0.83	Temperature = 37°C, humidity = 14.5g/m^3
0.10	+64	F	0.85	Temperature = 37°C, humidity = 16.5g/m^3
0.10	+65	F	0.87	Temperature = 37°C, humidity = 18.5g/m^3
0.10	+66	F	0.88	Temperature = 37°C, humidity = 20.5g/m^3
0.10	+68	F	0.91	Temperature = 37°C, humidity = 24.5g/m^3;
0.15	+80	F	0.80	Temperature = 32°C, humidity = 12.5g/m^3
0.15	+82	F	0.82	Temperature = 32°C, humidity = 16g/m^3
0.15	+83	F	0.83	Temperature = 32°C, humidity = 17.5g/m^3
0.15	+84	F	0.84	Temperature = 32°C, humidity = 19.5g/m^3
0.15	+85	F	0.85	Temperature = 32°C, humidity = 21g/m^3
0.15	+78	F	0.78	Temperature = 35°C, humidity = 14g/m^3
0.15	+80	F	0.80	Temperature = 35°C, humidity = 15.5g/m^3
0.15	+81	F	0.81	Temperature = 35°C, humidity = 17.5g/m^3
0.15	+83	F	0.83	Temperature = 35°C, humidity = 19.5g/m^3
0.15	+85	F	0.85	Temperature = 35°C, humidity = 24g/m^3
0.15	+76	F	0.76	Temperature = 37°C, humidity = 14.5g/m^3
0.15	+77	F	0.77	Temperature = 37°C, humidity = 16.5g/m^3
0.15	+78	F	0.78	Temperature = 37°C, humidity = 18.5g/m^3
0.15	+80	F	0.80	Temperature = 37°C, humidity = 20.5g/m^3
0.15	+83	F	0.83	Temperature = 37°C, humidity = 24.5g/m^3
0.20	+95	F	0.76	Temperature = 32°C, humidity = 12.5g/m^3
0.20	+97	F	0.78	Temperature = 32°C, humidity = 16g/m^3
0.20	+99	F	0.79	Temperature = 32°C, humidity = 17.5g/m^3
0.20	+100	F	0.80	Temperature = 32°C, humidity = 19.5g/m^3
0.20	+102	F	0.82	Temperature = 32°C, humidity = 1g/m^3

Table A1 cont…

D (m)	U_{sp} (kV)	T/F	Gap Factor	Comments
0.20	+95	F	0.76	Temperature = 35°C, humidity = 14g/m^3
0.20	+96	F	0.77	Temperature = 35°C, humidity = 15.5g/m^3
0.20	+97	F	0.78	Temperature = 35°C, humidity = 17.5g/m^3
0.20	+100	F	0.80	Temperature = 35°C, humidity = 19.5g/m^3
0.20	+102	F	0.82	Temperature = 35°C, humidity = 24g/m^3
0.20	+93	F	0.74	Temperature = 37°C, humidity = 14.5g/m^3
0.20	+94	F	0.75	Temperature = 37°C, humidity = 16.5g/m^3
0.20	+95	F	0.76	Temperature = 37°C, humidity = 18.5g/m^3
0.20	+96	F	0.77	Temperature = 37°C, humidity = 20.5g/m^3
0.20	+99	F	0.79	Temperature = 37°C, humidity = 24.5g/m^3
0.25	+111	F	0.74	Temperature = 32°C, humidity = 12.5g/m^3
0.25	+113	F	0.75	Temperature = 32°C, humidity = 16g/m^3
0.25	+115	F	0.77	Temperature = 32°C, humidity = 17.5g/m^3
0.25	+117	F	0.78	Temperature = 32°C, humidity = 19g/m^3
0.25	+120	F	0.80	Temperature = 32°C, humidity = 21g/m^3
0.25	+112	F	0.75	Temperature = 35°C, humidity = 14g/m;3
0.25	+114	F	0.76	Temperature = 35°C, humidity = 15.5g/m^3
0.25	+116	F	0.77	Temperature = 35°C, humidity = 17.5g/m^3
0.25	+118	F	0.79	Temperature = 35°C, humidity = 19.5g/m^3
0.25	+124	F	083	Temperature = 35°C, humidity = 24g/m^3
0.25	+109	F	0.73	Temperature = 37°C, humidity = 14.5g/m^3
0.25	+111	F	0.74	Temperature = 37°C, humidity = 16.5g/m^3
0.25	+114	F	0.76	Temperature = 37°C, humidity = 18.5g/m^3
0.25	+118	F	0.79	Temperature = 37°C, humidity = 20.5g/m^3
0.25	+124	F	0.83	Temperature = 37°C, humidity = 24.5g/m^3

APPENDIX B*:

Negative DC sparkover data for horizontal Rod-to-Rod Air gap

Table B1

D (m)	U_{sp} (kV)	T/F	Comments
0.05	–40	F	Temperature = 32°C, humidity = 12.5g/m^3
0.05	–43	F	Temperature = 32°C, humidity = 16g/m^3
0.05	–45	F	Temperature = 32°C, humidity = 17.5g/m^3
0.05	–47	F	Temperature = 32°C, humidity = 19.5g/m^3
0.05	–49	F	Temperature = 32°C, humidity = 21g/m^3
0.05	–40	F	Temperature = 35°C, humidity = 14g/m^3
0.05	–41	F	Temperature = 35°C, humidity = 16g/m^3
0.05	–42	F	Temperature = 35°C, humidity = 17.5g/m^3
0.05	–43	F	Temperature = 35°C, humidity = 19.5g/m^3
0.05	–44	F	Temperature = 35°C, humidity = 23.5g/m^3
0.05	–42	F	Temperature = 37°C, humidity = 14.5g/m^3
0.05	–42.5	F	Temperature = 37°C, humidity = 16.5g/m^3
0.05	–43	F	Temperature = 37°C, humidity = 18.5g/m^3
0.05	–43.5	F	Temperature = 37°C, humidity = 21.5g/m^3
0.05	–44	F	Temperature = 37°C, humidity = 24.5g/m^3
0.10	–62	F	Temperature = 32°C, humidity = 12.5g/m^3
0.10	–64	F	Temperature = 32°C; humidity = 16-21g/m^3
0.10	–64	F	Temperature = 35°C, humidity = 14g/m^3
0.10	–64.5	F	Temperature = 35°C, humidity = 16g/m^3;
0.10	–65	F	Temperature = 35°C, humidity = 17.5g/m^3
0.10	–66	F	Temperature = 35°C, humidity = 19.5g/m^3
0.10	–67	F	Temperature = 35°C, humidity = 23.5g/m^3
0.10	–62	F	Temperature = 37°C, humidity = 14.5g/m^3

**Extracted from [43], however the original source is [44].*

Table B1 cont…

D (m)	U_{sp} (kV)	T/F	Comments
0.10	–63	F	Temperature = 37°C; humidity = 16.5g/m^3;
0.10	–64	F	Temperature = 37°C, humidity = 18.5g/m^3
0.10	–65	F	Temperature = 37°C, humidity = 21.5g/m^3
0.10	–66	F	Temperature = 37°C, humidity = 24.5g/m^3
0.15	–78	F	Temperature = 32°C, humidity = 12.5g/m^3
0.15	–80	F	Temperature = 32°C, humidity = 16g/m^3
0.15	–82	F	Temperature = 32°C, humidity = 17.5g/m^3
0.15	–84	F	Temperature = 32°C, humidity = 21g/m^3
0.15	–76'	F	Temperature = 35°C, humidity = 14g/m^3
0.15	–77	F	Temperature = 35°C, humidity = 16g/m^3
0.15	–78	F	Temperature = 35°C, humidity = 17.5g/m^3
0.15	–79	F	Temperature = 35°C, humidity = 19.5g/m^3
0.15	–80	F	Temperature = 35°C, humidity = 23.5g/m^3
0.15	–74	F	Temperature = 37°C, humidity = 14.5g/m^3
0.15	–75	F	Temperature = 37°C, humidity = 16.5g/m^3
0.15	–77	F	Temperature = 37°C, humidity = 18.5g/m^3
0.15	–79	F	Temperature = 37°C, humidity = 21.5g/m^3
0.15	–81	F	Temperature = 37°C, humidity = 24.5g/m^3
0.20	–98	F	Temperature = 32°C, humidity = 12.5g/m^3
0.20	–100	F	Temperature = 32°C, humidity = 16g/m^3
0.20	–102	F	Temperature = 32°C, humidity = 17.5g/m^3
0.20	–104	F	Temperature = 32°C, humidity = 19.5g/m^3
0.20	–105	F	Temperature = 32°C, humidity = 21g/m^3
0.20	–94	F	Temperature = 35°C, humidity = 14g/m^3

Table B1 cont…

D (m)	U_{sp} (kV)	T/F	Comments
0.20	–96	F	Temperature = 35°C, humidity = 16g/m^3
0.20	–98	F	Temperature = 35°C, humidity = 17.5g/m^3
0.20	–99	F	Temperature = 35°C, humidity = 19.5g/m^3
0.20	–101	F	Temperature = 35°C, humidity = 23.5g/m^3
0.20	–91	F	Temperature = 37°C, humidity = 14.5g/m^3
0.20	–93	F	Temperature = 37°C, humidity = 16.5g/m^3
0.20	–95	F	Temperature = 37°C, humidity = 18.5g/m^3
0.20	–97	F	Temperature = 37°C, humidity = 21.5g/m^3
0.20	–106	F	Temperature = 37°C, humidity = 24.5g/m^3
0.25	–110	F	Temperature = 32°C, humidity = 12.5g/m^3
0.25	–119	F	Temperature = 32°C, humidity = 16g/m^3
0.25	–120	F	Temperature = 32°C, humidity = 17.5g/m^3
0.25	–122	F	Temperature = 32°C, humidity = 19g/m^3
0.25	–125	F	Temperature = 32°C, humidity = 21g/m^3
0.25	–111	F	Temperature = 35°C, humidity = 14g/m^3
0.25	–114	F	Temperature = 35°C, humidity = 16g/m^3
0.25	–117	F	Temperature = 35°C, humidity = 17.5g/m^3
0.25	–122	F	Temperature = 35°C, humidity = 19.5g/m^3
0.25	–129	F	Temperature = 35°C, humidity = 23.5g/m^3
0.25	–109	F	Temperature = 37°C, humidity = 14.5g/m^3
0.25	–115	F	Temperature = 37°C, humidity = 16.5g/m^3
0.25	–118	F	Temperature = 37°C, humidity = 18.5g/m^3
0.25	–123	F	Temperature = 37°C, humidity = 21.5g/m^3
0.25	–133	F	Temperature = 37°C, humidity = 24.5g/m^3

APPENDIX C*:

Power Frequency AC sparkover data for horizontal Rod-to-Rod Air gap

Table C1

D (m)	D (inches)	U_{sp} (kV_{peak})	T/F	Gap Factor
0.02	0.8	25	T	2.51
0.03	1.2	36	T	2.41
0.04	1.6	46	T	2.31
0.05	2.0	53	T	2.13
0.06	2.4	60	T	2.00
0.08	3.1	70	T	1.76
0.10	3.9	79	T	1.59
0.12	4.7	86	T	1.44
0.14	5.5	95	T	1.36
0.16	6.3	104	T	1.31
0.18	7.1	112	T	1.25
0.20	7.9	120	T	1.21
0.25	9.8	143	T	1.15
0.30	11.8	167	T	1.12
0.35	13.8	192	T	1.10
0.40	15.7	218	T	1.09
0.45	17.7	243	T	1.08
0.50	19.7	270	T	1.08
0.60	23.6	322	T	1.08
0.70	27.6	374	T	1.07
0.80	31.5	422	T	1.06
0.90	35.4	473	T	1.06
1.00	39.4	520	T	1.04
1.20	47.2	625	T	1.05

**Extracted from [43], however the original source is [45].*

APPENDIX D:
Positive dc Breakdown characteristics – Small Airgaps

Table D.1. Positive dc breakdown characteristics with no fire

Rod Geometry:	**Rod - Rod**	**Temperature (˚C)**	32
length (mm)	17	**Pressure (mb)**	994.3
breadth (mm)	17	**Humidity (%)**	48.7

	Breakdown Voltage (kV) Sample Reading Number					Average B/down
d (Gap size) in mm	**1**	**2**	**3**	**4**	**5**	**(kV)**
10	18.00	18.00	19.00	19.00	18.00	18.40
20	24.50	24.00	24.50	24.00	24.50	24.30
30	35.00	35.50	36.00	34.50	35.00	35.20
40	40.00	39.50	36.00	35.00	36.00	37.30
50	43.00	43.00	42.00	43.00	43.00	42.80
60	48.00	47.50	47.00	47.00	48.00	47.50
70	57.00	58.00	58.00	57.00	58.00	57.60
80	60.00	61.00	61.00	61.00	61.00	60.80
90	66.00	67.00	65.00	64.00	64.00	65.20
100	64.00	65.00	67.00	67.00	66.00	65.80
110	70.00	69.00	70.00	71.00	70.00	70.00
120	70.00	71.00	71.00	69.00	70.00	70.20
130	76.00	75.00	75.00	76.00	76.00	75.60
140	80.00	79.00	80.00	79.00	78.00	79.20
150	84.00	85.00	84.00	84.00	83.00	84.00

Table D.2. Positive dc breakdown characteristics (T_gap = 50^0C)

Rod Geometry:	**Rod - Rod**	**Temperature (˚C)**	21.5
length (mm)	17	**Pressure (mb)**	1011
breadth (mm)	17	**Humidity (%)**	69.5

	Breakdown Voltage (kV) Sample Reading Number					Average B/down	Air-gap Temp
d (Gap size) in mm	**1**	**2**	**3**	**4**	**5**	**(kV)**	**(˚C)**
10	21.00	21.00	21.00	21.00	21.00	21.00	49.00
20	29.00	29.00	29.00	29.00	29.00	29.00	49.00
30	32.00	32.00	32.00	32.00	32.00	32.00	51.00
40	36.00	36.00	36.00	36.00	36.00	36.00	52.00
50	41.00	41.00	41.00	41.00	41.00	41.00	50.00
60	46.00	45.00	46.00	45.00	46.00	45.60	51.00
70	53.00	52.00	52.00	53.00	53.00	52.60	50.00
80	58.00	58.00	58.00	58.00	57.00	57.80	51.00
90	58.00	59.00	60.00	60.00	60.00	59.40	50.00
100	69.00	69.00	69.00	70.00	69.00	69.20	51.00
110	74.00	74.00	75.00	74.00	75.00	74.40	49.00
120	76.00	76.00	76.00	76.00	76.00	76.00	53.00
130	78.00	78.00	80.00	79.00	79.00	78.80	51.00
140	83.00	82.00	83.00	84.00	83.00	83.00	49.00
150	85.00	85.00	86.00	86.00	86.00	85.60	53.00
Average Temperature of air-gap (˚C)							**50.60**

Table D3. Positive dc breakdown characteristics (T_gap = 75^{0}C)

Rod Geometry:	**Rod - Rod**	**Temperature (˚C)**	25.1
length (mm)	17	**Pressure (mb)**	1003.3
breadth (mm)	17	**Humidity (%)**	64.7

	Breakdown Voltage (kV) Sample Reading Number					Average B/down	Air-gap Temp
d (Gap size) in mm	**1**	**2**	**3**	**4**	**5**	**(kV)**	**(˚C)**
10	22.00	22.00	22.00	22.00	22.00	22.00	76.00
20	28.00	28.00	28.00	28.00	28.00	28.00	76.00
30	31.00	31.00	32.00	31.00	31.00	31.20	75.00
40	35.00	35.00	35.00	35.00	35.00	35.00	74.00
50	39.00	39.00	39.00	39.00	39.00	39.00	75.00
60	43.00	43.00	42.00	44.00	44.00	43.20	76.00
70	48.00	49.00	49.00	50.00	49.00	49.00	75.00
80	54.00	54.00	55.00	55.00	55.00	54.60	74.00
90	58.00	58.00	58.00	58.00	58.00	58.00	75.00
100	60.00	60.00	61.00	60.00	60.00	60.20	76.00
110	64.00	64.00	64.00	64.00	64.00	64.00	73.00
120	68.00	68.00	67.00	68.00	68.00	67.80	74.00
130	69.00	72.00	72.00	72.00	71.00	71.20	75.00
140	75.00	75.00	75.00	75.00	75.00	75.00	75.00
150	77.00	75.00	75.00	76.00	77.00	76.00	75.00
Average Temperature of air-gap (˚C)							**74.93**

Table D.4. Positive dc breakdown characteristics (T_gap = 100^{0}C)

Rod Geometry:	**Rod - Rod**	**Temperature (˚C)**	23.3
length (mm)	17	**Pressure (mb)**	1004.3
breadth (mm)	17	**Humidity (%)**	69.4

	Breakdown Voltage (kV) Sample Reading Number					Average B/down	Air-gap Temp
d (Gap size) in mm	**1**	**2**	**3**	**4**	**5**	**(kV)**	**(˚C)**
10	20.00	20.00	19.00	20.00	20.00	19.80	99.00
20	27.00	28.00	27.00	26.00	27.00	27.00	100.00
30	31.00	31.00	31.00	31.00	32.00	31.20	101.00
40	34.00	35.00	34.00	34.00	35.00	34.40	100.00
50	39.00	39.00	38.00	38.00	39.00	38.60	102.00
60	42.00	43.00	42.00	42.00	43.00	42.40	101.00
70	46.00	46.00	46.00	46.00	46.00	46.00	102.00
80	49.00	50.00	51.00	50.00	50.00	50.00	102.00
90	53.00	54.00	54.00	53.00	54.00	53.60	98.00
100	58.00	57.00	57.00	57.00	56.00	57.00	99.00
110	62.00	62.00	62.00	61.00	62.00	61.80	102.00
120	64.00	64.00	63.00	63.00	63.00	63.40	102.00
130	67.00	67.00	68.00	68.00	68.00	67.60	101.00
140	72.00	72.00	72.00	71.00	71.00	71.60	100.00
150	75.00	75.00	76.00	75.00	75.00	75.20	98.00
Average Temperature of air-gap (˚C)							**100.47**

Table D.5. Positive dc breakdown characteristics (T_gap = 125^{0}C)

Rod Geometry:	**Rod - Rod**	**Temperature (˚C)**	22.3
length (mm)	17	**Pressure (mb)**	1001.7
breadth (mm)	17	**Humidity (%)**	47.3

	Breakdown Voltage (kV) Sample Reading Number					Average B/down	Air-gap Temp
d (Gap size) in mm	**1**	**2**	**3**	**4**	**5**	**(kV)**	**(˚C)**
10	20.00	18.00	19.00	19.00	19.00	19.00	127.00
20	25.00	25.00	25.00	25.00	25.00	25.00	124.00
30	29.00	28.00	29.00	28.00	28.00	28.40	125.00
40	30.00	30.00	30.00	30.00	30.00	30.00	124.00
50	34.00	35.00	35.00	35.00	34.00	34.60	125.00
60	39.00	39.00	39.00	40.00	39.00	39.20	124.00
70	40.00	41.00	41.00	41.00	42.00	41.00	124.00
80	44.00	44.00	45.00	44.00	45.00	44.40	126.00
90	48.00	48.00	46.00	47.00	47.00	47.20	126.00
100	51.00	50.00	51.00	51.00	51.00	50.80	125.00
110	53.00	53.00	53.00	52.00	54.00	53.00	124.00
120	57.00	57.00	56.00	57.00	58.00	57.00	123.00
130	62.00	62.00	62.00	62.00	61.00	61.80	127.00
140	61.00	62.00	63.00	64.00	63.00	62.60	127.00
150	65.00	64.00	64.00	64.00	64.00	64.20	125.00
Average Temperature of air-gap (˚C)							**125.07**

Table D.6. Positive dc breakdown characteristics (T_gap = 150^{0}C)

Rod Geometry:	**Rod - Rod**	**Temperature (˚C)**	22.0
length (mm)	17	**Pressure (mb)**	1005.5
breadth (mm)	17	**Humidity (%)**	67.5

	Breakdown Voltage (kV) Sample Reading Number					Average B/down	Air-gap Temp
d (Gap size) in mm	**1**	**2**	**3**	**4**	**5**	**(kV)**	**(˚C)**
10	17.00	18.00	17.00	17.00	17.00	17.20	150.00
20	24.00	24.00	25.00	25.00	25.00	24.60	149.00
30	28.00	28.00	27.00	28.00	29.00	28.00	152.00
40	30.00	30.00	31.00	32.00	30.00	30.60	152.00
50	32.00	32.00	32.00	32.00	32.00	32.00	149.00
60	37.00	38.00	37.00	38.00	38.00	37.60	149.00
70	42.00	43.00	43.00	42.00	43.00	42.60	148.00
80	47.00	46.00	47.00	47.00	46.00	46.60	150.00
90	49.00	50.00	49.00	49.00	50.00	49.40	149.00
100	54.00	53.00	53.00	53.00	53.00	53.20	151.00
110	57.00	57.00	57.00	57.00	57.00	57.00	148.00
120	59.00	58.00	59.00	59.00	58.00	58.60	152.00
130	63.00	62.00	62.00	63.00	63.00	62.60	149.00
140	67.00	66.00	66.00	66.00	65.00	66.00	149.00
150	70.00	68.00	70.00	69.00	69.00	69.20	150.00
Average Temperature of air-gap (˚C)							**149.80**

Table D.7. Positive dc breakdown characteristics (T_gap = 200^{0}C)

Rod Geometry:	**Rod - Rod**	**Temperature (˚C)**	22.0
length (mm)	17	**Pressure (mb)**	1005.5
breadth (mm)	17	**Humidity (%)**	67.5

	Breakdown Voltage (kV) Sample Reading Number					Average B/down	Air-gap Temp
d (Gap size) in mm	**1**	**2**	**3**	**4**	**5**	**(kV)**	**(˚C)**
10	16.00	16.00	16.00	16.00	16.00	16.00	200.00
20	22.00	22.00	22.00	22.00	22.00	22.00	199.00
30	24.00	25.00	24.00	24.00	24.00	24.20	202.00
40	26.00	26.00	27.00	26.00	26.00	26.20	198.00
50	28.00	29.00	28.00	29.00	29.00	28.60	201.00
60	32.00	32.00	32.00	33.00	32.00	32.20	202.00
70	37.00	37.00	36.00	36.00	36.00	36.40	200.00
80	43.00	44.00	43.00	43.00	43.00	43.20	200.00
90	43.00	44.00	44.00	44.00	44.00	43.80	201.00
100	49.00	49.00	48.00	48.00	49.00	48.60	201.00
110	51.00	51.00	49.00	52.00	51.00	50.80	202.00
120	52.00	53.00	53.00	53.00	54.00	53.00	201.00
130	57.00	57.00	57.00	57.00	57.00	57.00	202.00
140	60.00	59.00	60.00	61.00	61.00	60.20	200.00
150	62.00	62.00	61.00	62.00	61.00	61.60	200.00
Average Temperature of air-gap (˚C)							**200.60**

Table D.8. Positive dc breakdown characteristics (T_gap = 250^{0}C)

Rod Geometry:	**Rod - Rod**	**Temperature (˚C)**	25.3
length (mm)	17	**Pressure (mb)**	1006
breadth (mm)	17	**Humidity (%)**	60.6

	Breakdown Voltage (kV) Sample Reading Number					Average B/down	Air-gap Temp
d (Gap size) in mm	**1**	**2**	**3**	**4**	**5**	**(kV)**	**(˚C)**
10	10.00	11.00	11.00	11.00	11.00	10.80	251.00
20	18.00	18.00	20.00	20.00	19.00	19.00	249.00
30	22.00	23.00	22.00	22.00	23.00	22.40	249.00
40	24.00	24.00	24.00	24.00	23.00	23.80	250.00
50	25.00	26.00	26.00	26.00	26.00	25.80	248.00
60	27.00	27.00	27.00	26.00	27.00	26.80	249.00
70	31.00	31.00	31.00	31.00	31.00	31.00	249.00
80	33.00	33.00	34.00	34.00	34.00	33.60	249.00
90	38.00	38.00	38.00	39.00	37.00	38.00	248.00
100	41.00	43.00	43.00	43.00	43.00	42.60	252.00
110	46.00	46.00	46.00	47.00	47.00	46.40	250.00
120	50.00	50.00	50.00	50.00	50.00	50.00	250.00
130	52.00	52.00	52.00	52.00	52.00	52.00	249.00
140	54.00	54.00	54.00	53.00	55.00	54.00	252.00
150	58.00	56.00	56.00	57.00	57.00	56.80	248.00
Average Temperature of air-gap (˚C)							**249.53**

Table D.9. Positive dc breakdown characteristics (T_gap = 300^{0}C)

Rod Geometry:	**Rod - Rod**	**Temperature (˚C)**	24.6
length (mm)	17	**Pressure (mb)**	1005.5
breadth (mm)	17	**Humidity (%)**	71.3

	Breakdown Voltage (kV) Sample Reading Number					Average B/down	Air-gap Temp
d (Gap size) in mm	**1**	**2**	**3**	**4**	**5**	**(kV)**	**(˚C)**
10	13.00	12.00	12.00	12.00	12.00	12.20	299.00
20	15.00	15.00	15.00	15.00	15.00	15.00	299.00
30	17.00	18.00	18.00	19.00	19.00	18.20	299.00
40	19.00	20.00	20.00	18.00	20.00	19.40	301.00
50	22.00	22.00	22.00	23.00	22.00	22.20	300.00
60	23.00	23.00	23.00	24.00	24.00	23.40	299.00
70	26.00	26.00	25.00	25.00	25.00	25.40	299.00
80	29.00	29.00	30.00	31.00	31.00	30.00	299.00
90	33.00	34.00	34.00	35.00	34.00	34.00	298.00
100	41.00	41.00	41.00	42.00	42.00	41.40	300.00
110	43.00	46.00	46.00	45.00	45.00	45.00	301.00
120	48.00	47.00	47.00	48.00	48.00	47.60	301.00
130	48.00	48.00	48.00	48.00	48.00	48.00	300.00
140	49.00	49.00	49.00	49.00	50.00	49.20	300.00
150	51.00	50.00	50.00	50.00	52.00	50.60	302.00
Average Temperature of air-gap (˚C)							**299.80**

APPENDIX E:
Negative dc Breakdown characteristics – Small Airgaps

Table E.1. Negative dc breakdown characteristics with no fire

Rod Geometry:	**Rod - Rod**	**Temperature (˚C)**	32
length (mm)	17	**Pressure (mb)**	994.3
breadth (mm)	17	**Humidity (%)**	48.7

	Breakdown Voltage (kV) Sample Reading Number					Average B/down
d (Gap size) in mm	**1**	**2**	**3**	**4**	**5**	**(kV)**
10	18.00	18.00	19.00	19.00	18.00	18.40
20	24.50	24.00	24.50	24.00	24.50	24.30
30	35.00	35.50	36.00	34.50	35.00	35.20
40	40.00	39.50	36.00	35.00	36.00	37.30
50	43.00	43.00	42.00	43.00	43.00	42.80
60	48.00	47.50	47.00	47.00	48.00	47.50
70	57.00	58.00	58.00	57.00	58.00	57.60
80	60.00	61.00	61.00	61.00	61.00	60.80
90	66.00	67.00	65.00	64.00	64.00	65.20
100	64.00	65.00	67.00	67.00	66.00	65.80
110	70.00	69.00	70.00	71.00	70.00	70.00
120	70.00	71.00	71.00	69.00	70.00	70.20
130	76.00	75.00	75.00	76.00	76.00	75.60
140	80.00	79.00	80.00	79.00	78.00	79.20
150	84.00	85.00	84.00	84.00	83.00	84.00

Table E.2. Negative dc breakdown characteristics (T_gap = 50^{0}C)

Rod Geometry:	**Rod - Rod**	**Temperature (˚C)**	21.5
length (mm)	17	**Pressure (mb)**	1011
breadth (mm)	17	**Humidity (%)**	69.5

	Breakdown Voltage (kV) Sample Reading Number					Average B/down	Air-gap Temp
d (Gap size) in mm	**1**	**2**	**3**	**4**	**5**	**(kV)**	**(˚C)**
10	21.00	21.00	21.00	21.00	21.00	21.00	49.00
20	29.00	29.00	29.00	29.00	29.00	29.00	49.00
30	32.00	32.00	32.00	32.00	32.00	32.00	51.00
40	36.00	36.00	36.00	36.00	36.00	36.00	52.00
50	41.00	41.00	41.00	41.00	41.00	41.00	50.00
60	46.00	45.00	46.00	45.00	46.00	45.60	51.00
70	53.00	52.00	52.00	53.00	53.00	52.60	50.00
80	58.00	58.00	58.00	58.00	57.00	57.80	51.00
90	58.00	59.00	60.00	60.00	60.00	59.40	50.00
100	69.00	69.00	69.00	70.00	69.00	69.20	51.00
110	74.00	74.00	75.00	74.00	75.00	74.40	49.00
120	76.00	76.00	76.00	76.00	76.00	76.00	53.00
130	78.00	78.00	80.00	79.00	79.00	78.80	51.00
140	83.00	82.00	83.00	84.00	83.00	83.00	49.00
150	85.00	85.00	86.00	86.00	86.00	85.60	53.00
Average Temperature of air-gap (˚C)							**50.60**

Table E.3. Negative dc breakdown characteristics (T_gap = 75^{0}C)

Rod Geometry:	**Rod - Rod**	**Temperature (˚C)**	25.1
length (mm)	17	**Pressure (mb)**	1003.3
breadth (mm)	17	**Humidity (%)**	64.7

	Breakdown Voltage (kV) Sample Reading Number					Average B/down	Air-gap Temp
d (Gap size) in mm	**1**	**2**	**3**	**4**	**5**	**(kV)**	**(˚C)**
10	22.00	22.00	22.00	22.00	22.00	22.00	76.00
20	28.00	28.00	28.00	28.00	28.00	28.00	76.00
30	31.00	31.00	32.00	31.00	31.00	31.20	75.00
40	35.00	35.00	35.00	35.00	35.00	35.00	74.00
50	39.00	39.00	39.00	39.00	39.00	39.00	75.00
60	43.00	43.00	42.00	44.00	44.00	43.20	76.00
70	48.00	49.00	49.00	50.00	49.00	49.00	75.00
80	54.00	54.00	55.00	55.00	55.00	54.60	74.00
90	58.00	58.00	58.00	58.00	58.00	58.00	75.00
100	60.00	60.00	61.00	60.00	60.00	60.20	76.00
110	64.00	64.00	64.00	64.00	64.00	64.00	73.00
120	68.00	68.00	67.00	68.00	68.00	67.80	74.00
130	69.00	72.00	72.00	72.00	71.00	71.20	75.00
140	75.00	75.00	75.00	75.00	75.00	75.00	75.00
150	77.00	75.00	75.00	76.00	77.00	76.00	75.00
Average Temperature of air-gap (˚C)							**74.93**

Table E.4. Negative dc breakdown characteristics (T_gap = 100^{0}C)

Rod Geometry:	**Rod - Rod**	**Temperature (˚C)**	23.3
length (mm)	17	**Pressure (mb)**	1004.3
breadth (mm)	17	**Humidity (%)**	69.4

	Breakdown Voltage (kV) Sample Reading Number					Average B/down	Air-gap Temp
d (Gap size) in mm	**1**	**2**	**3**	**4**	**5**	**(kV)**	**(˚C)**
10	20.00	20.00	19.00	20.00	20.00	19.80	99.00
20	27.00	28.00	27.00	26.00	27.00	27.00	100.00
30	31.00	31.00	31.00	31.00	32.00	31.20	101.00
40	34.00	35.00	34.00	34.00	35.00	34.40	100.00
50	39.00	39.00	38.00	38.00	39.00	38.60	102.00
60	42.00	43.00	42.00	42.00	43.00	42.40	101.00
70	46.00	46.00	46.00	46.00	46.00	46.00	102.00
80	49.00	50.00	51.00	50.00	50.00	50.00	102.00
90	53.00	54.00	54.00	53.00	54.00	53.60	98.00
100	58.00	57.00	57.00	57.00	56.00	57.00	99.00
110	62.00	62.00	62.00	61.00	62.00	61.80	102.00
120	64.00	64.00	63.00	63.00	63.00	63.40	102.00
130	67.00	67.00	68.00	68.00	68.00	67.60	101.00
140	72.00	72.00	72.00	71.00	71.00	71.60	100.00
150	75.00	75.00	76.00	75.00	75.00	75.20	98.00
Average Temperature of air-gap (˚C)							**100.47**

Table E.5. Negative dc breakdown characteristics (T_gap = 125^{0}C)

Rod Geometry:	**Rod - Rod**	**Temperature (˚C)**	23.7
length (mm)	17	**Pressure (mb)**	992.4
breadth (mm)	17	**Humidity (%)**	68.7

	Breakdown Voltage (kV) Sample Reading Number					Average B/down	Air-gap Temp
d (Gap size) in mm	**1**	**2**	**3**	**4**	**5**	**(kV)**	**(˚C)**
10	18.00	18.00	18.00	18.00	18.00	18.00	126.00
20	23.00	24.00	24.00	24.00	24.00	23.80	125.00
30	26.00	26.00	27.00	27.00	28.00	26.80	124.00
40	33.00	33.00	33.00	33.00	34.00	33.20	123.00
50	36.00	36.00	36.00	37.00	37.00	36.40	127.00
60	41.00	41.00	42.00	41.00	41.00	41.20	125.00
70	45.00	45.00	46.00	44.00	44.00	44.80	126.00
80	48.00	49.00	48.00	48.00	48.00	48.20	127.00
90	50.00	51.00	51.00	51.00	51.00	50.80	126.00
100	52.00	53.00	53.00	54.00	54.00	53.20	126.00
110	57.00	57.00	57.00	57.00	57.00	57.00	124.00
120	59.00	59.00	59.00	60.00	60.00	59.40	125.00
130	63.00	64.00	65.00	65.00	65.00	64.40	123.00
140	66.00	67.00	67.00	68.00	67.00	67.00	127.00
150	68.00	69.00	69.00	69.00	69.00	68.80	125.00
Average Temperature of air-gap (˚C)							**125.27**

Table E.6. Negative dc breakdown characteristics (T_gap = 150^{0}C)

Rod Geometry:	**Rod - Rod**	**Temperature (˚C)**	23
length (mm)	17	**Pressure (mb)**	1004.2
breadth (mm)	17	**Humidity (%)**	70.4

	Breakdown Voltage (kV) Sample Reading Number					Average B/down	Air-gap Temp
d (Gap size) in mm	**1**	**2**	**3**	**4**	**5**	**(kV)**	**(˚C)**
10	18.00	17.00	17.00	17.00	16.00	17.00	149.00
20	24.00	25.00	24.00	24.00	24.00	24.20	151.00
30	26.00	26.00	27.00	26.00	26.00	26.20	150.00
40	30.00	29.00	29.00	29.00	29.00	29.20	152.00
50	33.00	33.00	34.00	33.00	33.00	33.20	148.00
60	36.00	35.00	36.00	35.00	36.00	35.60	152.00
70	39.00	38.00	37.00	38.00	39.00	38.20	150.00
80	46.00	46.00	45.00	46.00	46.00	45.80	150.00
90	47.00	48.00	48.00	47.00	47.00	47.40	149.00
100	49.00	49.00	50.00	50.00	50.00	49.60	148.00
110	50.00	51.00	50.00	51.00	51.00	50.60	151.00
120	52.00	52.00	52.00	51.00	52.00	51.80	150.00
130	56.00	57.00	56.00	56.00	56.00	56.20	150.00
140	62.00	62.00	62.00	62.00	62.00	62.00	151.00
150	64.00	64.00	64.00	63.00	64.00	63.80	149.00
Average Temperature of air-gap (˚C)							**150.00**

Table E.7. Negative dc breakdown characteristics (T_gap = 200^{0}C)

Rod Geometry:	**Rod - Rod**	**Temperature (˚C)**	23.1
length (mm)	17	**Pressure (mb)**	1006.9
breadth (mm)	17	**Humidity (%)**	60.9

	Breakdown Voltage (kV) Sample Reading Number					Average B/down	Air-gap Temp
d (Gap size) in mm	**1**	**2**	**3**	**4**	**5**	**(kV)**	**(˚C)**
10	15.00	15.00	15.00	15.00	15.00	15.00	200.00
20	19.00	19.00	19.00	19.00	19.00	19.00	200.00
30	23.00	23.00	23.00	23.00	22.00	22.80	201.00
40	26.00	25.00	25.00	25.00	26.00	25.40	200.00
50	29.00	29.00	29.00	30.00	29.00	29.20	199.00
60	32.00	31.00	32.00	32.00	31.00	31.60	201.00
70	36.00	36.00	37.00	36.00	36.00	36.20	200.00
80	42.00	41.00	42.00	42.00	41.00	41.60	200.00
90	46.00	46.00	45.00	45.00	46.00	45.60	202.00
100	49.00	48.00	48.00	49.00	49.00	48.60	202.00
110	51.00	51.00	51.00	52.00	52.00	51.40	199.00
120	54.00	53.00	54.00	54.00	53.00	53.60	199.00
130	57.00	56.00	56.00	57.00	57.00	56.60	201.00
140	57.00	56.00	58.00	57.00	58.00	57.20	199.00
150	61.00	62.00	63.00	63.00	62.00	62.20	198.00
Average Temperature of air-gap (˚C)							**200.07**

Table E.8. Negative dc breakdown characteristics (T_gap = 250^{0}C)

Rod Geometry:	**Rod - Rod**	**Temperature (˚C)**	24.9
length (mm)	17	**Pressure (mb)**	1007.5
breadth (mm)	17	**Humidity (%)**	59.3

	Breakdown Voltage (kV) Sample Reading Number					Average B/down	Air-gap Temp
d (Gap size) in mm	**1**	**2**	**3**	**4**	**5**	**(kV)**	**(˚C)**
10	13.00	14.00	14.00	14.00	14.00	13.80	248.00
20	18.00	18.00	17.00	18.00	17.00	17.60	248.00
30	17.00	20.00	19.00	19.00	19.00	18.80	251.00
40	19.00	20.00	21.00	21.00	21.00	20.40	250.00
50	22.00	23.00	23.00	22.00	22.00	22.40	251.00
60	25.00	24.00	24.00	24.00	25.00	24.40	250.00
70	28.00	27.00	26.00	26.00	27.00	26.80	248.00
80	27.00	28.00	29.00	28.00	28.00	28.00	248.00
90	30.00	32.00	31.00	31.00	30.00	30.80	252.00
100	34.00	34.00	35.00	34.00	35.00	34.40	251.00
110	38.00	37.00	37.00	37.00	37.00	37.20	252.00
120	41.00	41.00	41.00	41.00	42.00	41.20	249.00
130	44.00	44.00	45.00	45.00	46.00	44.80	249.00
140	48.00	47.00	49.00	48.00	48.00	48.00	252.00
150	51.00	52.00	49.00	52.00	53.00	51.40	251.00
Average Temperature of air-gap (˚C)							**250.00**

Table E.9. Negative dc breakdown characteristics (T_gap = 300^{0}C)

Rod Geometry:	**Rod - Rod**	**Temperature (˚C)**	25
length (mm)	17	**Pressure (mb)**	1006
breadth (mm)	17	**Humidity (%)**	75.3

	Breakdown Voltage (kV) Sample Reading Number					Average B/down	Air-gap Temp
d (Gap size) in mm	**1**	**2**	**3**	**4**	**5**	**(kV)**	**(˚C)**
10	11.00	12.00	12.00	11.00	11.00	11.40	302.00
20	14.00	14.00	14.00	15.00	14.00	14.20	302.00
30	16.00	15.00	16.00	16.00	16.00	15.80	302.00
40	17.00	18.00	18.00	18.00	18.00	17.80	300.00
50	23.00	23.00	22.00	23.00	24.00	23.00	298.00
60	25.00	25.00	26.00	25.00	24.00	25.00	302.00
70	28.00	28.00	27.00	27.00	27.00	27.40	300.00
80	29.00	30.00	29.00	29.00	31.00	29.60	299.00
90	30.00	30.00	31.00	31.00	32.00	30.80	300.00
100	32.00	33.00	33.00	32.00	33.00	32.60	300.00
110	36.00	36.00	36.00	37.00	37.00	36.40	302.00
120	40.00	41.00	41.00	42.00	41.00	41.00	299.00
130	44.00	43.00	44.00	43.00	44.00	43.60	301.00
140	45.00	47.00	45.00	47.00	46.00	46.00	299.00
150	48.00	49.00	50.00	50.00	50.00	49.40	299.00
Average Temperature of air-gap (˚C)							**300.33**

APPENDIX F:
Positive dc Breakdown characteristics – Large Airgaps

Table F.1. Positive dc breakdown characteristics with no fire

Rod Geometry:	**Rod - Rod**	**Temperature (˚C)**	24.0
length (mm)	17	**Pressure (mb)**	995.3
breadth (mm)	17	**Humidity (%)**	51.1

	Breakdown Voltage (kV) Sample Reading Number				Average B/down	Air-gap Temp
d (Gap size) in mm	**1**	**2**	**3**	**4**	**(kV)**	**(˚C)**
200	128.00	122.00	121.00	122.00	123.3	24.00
250	152.00	150.00	153.00	150.00	151.3	24.00
300	185.00	180.00	181.00	181.00	181.8	24.00
350	210.00	209.00	207.00	210.00	209.0	24.00
400	240.00	242.00	241.00	242.00	241.3	24.00
450	270.00	269.00	269.00	269.00	269.3	24.00
Average Temperature of air-gap (˚C)						**24.00**

Table F.2. Positive dc breakdown characteristics (T_gap = 50^0C)

Rod Geometry:	**Rod - Rod**	**Temperature (˚C)**	22.0
length (mm)	17	**Pressure (mb)**	1006
breadth (mm)	17	**Humidity (%)**	60.6

	Breakdown Voltage (kV) Sample Reading Number				Average B/down	Air-gap Temp
d (Gap size) in mm	**1**	**2**	**3**	**4**	**(kV)**	**(˚C)**
200	115.00	110.00	112.00	113.00	112.50	50.50
250	141.00	142.00	136.00	142.00	140.25	50.50
300	162.00	160.00	162.00	162.00	161.50	50.50
350	197.00	192.00	192.00	190.00	192.75	50.50
400	220.00	220.00	218.00	223.00	220.25	50.50
450	252.00	246.00	247.00	245.00	247.50	50.50
Average Temperature of air-gap (˚C)						**50.50**

Table F.3. Positive dc breakdown characteristics (T_gap = 100^{0}C)

Rod Geometry:	**Rod - Rod**	**Temperature (˚C)**	23.5
length (mm)	17	**Pressure (mb)**	997.5
breadth (mm)	17	**Humidity (%)**	64.6

	Breakdown Voltage (kV) Sample Reading Number				Average B/down	Air-gap Temp
d (Gap size) in mm	**1**	**2**	**3**	**4**	**(kV)**	**(˚C)**
200	105.00	106.00	104.00	103.00	104.5	97.0
250	125.00	120.00	121.00	124.00	122.5	102.0
300	156.00	152.00	151.00	151.00	152.5	98.0
350	177.00	177.00	181.00	182.00	179.3	98.0
400	207.00	207.00	200.00	200.00	203.5	102.0
450	231.00	231.00	230.00	235.00	231.8	100.0
500	255.00	261.00	261.00	267.00	261.00	105.0
Average Temperature of air-gap (˚C)						**100.29**

Table F.5. Positive dc breakdown characteristics (T_gap = 150^{0}C)

Rod Geometry:	**Rod - Rod**	**Temperature (˚C)**	23.5
length (mm)	17	**Pressure (mb)**	1003
breadth (mm)	17	**Humidity (%)**	61.5

	Breakdown Voltage (kV) Sample Reading Number				Average B/down	Air-gap Temp
d (Gap size) in mm	**1**	**2**	**3**	**4**	**(kV)**	**(˚C)**
200	94.00	95.00	91.00	93.00	93.3	148.0
250	116.00	114.00	114.00	113.00	114.3	149.0
300	143.00	140.00	141.00	143.00	141.8	152.0
350	171.00	171.00	169.00	170.00	170.3	151.0
400	195.00	197.00	197.00	196.00	196.3	152.0
450	222.00	222.00	223.00	224.00	222.8	151.0
500	243.00	241.00	241.00	244.00	242.25	152.0
Average Temperature of air-gap (˚C)						**150.71**

APPENDIX G:
Negative dc Breakdown characteristics – Large Airgaps

Table G.1. Negative dc breakdown characteristics with no fire

Rod Geometry:	**Rod - Rod**	Temperature (˚C)	24.0
length (mm)	17	Pressure (mb)	995.3
breadth (mm)	17	Humidity (%)	51.1

	Breakdown Voltage (kV) Sample Reading Number				Average B/down	Air-gap Temp
d (Gap size) in mm	**1**	**2**	**3**	**4**	**(kV)**	**(˚C)**
200	131.00	131.00	133.00	132.00	131.8	24.00
250	156.00	151.00	152.00	152.00	152.8	24.00
300	187.00	189.00	190.00	190.00	189.0	24.00
350	217.00	215.00	214.00	215.00	215.3	24.00
400	249.00	248.00	250.00	251.00	249.5	24.00
450	278.00	277.00	277.00	278.00	277.5	24.00
Average Temperature of air-gap (˚C)						**24.00**

Table G.2. Negative dc breakdown characteristics (T_gap = 50^0C)

Rod Geometry:	**Rod - Rod**	Temperature (˚C)	22.0
length (mm)	17	Pressure (mb)	1006
breadth (mm)	17	Humidity (%)	60.6

	Breakdown Voltage (kV) Sample Reading Number				Average B/down	Air-gap Temp
d (Gap size) in mm	**1**	**2**	**3**	**4**	**(kV)**	**(˚C)**
200	121.00	122.00	121.00	122.00	121.50	50.50
250	141.00	141.00	140.00	142.00	141.00	50.50
300	166.00	165.00	166.00	167.00	166.00	50.50
350	203.00	200.00	200.00	201.00	201.00	50.50
400	234.00	234.00	230.00	231.00	232.25	50.50
450	260.00	258.00	255.00	256.00	257.25	50.50
Average Temperature of air-gap (˚C)						**50.50**

Table G.3. Negative dc breakdown characteristics (T_gap = 100^{0}C)

Rod Geometry:	**Rod - Rod**	Temperature (˚C)	23.5
length (mm)	17	Pressure (mb)	987
breadth (mm)	17	Humidity (%)	50

	Breakdown Voltage (kV) Sample Reading Number				Average B/down	Air-gap Temp
d (Gap size) in mm	**1**	**2**	**3**	**4**	**(kV)**	**(˚C)**
200	105.00	106.00	104.00	103.00	104.5	100.0
250	125.00	120.00	121.00	124.00	122.5	100.0
300	156.00	152.00	151.00	151.00	152.5	100.0
350	177.00	177.00	181.00	182.00	179.3	100.0
400	207.00	207.00	200.00	200.00	203.5	100.0
450	231.00	231.00	230.00	235.00	231.8	100.0
500	255.00	261.00	261.00	267.00	261.00	100.0
Average Temperature of air-gap (˚C)						**100.00**

Table G.4. Negative dc breakdown characteristics (T_gap = 150^{0}C)

Rod Geometry:	**Rod - Rod**	Temperature (˚C)	26.0
length (mm)	17	Pressure (mb)	1007
breadth (mm)	17	Humidity (%)	48

	Breakdown Voltage (kV) Sample Reading Number				Average B/down	Air-gap Temp
d (Gap size) in mm	**1**	**2**	**3**	**4**	**(kV)**	**(˚C)**
200	94.00	95.00	91.00	93.00	93.3	149.0
250	116.00	114.00	114.00	113.00	114.3	149.0
300	143.00	140.00	141.00	143.00	141.8	153.0
350	171.00	171.00	169.00	170.00	170.3	153.0
400	195.00	197.00	197.00	196.00	196.3	153.0
450	222.00	222.00	223.00	224.00	222.8	151.0
500	243.00	241.00	241.00	244.00	242.25	152.0
Average Temperature of air-gap (˚C)						**151.43**

APPENDIX H:
Positive dc Breakdown characteristics – Small Airgaps (Particles)

Table H.1. Positive dc breakdown characteristics (T_gap = 50^{0}C)

Rod Geometry: **Rod - Rod**

length (mm) 17
breadth (mm) 17

Temp. (˚C) 24.3
Pressure (mb) 996
Humidity (%) 64

	Breakdown Voltage (kV) Sample Reading Number					Average B/down	Air-gap Temp
d (Gap size) in mm	**1**	**2**	**3**	**4**	**5**	**(kV)**	**(˚C)**
10	15.00	15.00	16.00	15.00	15.00	15.20	49.00
20	22.00	22.00	21.00	23.00	22.00	22.00	50.00
30	27.00	27.00	26.00	27.00	28.00	27.00	50.00
40	31.00	32.00	31.00	31.00	31.00	31.20	50.00
50	34.00	36.00	37.00	36.00	36.00	35.80	51.00
60	38.00	34.00	40.00	40.00	39.00	38.20	50.00
70	44.00	43.00	45.00	44.00	45.00	44.20	50.00
80	52.00	51.00	51.00	51.00	51.00	51.20	51.00
90	54.00	55.00	56.00	56.00	56.00	55.40	50.00
100	62.00	62.00	64.00	64.00	62.00	62.80	49.00
110	67.00	67.00	68.00	69.00	68.00	67.80	50.00
120	70.00	71.00	70.00	72.00	69.00	70.40	51.00
130	73.00	75.00	74.00	73.00	74.00	73.80	52.00
140	77.00	78.00	79.00	77.00	78.00	77.80	50.00
150	81.00	83.00	81.00	83.00	83.00	82.20	51.00
Average Temperature of air-gap (˚C)							**50.27**

Table H2. Positive dc breakdown characteristics (T_gap = 75^{0}C)

Rod Geometry: **Rod - Rod**

length (mm) 17
breadth (mm) 17

Temp. (˚C) 26
Pressure (mb) 999
Humidity (%) 48

	Breakdown Voltage (kV) Sample Reading Number					Average B/down	Air-gap Temp
d (Gap size) in mm	**1**	**2**	**3**	**4**	**5**	**(kV)**	**(˚C)**
10	16.00	16.00	16.00	17.00	16.00	16.20	74.00
20	23.00	24.00	23.00	23.00	24.00	23.40	77.00
30	26.00	27.00	25.00	26.00	27.00	26.20	73.00
40	31.00	30.00	31.00	30.00	31.00	30.60	78.00
50	35.00	35.00	36.00	35.00	35.00	35.20	73.00
60	38.00	38.00	39.00	38.00	38.00	38.20	79.00
70	42.00	42.00	43.00	43.00	43.00	42.60	76.00
80	47.00	47.00	46.00	47.00	48.00	47.00	79.00
90	52.00	52.00	54.00	54.00	54.00	53.20	76.00
100	57.00	57.00	56.00	58.00	58.00	57.20	76.00
110	59.00	59.00	60.00	61.00	61.00	60.00	77.00
120	64.00	64.00	64.00	63.00	64.00	63.80	76.00
130	68.00	68.00	70.00	70.00	68.00	68.80	75.00
140	72.00	72.00	73.00	73.00	72.00	72.40	75.00
150	75.00	75.00	75.00	75.00	76.00	75.20	75.00
Average Temperature of air-gap (˚C)							**75.93**

Table H.3. Positive dc breakdown characteristics (T_gap = 100^{0}C)

Rod Geometry:	**Rod - Rod**	**Temperature (˚C)**	26
length (mm)	17	**Pressure (mb)**	999
breadth (mm)	17	**Humidity (%)**	48

	Breakdown Voltage (kV) Sample Reading Number					Average B/down	Air-gap Temp
d (Gap size) in mm	**1**	**2**	**3**	**4**	**5**	**(kV)**	**(˚C)**
10	13.00	15.00	14.00	14.00	13.00	13.80	100.00
20	20.00	21.00	22.00	20.00	21.00	20.80	97.00
30	23.00	25.00	24.00	24.00	24.00	24.00	102.00
40	29.00	28.00	29.00	28.00	28.00	28.40	101.00
50	33.00	33.00	32.00	32.00	30.00	32.00	99.00
60	33.00	36.00	34.00	33.00	33.00	33.80	101.00
70	37.00	37.00	36.00	36.00	36.00	36.40	97.00
80	40.00	41.00	41.00	42.00	41.00	41.00	100.00
90	45.00	43.00	43.00	44.00	44.00	43.80	100.00
100	48.00	49.00	48.00	48.00	49.00	48.40	98.00
110	52.00	54.00	53.00	52.00	54.00	53.00	102.00
120	57.00	58.00	59.00	58.00	58.00	58.00	102.00
130	61.00	63.00	62.00	62.00	63.00	62.20	102.00
140	65.00	64.00	66.00	66.00	66.00	65.40	103.00
150	69.00	68.00	68.00	70.00	70.00	69.00	104.00
Average Temperature of air-gap (˚C)							**100.53**

Table H.4. Positive dc breakdown characteristics (T_gap = 125^{0}C)

Rod Geometry:	**Rod - Rod**	**Temperature (˚C)**	26
length (mm)	17	**Pressure (mb)**	998
breadth (mm)	17	**Humidity (%)**	70

	Breakdown Voltage (kV) Sample Reading Number					Average B/down	Air-gap Temp
d (Gap size) in mm	**1**	**2**	**3**	**4**	**5**	**(kV)**	**(˚C)**
10	12.00	14.00	14.00	13.00	14.00	13.40	125.00
20	17.00	18.00	17.00	18.00	18.00	17.60	127.00
30	22.00	23.00	23.00	24.00	24.00	23.20	128.00
40	26.00	26.00	25.00	26.00	26.00	25.80	125.00
50	30.00	30.00	31.00	29.00	30.00	30.00	125.00
60	33.00	34.00	33.00	33.00	34.00	33.40	126.00
70	37.00	36.00	37.00	37.00	36.00	36.60	124.00
80	39.00	40.00	39.00	39.00	39.00	39.20	127.00
90	41.00	41.00	42.00	42.00	41.00	41.40	126.00
100	45.00	46.00	46.00	45.00	47.00	45.80	125.00
110	51.00	52.00	51.00	51.00	51.00	51.20	124.00
120	54.00	53.00	55.00	53.00	55.00	54.00	125.00
130	58.00	59.00	59.00	60.00	59.00	59.00	124.00
140	63.00	64.00	62.00	63.00	63.00	63.00	126.00
150	67.00	68.00	67.00	67.00	68.00	67.40	124.00
Average Temperature of air-gap (˚C)							**125.40**

Table H.5. Positive dc breakdown characteristics (T_gap = 150^{0}C)

Rod Geometry:	**Rod - Rod**	Temperature (˚C)	26.0
length (mm)	17	Pressure (mb)	998
breadth (mm)	17	Humidity (%)	70

	Breakdown Voltage (kV) Sample Reading Number					Average B/down	Air-gap Temp
d (Gap size) in mm	**1**	**2**	**3**	**4**	**5**	**(kV)**	**(˚C)**
10	13.00	14.00	13.00	13.00	13.00	13.20	150.00
20	16.00	17.00	16.00	16.00	16.00	16.20	149.00
30	19.00	20.00	19.00	19.00	19.00	19.20	152.00
40	24.00	25.00	25.00	24.00	25.00	24.60	155.00
50	27.00	28.00	27.00	27.00	27.00	27.20	154.00
60	30.00	31.00	31.00	30.00	31.00	30.60	154.00
70	33.00	34.00	34.00	35.00	33.00	33.80	151.00
80	35.00	36.00	37.00	37.00	37.00	36.40	150.00
90	40.00	39.00	41.00	41.00	41.00	40.40	149.00
100	43.00	42.00	43.00	43.00	43.00	42.80	151.00
110	45.00	46.00	46.00	45.00	46.00	45.60	153.00
120	49.00	48.00	48.00	48.00	49.00	48.40	152.00
130	50.00	51.00	51.00	52.00	51.00	51.00	149.00
140	55.00	55.00	56.00	55.00	55.00	55.20	149.00
150	60.00	59.00	60.00	59.00	59.00	59.40	150.00
Average Temperature of air-gap (˚C)							**151.20**

Table H.6. Positive dc breakdown characteristics (T_gap = 200^{0}C)

Rod Geometry:	**Rod - Rod**	Temperature (˚C)	22.0
length (mm)	17	Pressure (mb)	1005.5
breadth (mm)	17	Humidity (%)	67.5

	Breakdown Voltage (kV) Sample Reading Number					Average B/down	Air-gap Temp
d (Gap size) in mm	**1**	**2**	**3**	**4**	**5**	**(kV)**	**(˚C)**
10	11.00	12.00	12.00	11.00	12.00	11.60	200.00
20	14.00	15.00	15.00	15.00	16.00	15.00	199.00
30	18.00	18.00	19.00	18.00	18.00	18.20	202.00
40	21.00	22.00	22.00	21.00	21.00	21.40	198.00
50	25.00	26.00	26.00	26.00	26.00	25.80	201.00
60	27.00	28.00	28.00	28.00	28.00	27.80	202.00
70	31.00	32.00	33.00	31.00	31.00	31.60	200.00
80	34.00	35.00	34.00	34.00	34.00	34.20	205.00
90	36.00	37.00	36.00	36.00	44.00	37.80	204.00
100	40.00	40.00	39.00	39.00	49.00	41.40	201.00
110	42.00	42.00	43.00	43.00	51.00	44.20	202.00
120	45.00	46.00	45.00	46.00	54.00	47.20	201.00
130	48.00	49.00	48.00	49.00	48.00	48.40	202.00
140	50.00	51.00	52.00	52.00	52.00	51.40	198.00
150	55.00	56.00	55.00	55.00	56.00	55.40	198.00
Average Temperature of air-gap (˚C)							**200.87**

APPENDIX I:
Negative dc Breakdown characteristics – Small Airgaps (Particles)

Table I.1. Negative dc breakdown characteristics (T_gap = 50^{0}C)

Rod Geometry:	**Rod - Rod**	**Temperature (˚C)**	33
length (mm)	17	**Pressure (mb)**	983
breadth (mm)	17	**Humidity (%)**	46

	Breakdown Voltage (kV) Sample Reading Number					Average B/down	Air-gap Temp
d (Gap size) in mm	**1**	**2**	**3**	**4**	**5**	**(kV)**	**(˚C)**
10	17.00	18.00	17.00	16.00	16.00	16.80	50.00
20	24.00	23.00	24.00	24.00	24.00	23.80	52.00
30	29.00	30.00	31.00	30.00	30.00	30.00	53.00
40	35.00	36.00	35.00	36.00	36.00	35.60	51.00
50	41.00	41.00	42.00	41.00	42.00	41.40	48.00
60	46.00	45.00	46.00	46.00	46.00	45.80	48.00
70	49.00	49.00	51.00	51.00	50.00	50.00	48.00
80	56.00	55.00	55.00	56.00	56.00	55.60	49.00
90	59.00	59.00	60.00	60.00	59.00	59.40	51.00
100	64.00	64.00	65.00	64.00	64.00	64.20	51.00
110	68.00	69.00	69.00	68.00	68.00	68.40	53.00
120	72.00	72.00	72.00	73.00	72.00	72.20	51.00
130	75.00	76.00	75.00	75.00	75.00	75.20	51.00
140	78.00	79.00	79.00	79.00	78.00	78.60	51.00
150	83.00	83.00	82.00	84.00	83.00	83.00	53.00
Average Temperature of air-gap (˚C)							**50.67**

Table I2. Negative dc breakdown characteristics (T_gap = 75^{0}C)

Rod Geometry:	**Rod - Rod**	**Temperature (˚C)**	33
length (mm)	17	**Pressure (mb)**	983
breadth (mm)	17	**Humidity (%)**	46

	Breakdown Voltage (kV) Sample Reading Number					Average B/down	Air-gap Temp
d (Gap size) in mm	**1**	**2**	**3**	**4**	**5**	**(kV)**	**(˚C)**
10	16.00	17.00	16.00	16.00	16.00	16.20	76.00
20	23.00	24.00	23.00	23.00	23.00	23.20	76.00
30	27.00	26.00	27.00	26.00	27.00	26.60	76.00
40	34.00	35.00	34.00	34.00	34.00	34.20	75.00
50	38.00	37.00	38.00	38.00	38.00	37.80	77.00
60	42.00	41.00	41.00	41.00	41.00	41.20	78.00
70	45.00	45.00	46.00	45.00	45.00	45.20	78.00
80	49.00	50.00	49.00	50.00	50.00	49.60	75.00
90	54.00	55.00	55.00	55.00	55.00	54.80	73.00
100	58.00	58.00	58.00	59.00	58.00	58.20	73.00
110	61.00	61.00	61.00	62.00	61.00	61.20	75.00
120	65.00	64.00	65.00	65.00	65.00	64.80	73.00
130	70.00	69.00	70.00	70.00	70.00	69.80	77.00
140	74.00	73.00	73.00	73.00	73.00	73.00	75.00
150	75.00	74.00	75.00	75.00	76.00	76.00	75.00
Average Temperature of air-gap (˚C)							**75.47**

Table I.3. Negative dc breakdown characteristics (T_gap = 100^{0}C)

Rod Geometry:	**Rod - Rod**	**Temperature (˚C)**	33
length (mm)	17	**Pressure (mb)**	983
breadth (mm)	17	**Humidity (%)**	46

	Breakdown Voltage (kV) Sample Reading Number					Average B/down	Air-gap Temp
d (Gap size) in mm	**1**	**2**	**3**	**4**	**5**	**(kV)**	**(˚C)**
10	16.00	15.00	16.00	15.00	15.00	15.40	101.00
20	22.00	21.00	22.00	22.00	22.00	21.80	102.00
30	24.00	25.00	25.00	24.00	25.00	24.60	102.00
40	29.00	29.00	29.00	29.00	30.00	29.20	100.00
50	31.00	32.00	31.00	31.00	32.00	31.40	101.00
60	33.00	34.00	34.00	34.00	34.00	33.80	99.00
70	37.00	37.00	36.00	36.00	37.00	36.60	101.00
80	42.00	41.00	40.00	41.00	40.00	40.80	102.00
90	44.00	45.00	43.00	44.00	44.00	44.00	98.00
100	47.00	48.00	47.00	47.00	47.00	47.20	99.00
110	49.00	50.00	49.00	49.00	50.00	49.40	101.00
120	52.00	52.00	53.00	52.00	52.00	52.20	98.00
130	56.00	57.00	56.00	56.00	56.00	56.20	99.00
140	60.00	61.00	60.00	60.00	61.00	73.00	98.00
150	66.00	67.00	66.00	66.00	66.00	76.00	100.00
Average Temperature of air-gap (˚C)							**100.07**

Table I.4. Negative dc breakdown characteristics (T_gap = 125^{0}C)

Rod Geometry:	**Rod - Rod**	**Temperature (˚C)**	31
length (mm)	17	**Pressure (mb)**	984
breadth (mm)	17	**Humidity (%)**	51

	Breakdown Voltage (kV) Sample Reading Number					Average B/down	Air-gap Temp
d (Gap size) in mm	**1**	**2**	**3**	**4**	**5**	**(kV)**	**(˚C)**
10	15.00	16.00	15.00	15.00	15.00	15.20	125.00
20	19.00	19.00	20.00	20.00	20.00	19.60	126.00
30	24.00	24.00	25.00	25.00	25.00	24.60	126.00
40	31.00	30.00	30.00	31.00	30.00	30.40	125.00
50	33.00	34.00	34.00	35.00	35.00	34.20	128.00
60	37.00	36.00	37.00	37.00	37.00	36.80	127.00
70	39.00	40.00	39.00	39.00	40.00	39.40	127.00
80	42.00	43.00	43.00	42.00	43.00	42.60	125.00
90	46.00	46.00	46.00	45.00	46.00	45.80	125.00
100	48.00	48.00	47.00	48.00	47.00	47.60	124.00
110	51.00	51.00	50.00	51.00	51.00	50.80	124.00
120	54.00	53.00	55.00	53.00	54.00	59.00	123.00
130	58.00	59.00	58.00	58.00	59.00	63.00	125.00
140	60.00	60.00	61.00	61.00	60.00	60.40	125.00
150	63.00	62.00	63.00	63.00	63.00	62.80	126.00
Average Temperature of air-gap (˚C)							**125.40**

Table I.5. Negative dc breakdown characteristics (T_gap = 150^{0}C)

Rod Geometry:	**Rod - Rod**	**Temperature (˚C)**	28
length (mm)	17	**Pressure (mb)**	994
breadth (mm)	17	**Humidity (%)**	70

	Breakdown Voltage (kV) Sample Reading Number					Average B/down	Air-gap Temp
d (Gap size) in mm	**1**	**2**	**3**	**4**	**5**	**(kV)**	**(˚C)**
10	11.00	12.00	11.00	11.00	11.00	11.20	151.00
20	16.00	17.00	17.00	17.00	17.00	16.80	148.00
30	20.00	21.00	21.00	20.00	21.00	20.60	148.00
40	26.00	27.00	26.00	26.00	26.00	26.20	149.00
50	27.00	28.00	29.00	29.00	29.00	28.40	151.00
60	31.00	31.00	30.00	31.00	31.00	30.80	151.00
70	34.00	34.00	35.00	35.00	35.00	34.60	152.00
80	38.00	39.00	39.00	38.00	38.00	38.40	152.00
90	43.00	44.00	43.00	42.00	43.00	43.00	153.00
100	45.00	46.00	45.00	45.00	45.00	45.20	151.00
110	49.00	47.00	48.00	49.00	48.00	48.20	149.00
120	53.00	53.00	53.00	52.00	53.00	52.80	150.00
130	56.00	55.00	57.00	56.00	57.00	56.20	149.00
140	58.00	59.00	60.00	60.00	59.00	59.20	148.00
150	64.00	63.00	64.00	64.00	64.00	63.80	151.00
Average Temperature of air-gap (˚C)							**150.20**

Table I.6. Negative dc breakdown characteristics (T_gap = 200^{0}C)

Rod Geometry:	**Rod - Rod**	**Temperature (˚C)**	28
length (mm)	17	**Pressure (mb)**	994
breadth (mm)	17	**Humidity (%)**	70

	Breakdown Voltage (kV) Sample Reading Number					Average B/down	Air-gap Temp
d (Gap size) in mm	**1**	**2**	**3**	**4**	**5**	**(kV)**	**(˚C)**
10	10.00	11.00	11.00	10.00	11.00	10.60	200.00
20	16.00	17.00	16.00	17.00	17.00	16.60	202.00
30	21.00	20.00	20.00	21.00	20.00	20.40	203.00
40	23.00	24.00	23.00	23.00	23.00	23.20	202.00
50	27.00	27.00	26.00	26.00	27.00	26.60	201.00
60	29.00	31.00	30.00	30.00	30.00	30.00	201.00
70	34.00	34.00	35.00	34.00	34.00	34.20	200.00
80	36.00	36.00	37.00	37.00	36.00	36.40	201.00
90	39.00	40.00	40.00	39.00	39.00	39.40	202.00
100	43.00	43.00	43.00	44.00	43.00	43.20	198.00
110	46.00	46.00	47.00	46.00	46.00	46.20	198.00
120	49.00	49.00	49.00	49.00	49.00	49.00	199.00
130	54.00	54.00	53.00	53.00	53.00	53.40	202.00
140	57.00	56.00	56.00	57.00	56.00	56.40	199.00
150	59.00	59.00	60.00	60.00	59.00	59.40	198.00
Average Temperature of air-gap (˚C)							**200.40**

APPENDIX J:
Positive & Negative dc Breakdown characteristics Using Derived Model

V_tpos = 6.09x+10.07

V_tneg= 6.1x+13.36
Ut=Us*(0.386p)/(273+T)

Table J.1. Dc breakdown characteristics of a 200mm airgap using derived model

200mm							
temp_C	density	Vt_pos	Vt_neg	Us_pos	Us_neg	EPRI_pos	EPRI_neg
20	1	131.9	135.4	119.5	127.7	130.0	120.0
50	0.907	120.6	124.0	108.4	115.9	117.9	108.8
100	0.786	105.7	109.2	93.9	100.3	102.1	94.2
150	0.693	94.4	97.9	82.8	88.5	90.0	83.1
200	0.619	85.5	88.9	74.0	79.1	80.5	74.3
250	0.560	78.3	81.7	66.9	71.6	72.8	67.2
300	0.511	72.4	75.7	61.1	65.3	66.5	61.4

Table J.2. Dc breakdown characteristics of a 300mm airgap using derived model

300mm							
temp_C	density	Vt_pos	Vt_neg	Us_pos	Us_neg	EPRI_pos	EPRI_neg
20	1	192.8	196.4	176.2	183.2	185.0	180.0
50	0.907	175.8	179.4	159.8	166.2	167.8	163.3
100	0.786	153.6	157.1	138.4	143.9	145.3	141.4
150	0.693	136.6	140.1	122.0	126.9	128.1	124.7
200	0.619	123.2	126.7	109.1	113.5	114.6	111.5
250	0.560	112.4	115.9	98.7	102.6	103.6	100.8
300	0.511	103.5	106.9	90.1	93.7	94.6	92.0

Table J.3. Dc breakdown characteristics of a 400mm airgap using derived model

400mm							
temp_C	density	Vt_pos	Vt_neg	Us_pos	Us_neg	EPRI_pos	EPRI_neg
20	1	253.7	257.4	233.9	241.8	260.0	240.0
50	0.907	231.0	234.7	212.1	219.3	235.8	217.7
100	0.786	201.4	205.0	183.7	189.9	204.2	188.5
150	0.693	178.8	182.4	162.0	167.5	180.1	166.2
200	0.619	161.0	164.5	144.9	149.8	161.0	148.6
250	0.560	146.5	150.1	131.0	135.5	145.6	134.4
300	0.511	134.6	138.1	119.6	123.6	132.9	122.7

Table J.4. Dc breakdown characteristics of a 450mm airgap using derived model

450mm							
temp_C	density	Vt_pos	Vt_neg	Us_pos	Us_neg	EPRI_pos	EPRI_neg
20	1	284.1	287.9	261.0	268.9	280.0	270.0
50	0.907	258.7	262.4	236.8	244.0	254.0	244.9
100	0.786	225.3	229.0	205.0	211.3	219.9	212.1
150	0.693	199.9	203.5	180.8	186.3	193.9	187.0
200	0.619	179.8	183.4	161.7	166.6	173.4	167.2
250	0.560	163.6	167.1	146.2	150.7	156.8	151.2
300	0.511	150.2	153.7	133.5	137.5	143.2	138.0

References

[1]. E. Bussy, N.M. Ijumba and A.C. Britten, "A Literature Review of Air Insulation Strength as Affected by Temperature and Fire – The State of the Art", *Proceedings of the 2006 HVDC Congress*, Durban, South Africa, 12 – 14 July 2006.

[2]. Z. Ntshangase, N.M. Ijumba, E. Bussy, A. Naidoo and A.C. Britten, "Preliminary Study of Fire-Induced Voltage Breakdown Characteristics under HVDC Conditions", *Proceedings of the 15th International Symposium on High Voltage Engineering*, Ljubljana, Slovenia, 27 – 31 August 2007, pp T9-342.

[3] K.J. Sadurski and J.P. Reynders, "High Voltage AC Breakdown in Presence of Fires", *Proceedings of the 6th International Symposium on High Voltage Engineering*, New Orleans, LA, USA, 28 August – 1 September 1989.

[4] A. Sukhnandan and D.A. Hoch, "An Investigation of Fire Induced Flashovers of Transmission Lines", *SAUPEC 2004*, University of Stellenbosch, South Africa, 22 – 23 January 2004.

[5] J.R. Fonseca, A.L. Tan, V. Monassi, W.S. Junqueire, R.P. Silva, L.A.R. Assuncao and M.O.C. Melo, "Effects of Agricultural Fires on the Performance of Overhead Transmission Lines", *IEEE Transactions on Power Delivery*, Vol. 5, No. 2, April 1990, pp. 687-694.

[6] P.M. Cowan, J.A. Dunn, P. Naidoo and J. Masters, "Sugar Cane Induced Transmission Line Flashovers", *Electron*, January 1991, pp. 12-15.

[7] A. Sukhnandan and D.A. Hoch, "Fire Induced Flashovers of Transmission Lines: Theoretical Models", *Transactions of the SA Institute of Electrical Engineers*, September 2004, pp. 148-153.

[8] R. Lanoie and H.P. Mercure, "Influence of Forest Fires on Power Line Insulation", *Proceedings of the 6th International Symposium on High Voltage Engineering*, New Orleans, LA, USA, 28 August – 1 September 1989.

[9] A. Robledo-Martinez, E. Guzman and J.L. Hernandez, "Dielectric Characteristics of a Model Transmission Line in the Presence of Fire", *IEEE Transactions on Electrical Insulation*, Vol. 26, No. 4, August 1991, pp. 776 – 782.

.

[10] Eskom Archives, Eastern Region – Transmission, New Germany, Durban, South Africa 2008.

[11] Z. Ntshangase, N.M. Ijumba, E. Bussy, A. Naidoo and A.C. Britten, "Initial Study of Fire-Induced Air gap Breakdown Characteristics Under HVDC Conditions," *Proceedings of the 16th South African Power Engineering Universities' Conference*, Cape Town, South Africa, 25-26 January 2007

[12] E.H.R. Gaxiola and J.M. Wetzer, "Streamers and Transition to Breakdown," *Proceedings of the 11th International Symposium on High-Voltage Engineering*, Vol. 3, London, UK, 22-27 August 1999, pp. 33.11.S5-33.14.S5.

[13] C.R. Evert, "The detection of fires under high voltage transmission lines," M.Sc. dissertation, University of Natal, Durban, South Africa, 2003, pp. 25.

[14] A. Pederson, "On the Electrical Breakdown of Gaseous Dielectrics, An Engineering Approach", *IEEE Transactions on Electrical Insulation*, Vol. 24, No. 5, October 1989, pp. 721-739.

[15] N.M. Ijumba, "Study of time lags to breakdown in SF_6 with insulated coverings on the electrode", M.Sc. dissertation, University of Salford, Scotland, 1979, pp. 7.

[16] R.W. Crowe, J.K. Bragg and Virginia G. Thomas, "Space Charge Formation and the Townsend Mechanism of Spark Breakdown in Gases," *Physical Review*, Vol. 96, No. 1, 1 October 1954, pp. 10-14.

[17] F. Llewellyn Jones, "Ionization Processes in the Electrical Breakdown of Gases," *British Journal of Applied Physics*, Vol. 5, 5 February 1954, pp. 49-54.

[18] J. Dutton and W.T. Morris, "The Mechanism of the Electrical Breakdown of Air in Uniform Fields at Voltages Up To 400 kV," *British Journal of Applied Physics*, Vol. 18, 1967, pp. 1115-1120.

[19] F. Llewellyn Jones and A.B. Parker, "Electrical Breakdown of Gases. I. Spark Mechanism in Air," *Proceedings of the Royal Society of London, Series A, Mathematical and Physical Sciences*, Vol. 213, No. 1113, 24 June 1952, pp. 185-202.

[20] P.J. Harrop, *Dielectrics*, Butterworth & Co., ISBN: 0 408 70387 3, Durban, South Africa, 1972, Chapter 3, pp. 42 – 91.

[21] S.C. Brown, *Introduction to Electrical Discharges in Gases*, John Wiley & Sons, Inc., ISBN: New York, USA, 1966, Chapter 6, pp. 94 – 110.

[22] E. Kuffel, W.S. Zaengl and J. Kuffel, *High Voltage Engineering: Fundamentals – 2nd Ed.*, Butterworth-Heinemann, ISBN: 0 7506 6364 3, Norfolk, Great Britain, 2000, Chapter 5, pp. 281 – 364 [22]

[23] D.V. Razevig, *High Voltage Engineering*, Khanna Publishers, Dehli, India 1978, Chapter 2, pp. 13 – 26.

[24] D. Kind and H. Karner, *High-Voltage Insulation Technology*, Friedr. Vieweg & Sohn, ISBN: 3-528-08599-1, Germany, 1985, Chapter 1, pp. 1 – 62.

[25] H. Raether, *Electron Avalanches and Breakdown in Gases*, Butterworths, London, 1964.

[26] L.B. Loeb, *Basic Processes of Gaseous Electronics*, University of California Press, Los Angeles, USA, 1960.

[27] J.M. Meek and J.D. Craggs, *Electrical Breakdown of Gases*, Clarendon Press, Oxford, 1978.

[28] K. Petcharaks, "A Contribution to the Streamer Breakdown Criterion", *Proceedings of the 11th International Symposium on High-Voltage Engineering*, Vol. 3, London, UK, 22-27 August 1999, pp. 3.19.S5-3.22.S5.

[29] F.G. Heymann, "Corona on Wires in Air", *Transactions of the South African Institute of Electrical Engineers (SAIEE)*, Vol. 56, Pt. 11, 1965, pp. 271 – 290.

[30] R.T. Waters and W.B. Stark, "Characteristics of Stabilized Glow Discharge in Air", *J. Phys. D: Applied Physics*, Vol. 8, 1975, pp. 416 – 426.

[31] W.S. Zaengl, S. Yimvuthikul and G. Friedrich, "The Temperature Dependence of Homogenous Field Breakdown in Synthetic Air, *IEEE Transactions on Electrical Insulation*, Vol. E1-26, No. 3, pp. 380 – 390, 1991.

[32] K. Petcharaks and W.S. Zaengl, "Numerical Calculation of Breakdown Voltages of Standard Air Gaps (IEC52) based on Streamer Breakdown Criteria", *Proceedings of the 9th International Symposium on High-Voltage Engineering*, Vol. 2, Paper No. 2173, Graz, Austria, 1995.

[33] R.V. Hodges, R.N. Varney and J.F. Riley, "Probability of Electrical Breakdown: Evidence for a transition between the Townsend and Streamer Breakdown Mechanisms", *Physical Review A*, Vol. 31, No. 4, April 1985, pp. 2610 – 2620.

[34] J.M. Meek, "A Theory of Spark Discharge", *Physical Review*, No. 57, Issue 8, April 1940, pp. 722 – 728.

[35] V. Cooray, *The Lightning Flash*, The Institution of Electrical Engineers (IEE) Power Series - 34, Stevenage, UK, 2003, Chapter 3, pp. 45 – 126.

[36] Han S. Uhm, "Properties of Plasmas Generated by Electrical Breakdown in Flames", *Journal of Physics of Plasmas*, Vol. 6, No. 11, November 1999, pp. 4366 – 4374.

[37] R. Arora and W. Mosch, *High Voltage Insulation Engineering*, New Age International Publishers Limited, Wiley Eastern LTD., ISBN: 81-224-0619-X, India, 1995, Chapter 2, pp. 54 – 176.

[38] K. Feser and J. Schmid, "Temperature Effect on the Streamer Breakdown in Air", *Proceedings of the 6th International Symposium on High-Voltage Engineering*, New Orleans, LA, USA, 28 August – 1 September 1989, Paper No. *46.04*.

[39] Earl W. McDaniel, *Collision Phenomena in Ionized Gases*, John Wiley & Sons, Inc., Catalog Card Number: 64-13219, New York, Unites States of America, 1964, Chapter 2, pp. 32 – 57.

[40] N.L Allen and A. Ghaffar, "Temperature and Density Effects on Streamer Propagation in Air", *Proceedings of the 8th International Symposium on High-Voltage Engineering*, Yokohama, Japan, 23 – 27 August 1993, Paper No. *40.02*, pp. 5 – 8.

[41] EPRI, *Transmission Line Reference Book – HVDC To ±600 kV,* Electric Power Research Institute, California, USA, 1977, Chapter 10, pp. 144 – 146.

[42] B. Hutzler, "Dielectric Properties of Air Gaps", *Proceedings of the Sixth International Symposium on High Voltage Engineering*, New Orleans, LA, USA, 28 August – 1 September 1989.

[43] EPRI, "Sparkover performance and gap factors of air gaps below 1 meter", Electric Power Research Institute, Inc., CA, USA, Report no. *TR-106335*, 1998.

[44] A.P. Abraham, B.R. Prabhakar, "Effect of Humidity and Temperature on the DC Breakdown of Rod-Rod and Rod-Plane Gaps", *IEEE Transactions on Electrical Insulation*, Vol. 27, No. 2, April 1991, pp. 207 – 213.

[45] R. Gobbo & G. Pesavento, "Rod-rod Gaps under DC Voltage", *Proceedings of the 12th International Symposium on High-Voltage Engineering*, Bangalore, India, 20 – 24 August 2001, pp. 1174 – 1177.

[46] N.L. Allen, M. Boutlendj & H.A. Lightfoot, "Dielectric Breakdown in Nonuniform Field Air Gaps", *IEEE Transactions on Electrical Insulation*, Vol. 28, No. 2, April 1993, pp. 183 – 191.

[47] J.L. Lowke, "Theory of Electrical Breakdown in Air in Non-uniform Fields", *Proceedings of the Tenth International Conference on Gas Discharges & Their Applications*", SWANSEA, Vol. 2, 1992, pp. 616 – 619.

[48] IEC Publication 60-1, 2nd Edition, *High-voltage Test Techniques – Part 1: General Definitions and Test Requirements*, IEC, 1989.

[49] L.L. Alston, "High Temperature Effects on Flashover in Air", *Proceedings of The Institute of Electrical Engineers (IEE)*, Vol. 105-A, No. 24, December 1958, pp. 549 – 553.

[50] M. Hara, J. Suehero, S. Sumiyoshitani and M. Akazaki, "Modes and Characteristics of Corona Discharge in High-Temperature Air", *Proceedings of Electrical Engineering in Japan*, Vol. 108, No. 3, 1988, pp. 10 – 21.

[51] A. Robledo-Martinez & P.A. Calva, "DC Breakdown Characteristics of Rod-rod and Rod-plane Gaps in Reduced-Density Air", *Proceedings of the 6th International Symposium on High-Voltage Engineering*, New Orleans, LA, USA, 28 August – 1 September 1989.

[52] D.B. Watson, S.K. Kho, K.A. Samuels and S. Chee, "Electrical Flashover Through Heated Air", *J. Phys. D: Applied Physics*, Vol. 26,1993, pp. 1067 – 1072.

[53] M. Moreno, "Performance of External Insulation in Presence of Flames Due to Sugar Cane Burning", *CIGRE 33-85 (WG-07)*, Prague, September 1985.

[54] K.J. Sadurski, "Effects of bush, grass and cane fires below transmission lines", Eskom Electrical Report No. 123/2/97, Project No. 72E9, pp. 6

[55] H.F. Vosloo, "The need for and contents of a life Cycle Management Plan for Eskom Transmission Line Servitudes," M.Sc. dissertation, Rand Afrikaans University (RAU), December 2004.

[56] R. Lanoie and H.P. Mercure, "Influence of Forest Fires on Power Line Insulation", *Proceedings of the 6th International Symposium on High-Voltage Engineering*, New Orleans, LA, USA, 28 August – 1 September 1989.

[57] B. Hutzler, "Space Charge in Large Air gaps", *Proceedings of the 4th International Symposium on High-Voltage Engineering*, Athens, Greece, 05 – 09 September 1983, Paper No. *42.02*.

[58] T.E. Broadbent and J.K. Wood, "A Thermally triggered Spark Gap", *British Journal of Applied Physics*, Vol. 6, 1955, pp. 368.

[59] A.M. Sletten and T.J. Lewis, "Characteristics of the Trigatron Spark Gap", *Proceedings of the IEE*, Monograph No. 193M, August 1956, 104C, pp. 54.

[60] J.L. Hernandez-Avilla and A. Robledo-Martinez, "Effect of Polarity on DC Flame Breakdown", *Proceedings of the 12th International Symposium on High-Voltage Engineering*, Bangalore, India, 20 – 24 August 2001, pp. 310 – 313.

[61] *HVDC Test Set Instruction Manual*, MWB India Limited, 2000.

[62] *Instruction Manual – PK Series*, Glassman High Voltage Inc., New Jersey, USA, 18 December 2003.

[63] *Product Brochure – Full Face Mask 3S Basic Plus*, MSA – AUER GmbH, Berlin, Germany, 2009. Website: www.mas-auer.de